THE UNIVERSITY OF ALBERTA

A Study of Aggregative Fluidization.

Faculty of ~~Engineering~~ GRADUATE STUDIES

Department of Chemical and Petroleum Engineering

by

Geoffrey Davies

Edmonton, Alberta.

September, 1959.

THE UNIVERSITY OF ALBERTA

A Study of Aggregative Fluidization.

A DISSERTATION

SUBMITTED TO THE FACULTY OF GRADUATE STUDIES

IN PARTIAL FULFILMENT OF THE REQUIREMENTS FOR THE DEGREE

OF MASTER OF SCIENCE.

FACULTY OF ENGINEERING

DEPARTMENT OF CHEMICAL AND PETROLEUM ENGINEERING

BY

GEOFFREY DAVIES

EDMONTON, ALBERTA

September, 1959.

ACKNOWLEDGMENTS.

The investigations described in this thesis were conducted in the laboratories of the Research Council of Alberta, Edmonton. The work was carried out under the direction of a committee composed of Dr. D.B. Robinson and Dr. I.G. Dalla Lana of the Department of Chemical Engineering of the University of Alberta and Dr. C. Moreland of the Coal Section, Research Council of Alberta. Sincere appreciation is extended to the members of the committee for their helpful advice and guidance during the course of this work.

The author also wishes to extend his thanks to the other members of the staff of the Research Council of Alberta who have given of their time and assistance, and especially to Mr. E. Kyto whose assistance throughout this work and in the preparation of many of the drawings is greatly appreciated.

Finally, the author wishes to thank the Research Council of Alberta for the permission to submit this work towards the degree of Master of Science.

Table of Contents.

Table of Contents. (cont.)

Table of Contents. (cont.)

List of Tables.

List of Figures.

List of Figures. (cont.)

List of Figures. (cont.)

List of Plates.

ABSTRACT.

Fluidization tests have been carried out in a 2½ in. diameter column using glass beads and char particles, and air as the fluidizing medium.

Log-probability size distributions of 5,10,25 and 100-fold size variation, with an average size of 271 microns, were tested and changes in the average diameter due to elutriation were studied. Systematic tests with beds of closely sized particles ranging in size from 74 to 912 microns were also made. The results are presented as bed expansion curves and show that whilst size distributions of the same average diameter have no effect on the shape of these curves, the particle diameter has a considerable effect.

The data has also been correlated by the method suggested by Zenz for particulate fluidization, and the results show that this method is not applicable to the case of aggregative fluidization. Comparison with several other correlations show similar differences. It is concluded that up to the present time, no really satisfactory correlation for aggregative fluidization has been proposed.

Other system properties are considered, and data obtained from fixed-bed experiments are included.

A STUDY OF AGGREGATIVE FLUIDIZATION.

GENERAL INTRODUCTION.

Fluidization is achieved when a bed of solid particles is suspended in a continuously agitated state by the countergravity flow of a fluid. The fluidized state is common in nature; the transport of soil by rivers, drifting of sand in deserts, and the suspension of droplets of water in clouds are examples of an apparent fluidization. Similarly, quicksand is simply a partially fluidized system of sand in an upward seepage of water.

The mineral industry probably was the first to make use of fluidization, calling it the 'teeter' condition, where water was used as the fluidizing medium. Commercially, the first successful operation involving gas-fluidization was the Winkler process for gasification of German brown coals, which was operating by the mid-1920's. However, it was the introduction of fluidization to the petroleum industry, where it provided a simple and cheap means of handling the large quantities of cracking catalyst, that really established the process as a unit operation. The advantages of increased heat transfer, resulting in improvement of temperature control, and more uniform temperature distributions in the bed, also made fluidization very useful in dealing with

strongly exothermic reactions, such as the oxidation of napthalene and the Fischer-Tropsch reaction for synthetic gasoline manufacture.

In recent years the coal industry has shown considerable interest in the application of fluidization to the low temperature carbonisation of coal, due to its obvious advantages over the older fixed bed processes. The Research Council of Alberta is therefore studying the carbonisation of Alberta coals in a small scale fluidized bed reactor, with a view to obtaining information on the product yields, design and operation of such a process.

The aims of this thesis were to study the fluidization characteristics of a typical low-temperature char produced in the above reactor, so that the required design constants could be determined, and to use this data, together with data obtained from similar experiments with glass beads, to test the validity of a correlation proposed for particulate (liquid-solid) fluidization when applied to the aggregative type of fluidization (gas-solid.)

A. LITERATURE REVIEW.

1. INTRODUCTION.

The flow of a fluid past a body or group of particles covers a very wide field of operations in Chemical Engineering.

Fluidization, which has previously been defined as that operation involving the suspension of a bed of solid particles in an upward flow of a fluid, lies intermediate between the operations involving the flow of a fluid through a packed or fixed bed and that involving the flow of a fluid past isolated particles. Essentially, fluidization is the inverse operation of hindered settling, and several workers (16,28) have compared the results obtained by these two methods.

Since all these operations involve similar mechanisms, it would be thought that a general correlation could be used. However, at the present time, separate correlations are used to define each operation, and we must therefore consider each operation, and its relationship to fluidization, separately.

2. THE FIXED BED.

The flow of fluids through porous systems has long been studied in many fields of engineering. Natural

examples are common, and commercially, its main advantage lies in its high surface-area to volume ratio. In 1856, D'Arcy (1) first reported the proportionality between the pressure drop per unit height of bed and the flow of water through it. Since that time, many correlations (2) have been reported, and the effects of most of the experimental variables bave been determined. The similarity between D'Arcy's equation and Poiseuille's equation for viscous flow through capillaries led to semi-empirical correlations based on an analogy between the flow through packed beds and the flow through a group of capillaries. The length of these capillaries was assumed to depend on the particle shape, size, size distribution and orientation, and on bed porosity, as well as on the bed height.

The methods of dimensional analysis, first introduced by Blake (3), and later extended by other workers, are now commonly used. Chilton and Colburn (4) in a similar correlation did not account for the fraction voids in the bed; (this is now known to be of considerable importance). However, Carman (5,6) in dealing with beds of spheres, extended the Blake and Kozeny (7) equations to give the so called "Carman-Kozeny" equation for pressure drop in packed beds:

$$f = \frac{g \, \varphi \, \Delta p \, d_p \, \varepsilon^3}{2L \rho_f V^2 (1-\varepsilon)^2} = F\left(\frac{d_p V \rho_f}{\mu}\right) \quad \ldots (1)$$

Leva (2) developed the Carman-Kozeny equation further, and showed a more general relationship as;

$$f = \frac{\Delta P \, d_p g \, \varepsilon^3}{2 \rho_f V^2 L \, \lambda^{3-q} (1-\varepsilon)^{3-q}} = F\left(\frac{d_p V \rho_f}{\mu}\right) \quad . . . (2)$$

where λ is a shape factor.

The index 'q' was found to vary from one for completely viscous flow to two for completely turbulent flow. Leva defines the diameter d_p as the geometric mean of the sieve openings used to size the particles. He also shows that surface roughness has no effect in the viscous range, but has the definite effect of increasing the friction factor in the turbulent region.

Ergun (8) further modified the equations, and gave the following comprehensive equation, valid for all types of flow:

$$\frac{\Delta p \, g}{L} = 150 \frac{(1-\varepsilon)^2}{\varepsilon^3} \frac{\mu V}{d_p^2} + 1.75 \frac{(1-\varepsilon)}{\varepsilon^3} \frac{\rho_f V^2}{d_p} \quad . . (3)$$

The left-hand side of this equation defines the total friction energy losses, and the two terms on the right hand side represent the viscous and kinetic energy losses respectively. In this case, $d_p = (d_s x \phi)$.

Brownell and Katz (9) correlate the data of other workers together with their own results on the graph for

the flow of fluids through cylindrical ducts, and use the dimensionless groups

$$f = \frac{2g \; d_p \; (-\Delta p)}{F_f \; LV^2 \rho_f} \quad \text{and } Re = \frac{d_p V \rho_f}{\mu} \cdot F_{Re}$$

where F_f and F_{Re} are correction factors to bring the data onto the desired curve. Graphs are presented showing the factors F_f and F_{Re} as functions of the porosity, with sphericity (ϕ) as a parameter; d_p is defined for close size ranges as the average sieve diameter (d_m) and for mixed sizes as the mean surface diameter (9).

At the present time, orientation effects have not been studied separately. Wall effects have been discussed by some workers (5,10,11), showing a wide variation in effect, but it seems that wall effects become negligible when the tube dia./particle dia. ratio becomes greater than about 50:1. In a recent paper, Barclay (12) has shown that this is true for beds of anthracite at normal voids (ie. normal packing.) but at constant voids, he found that the wall effects decreased with increasing D_t/d_p ratio to a minimum, and then increased with further increases in D_t/d_p. He also found that this critical value of D_t/d_p at which wall effects became negligible increased markedly with decrease in particle size.

Unfortunately, the correlations developed for fixed

beds break down when applied to fluidized beds. The method of Brownell and Katz can cover the range of porosity from 0.2 - 0.9, but only for fixed beds. Similarly, the equations of Leva and Ergun can be used for fixed beds in the range of porosities from 0.35 - 0.6. Above this the function $\varepsilon^y/(1-\varepsilon)^x$ fails to give a satisfactory correlation, since this function tends to infinity as the porosity tends to unity.

However, at the point of fluidization, a bed can be considered to be a fixed bed at its loosest possible packing, and the correlations obtained from analysis of fixed bed data can be applied at the point of incipient fluidization.

3. THE ONSET OF FLUIDIZATION.

When a fluid stream is caused to flow upwards through a packed bed, the pressure drop first increases with increasing flow, without changing the bed height. Eventually, a point is reached where the frictional pressure drop approaches the buoyant weight of the bed, and further increases in flow rate then cause an increasing expansion of the bed, but produce little change in the pressure drop. In the fluidized state, the bed exhibits fluid-like properties, and Parent et al. (13) suggested that the pressure drop through the bed would be equal to the hydrostatic head (H.), together with the

head loss necessary to overcome frictional forces due to the motion of the particles (h) ie.

$$\Delta p = H + h \quad \ldots\ldots\ldots\ldots\ldots (4)$$

Working with gases they found that 'h' was negligible, and that the pressure drop was independent of the properties of the gas used.

Williamson and Garside (14) using air later confirmed Parent's observations.

Later, Wilhelm and Kwauk (15) and Leva (2) extended equation (4) as

$$\Delta p/L = (1-\varepsilon)\ (\rho_s - \rho_f) \quad \ldots\ldots\ldots\ldots\ldots (5)$$

showing that the pressure drop is not independent of the fluid density. (However, if the fluid be a gas, ρ_f may be neglected, and this is what Parent actually found.)

Lewis et al. (16) plotted the ratio of actual pressure drop to calculated pressure drop against Reynolds Number for beds of 0.0061 inch glass spheres fluidized with air, showing deviations up to 20% greater than the theoretical value of one. They interpret the deviations as being due to electrostatic and frictional drag forces on the walls of the vessel. Toomey and Johnstone (17) have proposed a mechanism to account for this excess pressure drop over that just required for fluidization, by taking account of the work done by the discontinuous

phase in rotating particles in the bed, and of wall effects, and correlate their own data, and that of Lewis.

4. THE POINT OF INCIPIENT FLUIDIZATION.

The transition from a fixed to a fluidized state is usually gradual, and proceeds over a range of flow rates depending on the nature of the bed. Practically, it is desirable to define some definite point of incipient fluidization at which the complete change is assumed to take place, and this lower limit of velocity is referred to as the critical or minimum fluidizing velocity. It is important that this reference point is reproducible, and fits easily into available correlations.

Leva et al. (2)(18) base their definitions of the critical fluidizing velocity on correlations obtained for fixed beds. By setting the pressure drop term in these equations equal to the weight of the bed, and then substituting the bed voidage obtained from a correlation of the maximum fixed bed voidage, they obtained the critical velocity.

Lewis et al. (16) plotted curves connecting the properties of the system and bed voidage against the modified Reynolds number for both the fixed and fluidized state, and suggest by simultaneously solving for porosity and velocity between the two curves that the critical conditions can be obtained. Sinclair and Robinson(19) however, show that this method is not generally applicable,

since at certain values of the Reynolds number, an imaginary solution is obtained.

Baerg, Klassen and Gishler (20) assumed that the discontinuity observed in the plot of heat transfer coefficient to the walls of the retaining vessel versus the superficial gas velocity through fixed and fluidized beds corresponded to the point of fluidization.

Agarwal and Storrow (21), defined the critical velocity by visual observation of beds fluidized in a transparent tube as being, for uniformly sized beds, the point at which the bed becomes settled as the velocity is reduced, and for beds of mixed particle sizes as the point at which all the bed is fluidized as the velocity is increased.

The variation of pressure drop with superficial velocity through beds of particles forms the basis of two definitions of critical velocity. Figure 1a. shows this relationship plotted on a log-log scale for an idealised system. During the fixed bed condition, the pressure drop increases linearly (for viscous flow.) with increasing velocity, the position of the line depending on the system and on the initial bed packing. The pressure drop becomes essentially constant during fluidization, and if the velocity is then reduced slowly, the curve retraces the same path in the fluidized region, but falls off at a higher velocity, when the bed settles

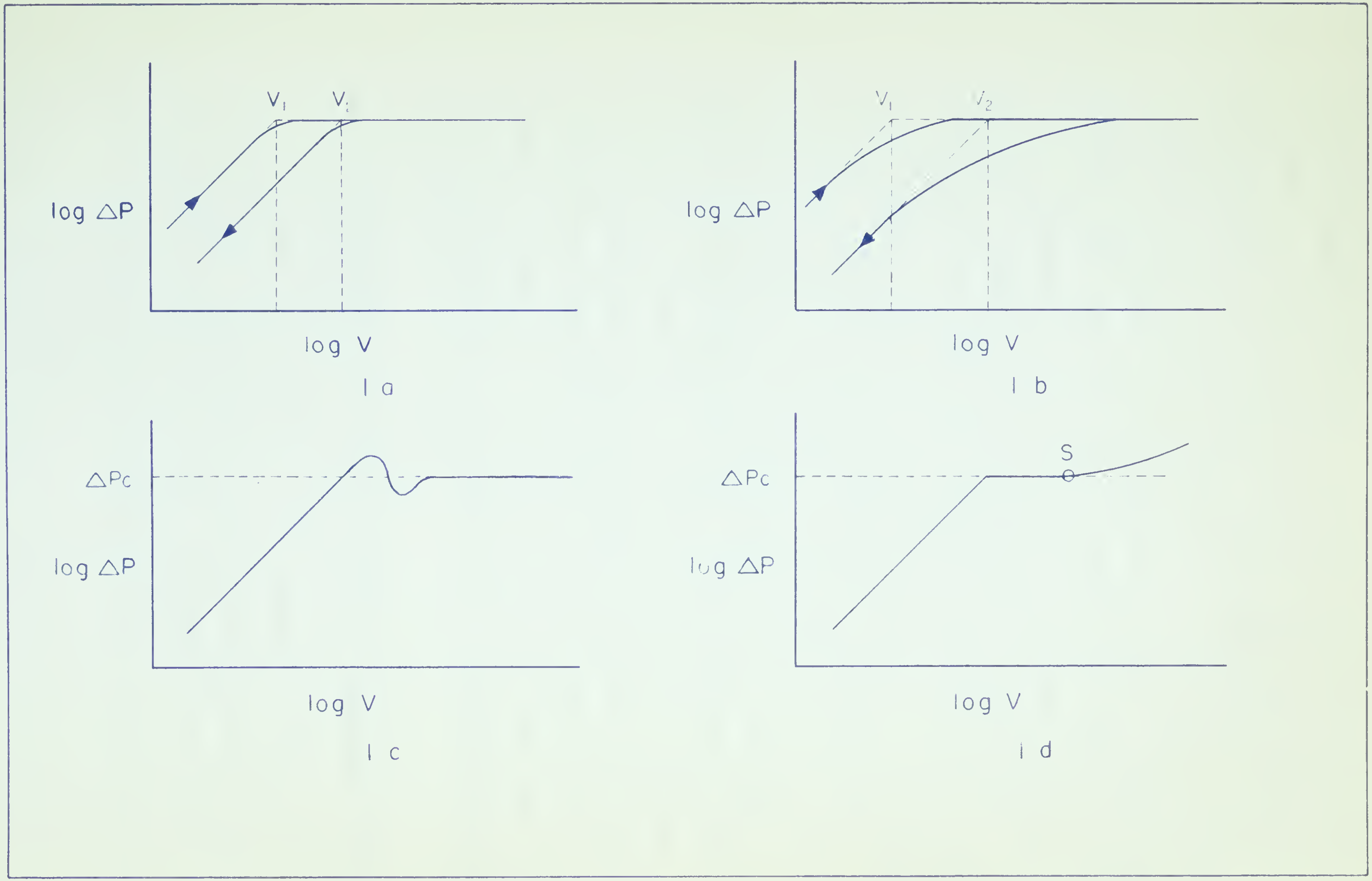

FIG I PRESSURE DROP CHARACTERISTICS

at its maximum porosity. If the fixed and fluidized regions are extrapolated as shown, two intersections are obtained at V_1 and V_2. The intersection V_1 will depend on the initial packing of the bed, and is therefore not suitable as a reproducible point. Jolley and Stanton (22) use this point to define the critical velocity, stipulating that the bed must be mechanically shaken. However, the intersection V_2 obtained by decreasing the flow rate through a fluidized bed is reproducible, since the bed always settles at a constant maximum voidage, and it represents a velocity above which the bed is fluidized. This definition was proposed independently by Van Heerden et al. (23) and Miller and Logwinuk (24), and is now favoured by most workers in this field. Difficulties arise, however, when dealing with wide size-range mixtures, since the pressure drop-velocity curves are much more curved as shown in Figure 1b. The significance of this type of curve, and the data obtainable from it are discussed in the results of this work.

5. CORRELATIONS FOR THE CRITICAL FLUIDIZING VELOCITY.

An excellent review of the suggested correlations for critical velocities is presented by Sinclair (19,25) in his associated work on the fluidization of coal in air, and the reader is recommended to consult this source for

a more detailed account of this topic.

Leva (2) and Van Heerden (23) developed correlations by substituting the identity

$$\frac{\Delta p}{L} = (1-\varepsilon_o)(\rho_s - \rho_f) \quad . \; . \; . \; . \; . \; . \; . \; (5a)$$

into equations developed from experiments on fixed beds. Leva et al. (2) obtained the expression:

$$G_o^2 = \frac{g \, d_p' \, \rho_f \, (\rho_s - \rho_f) \, \varepsilon_o^3}{2 \, f \, \lambda^{3-q} \, (1-\varepsilon_o)^{2-q}} \quad . \; . \; . \; . \; . \; (6)$$

for the critical fluidizing rate, and present graphs of f versus Re, and q versus Re, which must be used together with a plot of ε_o versus particle diameter to effect a solution. For purely viscous flow, the equation can be simplified by the substition of $q = 1$ and $f = 100/Re$ in equation 6.

Van Heerden et al. (23) studied fluidization only in the laminar region at Re<10, and confined their considerations to gas fluidization, so that for the fluidized state

$$\Delta p/L = g \, \rho_o \quad . \; . \; . \; . \; . \; . \; . \; . \; . \; . \; . \; . \; . \; (5b)$$

Substituting this relationship together with the fixed bed correlation $f = 77/Re$ for viscous flow obtained by

Lewis et al. (16), in the Carman-Kozeny equation, (equation 1) they obtained:

$$Re_0 = \frac{g \rho_f \rho_0 . d_p^3 \varepsilon_0^3}{154 \mu^2 \lambda^2 (1-\varepsilon_0)^2} \quad \ldots\ldots\ldots\ldots (7)$$

Van Heerden's data and that of Lewis et al. (16) indicated that spheres have a definite porosity of 0.406 at the critical point, and that this is independent of particle size. They therefore assumed that the effective voidage for gas flow would also be independent of particle size for irregular particles, and combined the shape factor with the porosity function to give a new shape factor B. By setting B equal to 1 for spheres, the following equation was obtained

$$Re_0 = \frac{0.00123\ g}{B \mu^2} . \rho_0 . \rho_f . d_p^3 \quad \ldots\ldots (8)$$

Finally, Van Heerden introduced an equivalent particle diameter which is defined as the diameter of the sphere with the same number of particles per unit volume of packed bed, both counted at maximum porosity. With this refinement, good agreement was obtained for all the size distributions studied, and the shape factor B was found to be approximately 1 in all cases.

Millar and Logwinuk (24) worked with non-spherical

particles in the laminar region only, and correlated their results using dimensional analysis by the equation:

$$G_0 = 0.00125 \ d_p^2 \ (\rho_s - \rho_f)^{0.9} \rho_f^{1.1} \ g / \mu \ . \ . \ . \ (9)$$

d_p is the geometric mean diameter and the ft.-lb.-hr. system of units is used.

More recently, Leva (26) has modified his correlation for critical velocities (for $Re_0 < 5$) by combining the terms $g_c \lambda^2 \varepsilon_0^3 / (1 - \varepsilon_0)$ as a constant C. Evaluation of C from extensive experimental data result in the equation:

$$G_0 = 688 \ d_p^{1.82} \left[\rho_f (\rho_s - \rho_f)\right]^{0.94} / \mu^{0.88} \ . \ . (10)$$

where d_p is in inches, μ in centipoises, and ρ_s and ρ_f in pounds per cubic foot. For $Re_0 > 5$, commonly met in liquid/solid systems, a correction factor must be applied.

Equations 8,9 and 10 are remarkably similar, and the differences are probably a matter of interpretation of the original experimental data. It is interesting to note that the dimensionless group $g \ (\rho_s - \rho_f) \rho_f \ d_p^3 / \mu^2$ closely matches the groups used in the above equations; this group also forms the basis for the correlations of Wilhelm and Kwauk (15), Zenz (27), Pinchbeck and Popper (29) and Becker (30), all of whom plot the group as a function of the modified particle Reynolds number, and it would seem that it adequately covers any variations in the properties of the system.

6. MINIMUM FLUID VOIDAGE. (ε_o)

The minimum fluidized-bed porosity is equivalent to the maximum fixed-bed porosity, and is often used in correlations for the critical fluidizing velocity. Most workers (eg. 2,21,19) present graphs of ε_o versus particle diameter, but in general, it is desirable to measure ε_o for the particles considered, since a small error in this value makes an appreciable difference in the value of the calculated velocity, powers of ε being involved.

A common method of measuring ε_o is to fluidize the bed intensely, and then gradually reduce the velocity to zero. However, visual observation of the bed height at the point when the particles settle is probably a more accurate interpretation. Leva (2) suggests that the minimum fluid voidage can be approximated by slowly pouring the particles into a measuring cylinder. The author agrees with Johnson (31) that this method gives low values of ε_o , and the error increases considerably for particles greater than about 150 microns. It should be noted that in all these methods, the slightest vibration of the apparatus will cause considerable error.

Matheson, Herbst and Holt (32) proposed the equation: (d_p in microns.)

$$\log d_p = 2.81 \left(\frac{\rho_o}{\rho_s}\right) + 1 \quad . \; . \; . \; . \; . \; . \; . \; . \quad (11)$$

to account for the effect of particle size on bed density. Although this equation gives the trend of the true relationships, it is useless from a quantitative point of view (31).

Figure 6 shows a plot of ε_0 versus particle diameter. For spheres, the minimum voidage is independent of the particle diameter (16,23); for all non-spherical particles, ε_0 is approximately constant for larger particles, but increases repidly for smaller particles (below 300 microns.) The absolute value of ε_0 depends on the shape of the particles, increasing as the particles become more irregular. Leva et al. (2) explain both these trends as surface effects, and also correlate their data for ε_0 by plotting $\lambda^2 \varepsilon_0^3/(1-\varepsilon_0)$ against d_p.(26,33)

The significance of the minimum fluid voidage when dealing with wide size distributions is more complex, and will be considered later. Further expansion of the bed beyond the critical point leads to two types of fluidization, depending on whether the fluid used is a liquid or a gas, and these will now be considered separately.

7. LIQUID-SOLID FLUIDIZATION.

In general, solid particles fluidized by a liquid are individually and uniformly dispersed throughout the

fluid-bed, and the upper level is quite sharp and horizontal. At lower flow rates, there is some tendency for channeling to develop, that is, for non-uniform flow distribution through the bed, and in cases where a large density difference exists between the solid and the liquid, slugging action has been reported. Normally however, uniformly agitated beds are obtained, and the agitation and mixing effects increase with increasing velocity, until the terminal velocity of the particles is reached when the bed is dispersed in the liquid and removed from the containing vessel. Wilhelm and Kwauk (15) defined this type as particulate fluidization, and showed that it is characterised by a Froude number (V^2/gd_p) of less than 1.

Since liquid fluidization is essentially the same operation as hindered settling, it is convenient to consider the correlations proposed for both these liquid-solid systems together.

Hancock (34,35) has described these phenomena and correlated the data of Hirst (36) for the hindered settling of anthracite, granite and galena, and for the fluidization of sand with water, by introducing the term ε^6 into the basic correlation for the free fall of spheres. (42) He plotted

$$C_D . \varepsilon^6 = \frac{4}{3} \; \frac{g \, d_p \, (\rho_s - \rho_f) . \varepsilon^6}{V^2 \rho_f} .$$

against the Reynolds number. The choice of the function ε^6 was purely empirical, but in a later paper (37), Hancock showed that it also held in the turbulent region, and compared his function with the more complex function obtained by Steinour (38) from his experiments on sedimentation.

Wilhelm and Kwauk (15) correlated their data for the fluidization of sand and beads with water by means of plots of the group $K_{\Delta\rho} = d_p^3 \; g \; \rho_f (\rho_s - \rho_f) \; / \; 2 \; \mu^2$ against the Reynolds number, with the bed voidage as parameter. They made no attempt to determine a function of bed voidage which would bring all their points onto one curve, concluding only that the function would be complicated.

Morse (39) attempted to obtain a single line plot using the voidage function $\varepsilon^3/(1-\varepsilon)$, but was not too successful.

Lewis et al. (16) from their settling and fluidization work with glass spheres correlated their data using the function $\varepsilon^{4.65}$ as a multiplier for the drag coefficient (C_D) plotted against the Reynolds number, and obtained a curve approximating to that for the free fall of spheres (42).

Leva (2,26) states that the modified equation:

$$G = \frac{0.005 \; d_p^2 \; g \; \rho_f (\rho_s - \rho_f) \; \varepsilon^3}{\mu \; \lambda^2 (1-\varepsilon)} \quad \ldots\ldots \quad (12)$$

developed from his work on fixed beds, can be used to correlate expansion data up to a voidage of 80-85%, provided that Re<10.

Jottrand (40) presents data for the fluidization of crushed sand with water for Re<0.5. He found that the function $\varepsilon^3/(1-\varepsilon)^2$ as proposed by Leva (2) was not satisfactory in correlating his data; instead, he proposed the function $\varepsilon^{5.6}$. However, he also showed that the data of Wilhelm and Kwauk gave different powers of the voidage, and concluded that the function varied with the Reynolds number.

Young (41) considered the problem in two ways. The first, based on the Blake-Carman correlation for fixed beds (5), determines $F(\varepsilon)$ in the relation,

$$\frac{(\rho_s - \rho_f)\, g\, d_p}{\rho_f V^2} \cdot F(\varepsilon) = F'\left(\frac{V\, d_p\, \rho_f}{6\mu\,(1-\varepsilon)}\right) \quad . \; . \; (13)$$

where the first group is called the Blake number, and the second is the modified Reynolds number according to Carman (5). The other method involves the determination of $F''(\varepsilon)$ and $F'''(\varepsilon)$ in the equation: $Bl.\, F''(\varepsilon) = \overline{F}\left[Re.F'''(\varepsilon)\right]$ where the function $\overline{F}$ is given by the standard curve for free-falling spheres (42). He presents graphs of the functions of voidage considered, and obtains reasonably good correlations.

Johnson (31) used the equations for the density and viscosity of suspensions together with Stoke's equation to correlate his data on the fluidization of irregular particles in both water and air. He presents the equations:

$$V = \frac{g \; d_p^2 \; \phi^2}{18\,\mu} (\rho_s - \rho_f) \frac{\varepsilon^5}{1 + 0.5\,(1-\varepsilon)} \quad . \; . \text{ for } Re_s < 2 \; . \quad (14)$$

$$V = 0.171 \; d_p \; \phi . \sqrt[3]{\frac{g^2 \; \rho_s \; . \varepsilon^6}{\mu(1-\varepsilon)\left[1+0.5(1-\varepsilon)\right]}} \left(\frac{\varepsilon}{1-\varepsilon}\right)^3 \text{for } Re_s > 2 . \quad (15)$$

$$\text{where } Re_s = 0.123 \; \frac{d_p \; V \left[\varepsilon \rho_f + (1-\varepsilon)\rho_s\right] \varepsilon^2}{\mu \; (1-\varepsilon)} \quad . \; . \; . \; . \; . \; . \; . \quad (16)$$

In general, equation (14) applies to liquid fluidization, but the equations have not found very wide acceptance due to their complexity.

Zaki (28) gives an excellent account of both liquid fluidization and sedimentation. Working with spherical particles he found that

$$\frac{V}{V_i} = \varepsilon^n \quad . \; . \; . \; . \; . \; . \; . \; . \; . \; . \; . \; . \quad (17)$$

where $V_i \equiv V_t$, for sedimentation.

and $\log V_i = \log V_t - d_p/D_t$, for fluidization.

For viscous flow ($Re_t < 0.2$), $n = 4.65 + 20\,d_p/D_t$ and for completely turbulent flow ($Re_t > 500$), $n = 2.39$. For $0.2 < Re_t < 500$, n is given as a function of d_p/D_t and Re_t. (see figure 38.)

It is interesting to note that for sedimentation, they obtained the equation:

$$V = \frac{d_p^2 \quad g \quad (\rho_s - \rho_f)}{18\,\mu} \cdot \varepsilon^{4.65} \quad \ldots\ldots\ldots \quad (18)$$

which agrees with the correlation proposed for the laminar region by Lewis et.al. (16).

Becker (30) and Zenz (27) have both given graphical correlations of sedimentation and liquid-fluidization based on the standard curve for the free-fall of spherical particles. (42)

Becker extended the method of Young (41), and plotted the dimensionless group

$K_B = C_D\,Re^2 = 4\,g\,d_p^3\,\rho_f\,(\rho_s - \rho_f)\,/\,3\,\mu^2$

as a function of the modified Reynolds number, $J = Re./\,F(\varepsilon).F'(\phi)$. Using the data of other workers, he obtained graphs of $F(\varepsilon)$ versus ε, and of $F'(\phi)$ versus ϕ, with K_B as parameter, for particulate fluidization. Modifying Ergun's equation for fixed beds (8), he derived the curves for $F(\varepsilon)$ versus ε at constant K_B mathematically, and showed fairly good agreement with the experimental

curves. He also showed that for viscous flow, $F(\varepsilon) = \varepsilon^{4.75}$, and for fully turbulent conditions, $F(\varepsilon) = \varepsilon^{2.4}$, both of which are in excellent agreement with the results of Zaki (28).

Zenz (27) replotted the standard drag coefficient correlation for spheres (42), using the groups: (See figure 34.).

$$(C_D Re^2)^{1/3} = d_p \Big/ \left(\frac{3}{4} \cdot \frac{\mu^2}{\rho_f (\rho_s - \rho_f)\, g} \right)^{1/3} \quad \ldots\ldots \quad (19)$$

$$(Re/C_D)^{1/3} = V_t \Big/ \left(\frac{4}{3} \; \frac{\mu (\rho_s - \rho_f)\, g}{\rho_f^{\,2}} \right)^{1/3} \quad \ldots\ldots \quad (20)$$

In effect, this is a plot of V_t versus d_p, with the denominators as constants based on the physical properties of the fluid and particles. Using the same co-ordinates, he replotted some of the available data on liquid-fluidization and sedimentation, and obtained a set of curves similar to the free-fall curve for spheres, with voidage as parameter. This is a simple, and most useful form of correlation, and since the product $(C_D Re^2)^{1/3} \cdot (Re/C_D)^{1/3} = Re$, the Reynolds number can be readily calculated for any point on the graph.

Beranek (43) correlates his own data, and that of Wilhelm and Kwauk (15) for particulate fluidization on

a log-log plot of $(\varepsilon-\varepsilon_o)/(1-\varepsilon_o)$ versus $(V-V_o)/(V_t-V_o)$. He explains the change in slope of the line obtained at high porosities as being due to wall effects.

8. <u>GAS-SOLID FLUIDIZATION.</u>

The state of knowledge concerning the fluidization of solid particles with a gas is limited at the present time due to its greater complexity. The sequence of events as the bed expands has been described by many workers (2,15,16,22,23,25,26,45), and will only be considered briefly here. Above the point of incipient fluidization, a bed of uniformly sized particles continues to rearrange itself from the loosest possible packing, and slight expansion occurs, allowing the particles to be freely supported by the fluidizing gas. With wider size distributions, increasing gas flow above the incipient fluidization point causes the finer material to break through the bed and fluidize at the top; this process continues until the static portion of the bed is reduced to zero. Further increases in gas flow result in <u>two phase</u> fluidization. The bulk of the bed constitutes a <u>dense phase</u>, which is in a state very close to that at the point of full fluidization, with the particles individually supported in the gas. The excess gas above that required to maintain this dense phase passes through the bed in "bubbles" or gas pockets, rising due to buoyancy effects. These gas bubbles usually carry

a dispersed population of particles, and are therefore referred to as the dilute phase. (An alternative nomenclature refers to them as the continuous and the discontinuous phase respectively.) These bubbles cause mixing and agitation in the bed, and therefore the degree of turbulence increases as the flow rate increases.

The behaviour of a fluid-bed depends on the physical and geometrical properties of the system. Channeling tendencies are common at low velocities, but are usually destroyed with increasing flow rate due to bed turbulence. A typical pressure drop curve is shown for a mildly channeling bed in Figure 1c. In certain cases, channels may be self-propagating causing severe channeling, and fluidization becomes impossible. Under normal circumstances the expanding bed is often likened to a boiling liquid, and waves are formed (44) as bubbles break at the surface. As the flow rate is increased, the bubbles grow larger, and the violent breaking action throws streamers of particles up from the bed. Under some conditions, the bubble diameter approaches the diameter of the retaining vessel, and whole sections of the bed are repeatedly projected upwards, disintegrate, and rain back through the enclosed piston of gas. This phenomenon is known as slugging, and is common in small diameter vessels. Figure 1d. shows a typical

pressure drop curve for such a system, the increase in pressure drop being due to the friction between the slugs of particles and the vessel walls. With further increasing gas flow, the superficial velocity approaches the terminal velocity of the particles in bed, and elutriation proceeds until the fluidized bed no longer exists.

Wilhelm and Kwauk (15) showed that this type of expansion, which they named <u>aggregative fluidization</u> to distinguish it from the smoother particulate fluidization, was characterised by a Froude number greater than 1. They also suggest that the tendency in aggregative fluidization towards the maintenance of a dense phase, in which conditions approximate a state of loosest particles contact, necessitates some form of interparticle attractive force which is responsible for the greater stability of the aggregated condition. It is likely that these forces are both fluid-dynamic and electrostatic in origin; both types have been reported as being significant (15,17). The existance of interparticle forces in a gas-solid system suggests a comparison with intermolecular forces in a true fluid. Matheson et al. (32) were probably the first to consider such an analogy in their investigations of the viscosity of fluidized beds. Becker (30) listed these similarities, and Furukawa and Ohmae (40) have measured the liquid-like properties of various beds of particles, and correlated their data using equations similar to those describing phase changes in liquids. The basis

of the analogy is the superficial velocity for fluidization, and the temperature for liquids, these properties being assumed equivalent. The expansion of gas-solid systems, as described, is more complex than the particulate case, and at the present time, none of the methods of correlation proposed in the literature has found wide acceptance. Many of the correlations used are the same as those discussed under liquid-solid fluidization, and some repetition will be necessary.

Wilhelm and Kwauk (15) using the dimensionless groups $K_{\Delta\rho}$ and Re, correlated their data for aggregative fluidization and that for liquid fluidization, with porosity as a parameter. However, Friend (15) showed that the relationship did not appear to be satisfactory in the case of small particles with wide size distributions.

Lewis et al. (16) also used the same correlation for both gas and liquid fluidization, and plotted the group $4gd_p(\rho_s - \rho_f)\,\varepsilon^{4.65}/3\rho_f V^2$ versus Re. on log-log coordinates. They also established the relationship:

$$\varepsilon - \varepsilon_o = 0.065 \quad (V - V_o) \,/\, d_p^{0.5} \qquad \ldots\ldots\ldots \quad (21)$$

where ε_o and V_o represent the quiescent state. It is interesting to note that for some of their experiments in which apparently 'good' fluidization was involved, the data did not agree with either of the above correlations.

Leva et al. (2,26) rearranged equation 12 to give

$$\frac{G \mu l_e}{\rho_f} = \text{constant} \left[\frac{(1-\varepsilon)^2}{\varepsilon^3} \right]^{-1} \quad \ldots\ldots\ldots \quad (22)$$

for a given system. They found that plots of log. $G \mu l_e / \rho_f$ against log $(1-\varepsilon)^2 / \varepsilon^3$ gave slopes ranging from -0.7 to -4.5, instead of -1 as would be expected from equation 22. To overcome this apparent disagreement, they introduced the term "fluidization efficiency" (E.) defined by:

$$E = \frac{G_F - G_e}{G_F} \quad \ldots\ldots\ldots\ldots\ldots \quad (23)$$

where G_F = mass flow required to fluidize the bed
and G_e = mass flow as calculated by equation 12 to expand the bed to the same porosity.

From this concept, they developed the equation:-

$$G_F = \frac{G_o}{l_e} \left(\frac{G_e \, l_e}{G_o} \right)^{|m|} \quad \ldots\ldots\ldots\ldots \quad (24)$$

where l_e = expansion ratio = height of the bed divided by height of the bed at incipient fluidization, and $|m|$ = numerical value of the slope. They present graphs of $|m|$ versus d_p and for the fluidization efficiency, and use

these together with equation 24 to obtain the expansion for any flow rate. This method is probably only satisfactory within the limits of the tested data, and the extrapolations of the fluidization efficiency curves presented should be used with caution. Morse (39) replotted the data of other workers (15,2) using the Carman equation (5) for fixed beds, and obtained poor agreement for air-fluidization data. He explained the deviations as being due to the inherent instability of the gas-solid system caused by the strong tendencies to segregate.

Ergun and Orning (18) developed the equation:

$$\frac{dp}{dL} = \frac{(1-\varepsilon)^2}{\varepsilon^3} \cdot 2\alpha\mu S_v^2 V + \frac{(1-\varepsilon)}{\varepsilon^3} \cdot \frac{\beta}{8} S_v \rho_f V^2 \quad . . . (25)$$

for the pressure drop through fixed beds, where α, β are constants. The porosity functions in this equation can be seen to be the same as those developed by Leva et al. (2) for viscous and turbulent flow respectively. Substituting equation 5, they obtained the equation:

$$\varepsilon^3 - \frac{2\alpha S_v^2 \mu V (1-\varepsilon)}{(\rho_s - \rho_f) g} = \frac{\beta . S_v \rho_f V^2}{8(\rho_s - \rho_f) g} \quad . . . (26)$$

The terms αS_v^2 and βS_v are obtained from fixed bed

experiments, and allow for the size and shape of the particles. Further, for small columns of fine, low density material, they approximate equation 26 as:

$$\frac{\Delta L}{L_0} = \frac{(\varepsilon - \varepsilon_0)}{(1-\varepsilon)} = \frac{2\alpha S_v^2 \mu}{c \rho_s g} (V - V_0) \quad \ldots\ldots(27)$$

which for a given system reduces to:

$$\frac{(\varepsilon - \varepsilon_0)}{(1-\varepsilon)} = \text{constant.} (V - V_0) \quad \ldots\ldots\ldots(28)$$

This equation is similar to that developed by Lewis et al. (16) and Beranek (43), and its limitations are clearly seen in this treatment.

Hancock (37), assumed that his correlation proposed for liquid-fluidization would apply to gas fluidization, but did not demonstrate this.

Johnson (31) obtained equations 14,15, and 16 in his work on fluidization, and concluded that when a gas was used as the fluidizing medium, equation 15 was generally to be used, (ie.) for $Re_s > 2$. He also showed that the approximate relationship proposed from equation 26 by Ergun (18) did not hold for aggregative fluidization.

Becker (30) used the same method of correlation as he did for particulate fluidization; replotting the data

of Leva (2) and Wilhelm and Kwauk (15) he obtained a graph of $F(\mathcal{E})$ versus $\mathcal{E}$, with $K_B = C_D Re^2$ as parameter, for aggregative fluidization. This showed that $F(\mathcal{E})$ increased more rapidly for gas-solid systems, tending to unity, at about $\mathcal{E} = 0.62$, for all values of K_B. Becker assumed that this was due to the essentially different mechanisms involved in the two types of fluidization.

Zenz (27) discusses aggregative fluidization, and shows that the data obtained for air-fluidization of a batch of cracking catalyst do not agree with the correlation obtained for particulate fluidization. This type of discrepancy has usually been attributed to the supposed differences between the aggregative and particulate mode of flow, but Zenz suggests that this might not be the case. He considers that for a batch of catalyst having a given size distribution, the characteristic diameter of the particles constituting the fluid-bed should be taken as the average diameter of the unelutriable portion of the charge at the velocity of operation. In the case of a laboratory test, the unelutriable part of the bed would represent the remaining charge after steady-state operation is obtained (ie. when the entrainment of fines is complete.) In commercial scale operations where the entrained material is returned to the bed via cyclone dip legs, the unelutriable portion would be again considered

as the stationary fluidized mass of coarser particles through which the "fines" flow at a mass velocity equal to the entrainment rate.

Zenz replotted his data for cracking catalyst using this interpretation, and found that the points were moved much closer to the corresponding particulate correlation. By further introducing a volume shape factor, he succeeded in moving the points onto his correlation. However, the point of incipient fluidization could not be brought into agreement by this method, and Zenz was forced to consider this point as a special case. Nevertheless, this method of correlation seemed to warrant further investigation, and part of the aim of this thesis was to consider this approach to aggregative fluidization.

9. ELUTRIATION FROM GAS-SOLID SYSTEMS.

In the region immediately above the surface of a fluidized bed, the bursting bubbles of gas thrust particles upward. The larger particles fall back, but the smaller ones are retained above the bed in a dispersed state, and the solids concentration in this zone decreases with distance above the bed. These surges of gas merge into a progressively more uniform flow profile, and at some height above the bed, the velocity profile becomes

constant and reference to a vessel superficial velocity is again significant. If this velocity is in the order of the terminal velocity of the particles in the disperse phase, entrainment will result, and particles will be removed from the vessel. Experiments have shown that the factor of major importance in controlling the rate of entrainment is the nature of the bubbling characteristics of the dense bed (49,51). Liquid-solid systems do not show entrainment, a uniform expansion of the bed taking place instead as the velocity is increased.

Lewis et al. (16) were probably the first to consider entraining fluidized systems in their work on "combined batch-continuous fluidization".

Leva (47) worked with a binary system of coarse and fine particles, and expressed the concentration of fines remaining in the bed as an exponential function of time, up to a certain "break point". He could not correlate this point in terms of the operating variables, but investigated the effect of system properties on the exponential "decay" constant. He also concluded that fluid-beds had a retentative capacity for fine particles.

Osberg and Charlesworth (48) working with similar systems could not correlate their data in the same manner, and found a continuous deviation from the exponential equation rather than a break point.

Jolley and Stanton (22) worked with pulverised coal in a 2 inch diameter column, with variable column height. They found that for closely sized materials, the entrainment rate was constant during a run, but for mixed sizes of coarse and fine material they found that the rate decreased, and the average particle size increased with time. They concluded that bed height had no effect on the rate of entrainment, and that the rate decreased with increasing outage (column space above the surface of the bed).

All of the above workers thought that the rate of entrainment reached a constant value at some high value of outage.

Hyman (49), Richards (50), and Lang (51) extensively studied entrainment from small diameter fluidized beds, and concluded that the entrainment rate was a complicated function of the gas velocity, column diameter, bed height, outage, and particle density and size. (Other properties such as size distribution shape, etc, were not studied, but obviously have an effect.) They found that the variables were all inter-related, and proposed only semi-quantitative correlations. One of the major discrepancies is the effect of column diameter; Lang (51) found that entrainment first decreased, and then increased again with increasing column diameter (in the range $\frac{1}{4}$ - $5\frac{3}{4}$ inches),

tending to a constant value at larger diameters. He therefore suggested that pilot-scale work should be used to estimate entrainment rates rather than the use of equations developed from data obtained when column diameter effects were significant.

Gregory (52) speculated that "it should be possible to establish equilibrium curves relating solids concentration (in the disperse phase) to gas velocity for any given particle size and to use these curves to determine entrainment in the same way as vapour pressure curves may be used to determine the composition of vapour in equilibrium with a multi-component liquid mixture at any temperature".

Recently, Zenz and Weil (53) have presented a means of calculating the rate of entrainment of solids from commercial-size fluidized beds, based on theoretical and empirical approaches, and show good agreement with experimental data obtained from an apparatus simulating flow characteristics in large-scale equipment.

10. TERMINAL VELOCITIES AND SHAPE FACTORS.

Correlations for the free-fall of particles in fluids form the basis of many correlations of fluidization

data, and represent the upper limit of expansion. (ie. $\mathcal{E} = 1$.) It is convenient to consider shape factors at the same time since the main problem in correlating data on terminal velocities is in the definition of a suitable shape correction factor: The same shape factors are also useful in dealing with fluidization. The free-fall drag coefficient for spheres correlated as a function of the Reynolds number is well established, and is aptly reviewed by Lapple and Shepherd (42). This involves a plot of $C_D = 4\ g\ d_p\ (\rho_s - \rho_f)/3\ \rho_f V_t^2$ versus $Re_t = d_p \rho_f V_t / \mu$, and covers a range of values of Re_t from 10^{-3} to 10^6; (it thus covers all flow regimes from the viscous (Stoke's law) to the fully turbulent (Newton's law) region).

For non-spherical particles, the C_D - Re_t curve is usually related to the standard curve for spheres by means of a shape factor. From purely theoretical considerations, it can be shown that for viscous flow:

$$C_D = F\ (A_S / A_P ,\ Re_t) \quad \ldots\ldots\ldots \quad (29)$$

Wadell (54) defined the ratio A_S / A_P as the sphericity (ϕ), and presented curves of C_D versus Re_t for non-spherical particles, with ϕ as parameter. He later approximated ϕ by ϕ, the degree of circularity, equal to the ratio of the circumference of a circle having the

same projected area as the particle and the actual perimeter of the projected area of the particle. The particle diameter in this case is taken as the diameter of the sphere with the same volume as the particle, d_s.

Heywood (55) introduced a volume coefficient defined by the equation $k = \overline{V}_p \,/\, d_n^3$ . . . . (30) where $\overline{V}_p$ = volume of the particle and d_n = diameter of a circle having the same projected area as the particle (A_n). In this case, $C_D = 8\ k\ (\rho_s - \rho_f)\ g\ d_p / \pi \rho_f V_t^2$ where d_p is defined as the mean projected diameter of the particle.

Pettyjohn and Christiansen (56) working with isometric particles found that the sphericity gave satisfactory correlation of their data, and presented equations relating C_D and ϕ for the viscous and turbulent regions, but gave only a graphical correlation for the transition zone. They found that the Heywood factor (k) was not apparently related to C_D as was the sphericity.

Heiss and Coull (57) studied the free-fall of non-isometric particles in the viscous region, and introduced a factor to allow for the orientation of the particles. They presented their results as graphs of K, a shape function, versus $d_s \,/\, d_n$ with sphericity as parameter; K is defined as the ratio of the terminal velocity of the

particle to that of the sphere with the same volume.

Beranek (43) replotted the data of Pettyjohn and Christiansen (56) using the new co-ordinates $Ar = Z_s / \rho_f \nu^2$ and $\Omega = V_t^3 \rho_f / g \nu (\rho_s - \rho_f)$, where Ar is called the Archimedes' criterion and Ω is a criterion of similarity. On this basis he obtained excellent agreement with his own data for crushed particles, and concluded that most crushed particles agree with the data for tetrahedrons.

Becker (59) has recently considered the drag on freely oriented bodies, and proposes the quadratic equation for the drag number (N_K);

$$N_K = 24\, Re_t + C_I\, Re_t^2 \quad \dots\dots\dots\dots (31)$$

where Re_t is based on the diameter of the sphere with the same surface area as the body. The first term in this equation allows for viscous, and the second for inertial, effects. Becker uses the sphericity (ϕ) and also introduces a "form" sphericity (ψ) = surface area of the sphere with the same volume as the particle divided by the projected area of the particle. ($\psi = \pi d_s^2 / A_n$.)

In general, the drag-curve for irregular particles is not exactly similar in shape to that for spheres, and the correlations obtained for regular non-spherical shapes can not be accurately used. Needham and Hill (58) attempted to correlate their own data for coal particles,

with that of many other workers shown in the literature, using Heywood's volume shape factor k. Using the same co-ordinates as Heywood (55), they found that the data for common minerals gave a band fairly close to the standard curve for spheres, but of a somewhat different shape. They called an average correlation of the points the "mineral line", and found that it crossed the standard curve for spheres at about $Re_t = 1.5$. This is in good agreement with the results of Heywood (55) on similar "crushed" particles.

It becomes obvious from the foregoing considerations that the Reynold's number as normally defined cannot be used as a criterion of dynamic similarity for dissimilar shapes. In general, the more irregular the particle, the lower is the Reynold's number at which a given degree of turbulence is developed. This is shown clearly by the data of Pettyjohn and Christiansen (56), where C_D becomes constant for tetrahedrons ($\phi = 0.67$) at $Re_t = 80$, for cubes ($\phi = 0.806$) at $Re_t = 200$, and for spheres at $Re_t = 1000$.

It is also obvious that the subject of shape factors is far from being understood, and some systematic studies of irregular particles are definitely needed. The large number of "effective" particle diameters used in the literature also tend to add confusion to this

branch of the subject.

In the correlations proposed for fluidization, the problem is especially complicated since, in the majority of caes, the data falls in the transition region. Johnson (31), Leva et al. (2) and others, have used the sphericity (ϕ) to allow for shape.

On the other hand, Hancock (37) used the volume coefficient k, and Richardson and Zaki (28), working in the fully turbulent region with regular non-spherical particles also found that the factor k better correlated their data than did the sphericity.

11. SIZE-DISTRIBUTION.

The effects of wide size-distributions have not been extensively studied; in general, work has been confined to studies involving mixtures of two or three closely-sized fractions, and the reciprocal mean diameter now seems to be accepted as the most suitable diameter to be used in characterising such systems. (26,23,60) This is defined as $d_p = 1 / \sum x_m / d_m$ . . . . (32)
where x_m = the weight fraction of average mesh size d_m.

In commercial operations, wide size-distributions are common and it has been found that for macroscopic size ranges, the distribution of ground materials closely follows the skew-probability type of distribution.

This is conveniently plotted on log-probability co-ordinates; (ie. a skew-probability distribution is such that if the size-frequency data is plotted with log d_p on the ordinate, and with the cumulative percent greater than, or less than, the corresponding diameter given on the ordinate plotted (on a frequency scale graduated according to the probability integral) on the abscissa, a straight line is obtained.) The 50 percent point represents the geometric mean particle size, and is used as the diameter of the mixture. The slope of the line through the data defines the size distribution. Due to its simplicity, and ease of extrapolation and interpolation, this method of size representation has been used throughout this work. (See figure 9 .)

The effects of size distribution on fluidization characteristics have only been qualitatively considered. Segregation in fluid-beds has been observed at velocities close to the point of incipient fluidization, and elutriation of the particles proceeds progressively according to size as the velocity is increased. The expansion process is usually smoother in the case of wide size-distributions, but quantitative effects have only been considered very briefly by Lewis and Bowerman (61) and Jacobs and Minet (60). The former workers studied the fluidization of a cracking catalyst in liquid hydrocarbons

in the viscous range only, and explained the difference between their data and that of Lewis et al. (16) as being due to the variation in size-distribution. The latter workers considered the air-fluidization of mixtures of coal and char particles, but confined most of their work to the study of simple mixtures of closely sized fractions.

Zenz (62) reviews the effects of particle size distribution on the fluidization characteristics of gas-solid systems. From the experimental work of Matheson et al. (32) and from the analytical approach of Trawinski (63), Zenz concludes that the optimum size distribution approaches that of a normal skew probability distribution, and that no advantage is obtained by exceeding about an elevenfold variation in size between the smallest and largest particle.

12. POROUS MATERIALS AND BED POROSITY.

In dealing with gas-solid fluidized systems, it is necessary to consider an average value of the voidage or porosity within the bed, assuming that the bed is reasonably homogeneous. This assumption is known to be false, and Bakker and Heertjes (64) have given an excellent account of the variation of porosity in such systems, showing the existence of three distinct regions. The

first of these allows for "entrance" or grid effects. Above this region is a zone of constant porosity extending to a height equivalent to the height of the bed at incipient fluidization. The third region is then a region of decreasing porosity above this level, and signifies the increasing height of the bed with increasing velocity.

With materials of little or no internal porosity, the determination of bed voidage is readily made by water-displacement methods. However, when dealing with porous materials such as coal and coke, it is necessary to define the bed voidage as only that part of the total voids which contributes to gas flow. Some workers (31,21) have ignored this problem completely, but several methods of dealing with such materials have been proposed.

Leva et al. (2) use equation 12, together with pressure drop data for the unexpanded bed to calculate an effective voidage. This calculated value is then compared with the value calculated using the apparent solid density, the bed height and weight, and a correction factor is found for each size of material; this factor is then applied to the data obtained during expansion. The main problem with this method is that it is necessary to estimate a shape factor for the porous

material. Leva presents photo-micrographs of particles for which the shape factor has been found by experiment, and suggests that the shape of porous particles can be found by direct comparison. This can only give an indication of the overall appearance of the particle, and does not make any allowance for the effects of surface cavities and irregularities. The errors involved in such estimations are probably of the same order of magnitude as the correction factor itself, and the method is therefore of doubtful value.

Ergun (65) also used an equation for fixed beds to estimate the true effective voidage in beds of porous particles. Pressure drop measurements are obtained for a series of different bulk densities, and equation 25 is then solved either graphically or by the method of least squares to give an apparent particle density. This density is then used in calculating the bed voidage in the normal manner. The main objection to this method is that it is necessary to do a considerable amount of experimental work if a large number of sizes of particle are to be studied.

Van Heerden et al. (23) in their work with coke and carborundum particles found that both the helium-density and the mercury-density remained essentially constant for

sizes of 75 - 500 microns. They suggested that the pores not accessible to mercury (< 10 μ.) could hardly contribute to the flow of gas through the bed, and therefore used the mercury-density to calculate bed voidage. This assumption seems reasonable, since in the fluidized state, the particles are individually supported in the gas stream, and it is the apparent weight of the particles which must be considered. The apparent density, as measured by mercury-displacement, has therefore been used in this work to define the bed voidage for char particles.

B. EXPERIMENTAL.

1. APPARATUS.

A line diagram of the apparatus is shown in figure 2, and the equipment used is essentially similar to that used by many other investigators. (See plates 1 and 11.)

Laboratory air at about 100 psig. passes through a simple air filter to a Moore Nullmatic pressure-regulation valve, which provides a constant pressure supply of air at about 5 psig. to the fluidizing column. The humidity of the air, measured by a sensitive diaphram-type hygrometer, is controlled by water or steam injection in the humidifier, and the air temperature is measured on a dial-type thermometer. The air flow is measured using an orifice plate and water manometer, and is controlled by a $\frac{3}{4}$ inch globe valve and a $\frac{1}{4}$ inch needle valve in parallel. From the orifice meter, the air passes to the fluidizing column, made from a $2\frac{1}{4}$ inch I.D. transparent Lucite tube, closed at each end with a conical section. The inlet cone is surmounted by a calming section consisting of a length of column packed with glass tubing, and the bed is supported above this on a porous bronze grid, sealed around its edge with varnish and held between two 9 inch diameter Lucite flanges. The static pressure at the base of the column is measured from a pressure tap

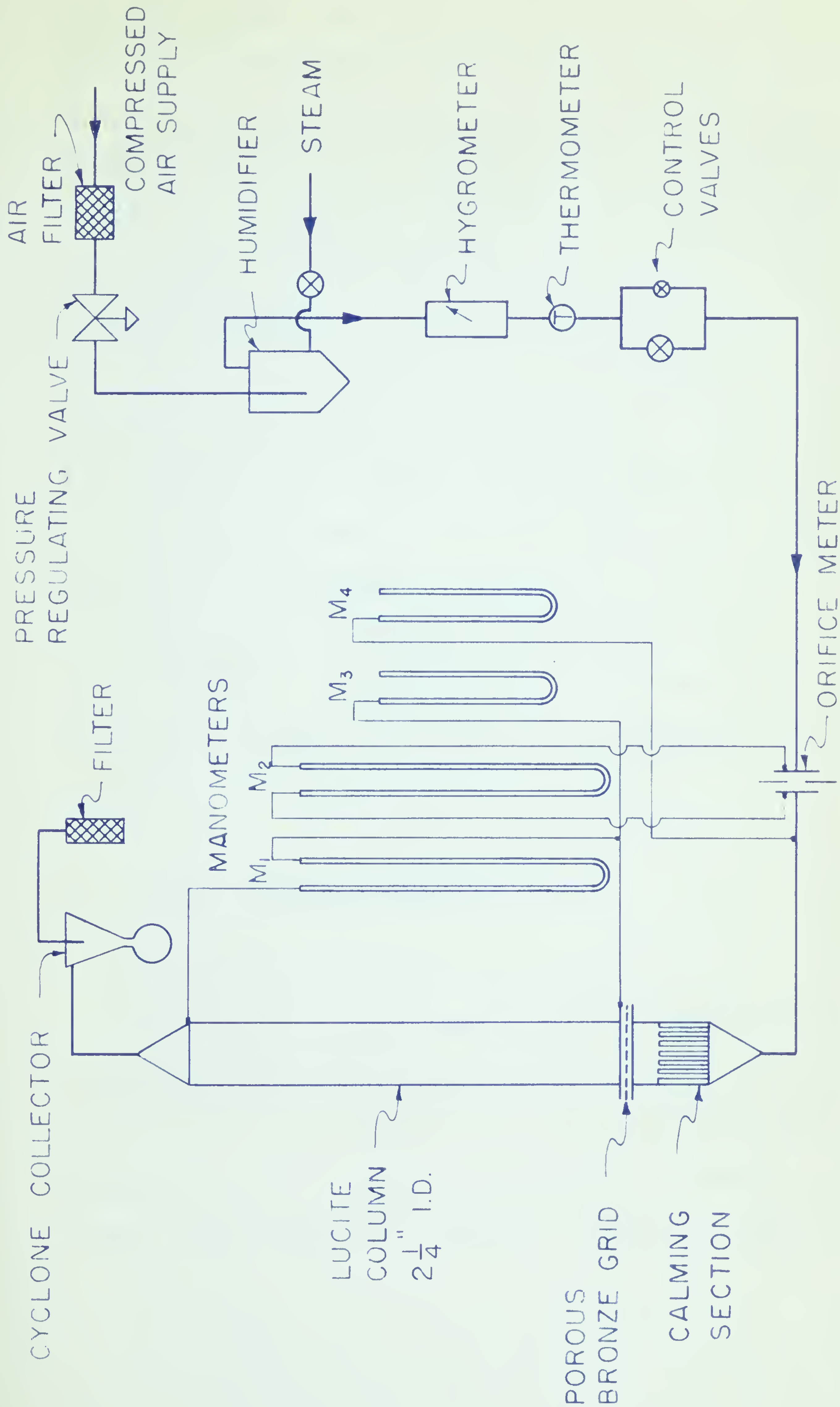

FIG. 2. LINE DIAGRAM OF THE APPARATUS

opening through the flange above the supporting screen, and the pressure drop across the bed is also measured from this tapping to one in the upper section of the column. Both these tappings are packed with glass wool to prevent the loss of fines from the bed into the manometer lines. Above the grid, the column is fitted with a scale graduated in inches, and multiple turns of earthed copper wire help reduce the static-electrical charges built up during the fluidization tests. The air leaving the column passes through a cyclone (made from a standard 500 ml. conical flask) to remove most of the entrained material, and through a simple bag filter, and is then exhausted to the atmosphere. Materials are charged to the column through a standard 1 inch pipe union at the top, and discharge is effected by simply inverting the column.

2. METER CALIBRATIONS.

(a) Orifice Meter.

The orifice meter consists of a standard $1\frac{1}{2}$ in. pipe union with its faces ground flat, preceded by 17 in. of $1\frac{1}{2}$ in. pipe and followed by 12 in. of $1\frac{1}{2}$ in. pipe. The pipe work is mounted vertically, and straightening vanes in the form of a bundle of plastic-tubes are enclosed

PLATE 1. CONTROL PANEL.

PLATE 11. REAR VIEW OF APPARATUS.

in the pipe upstream from the orifice, the length and free area of these 'vanes' being designed according to standard practice. The orifice plates were all constructed from 1/8 in. brass plate, and are held between two rubber gaskets in the union. Orifice diameters of 0.0371, 0.0781, 0.1875, 0.300, and 0.500, were chosen, (referred to as 01,2,3,4, and 5 respectively), and in all cases, the downstream side of the orifice is beveled at 45° so that the actual thickness of the orifice is always less than the smaller of one twentieth of an inch or one eighth of the orifice diameter. The pressure taps are $\frac{1}{4}$ in. brass fittings screwed at right angles into the union fitting, $1\frac{1}{8}$ in. upstream and 1 in. downstream of the orifice plate. These are connected to a four foot water manometer by standard $\frac{1}{4}$ in. copper lines.

Orifice plates 1 and 2 were calibrated using two wet test meters, both rated at 1/3 cu.ft./min. These had been previously calibrated against a meter testing system in the Chemical Engineering laboratories at the University, and carried ±1% accuracy limits. Orifice plates 3,4 and 5 were calibrated using dry gas meters (rated at 5 cu.ft./min. (10B) and 10 cu.ft./min. (25B) respectively). The 25B. meter was factory tested immediately before use, and found to be accurate within 1% up to 10 cu.ft./min.

The 10B meter was checked against the 25B by passing air through them in series, and a correction graph was obtained to bring the readings of the 10B into agreement with those for the 25B over all the flow rates used. The correction factor ranged from + 1% at 2 cu. ft./min. to about -3% at 5 cu.ft./min.

The equation used (66) to obtain the calibration curves shown in figure 3 is based on the equation:

$$Q_s = C_o A_o \frac{Z_s R T_s}{M P_s} \sqrt{\frac{2 g_c M P_2 \Delta h \cdot \rho_w}{12. Z R T_1 (1-D_o^4/D_1^4)}} \quad . (33)$$

where :-

Q_s = cu.ft./sec. flowing at T_s °R and P_s psfa.

A_o = area of the orifice ($ft.^2$).

C_o = orifice discharge coefficient.

Δh = manometer differential pressure (in. of water.)

P_2 = downstream pressure (psfa.).

P_s = reference pressure (taken as 2116 psfa.).

M = molecular weight of the gas.

Z_s = compressibility factor at reference conditions.

Z = compressibility factor.

T_s = reference temperature (taken as 520 °R.).

T_1 = upstream temperature. (°R.).

D_o = orifice diameter (ft.).

D_1 = pipe diameter (ft.).

Simplifying this equation, and substituting

$Z_S = 1$, $(1 - D_o^4 / D_1^4) = 1$, $R = 1545$ ft.lb/mole/°R

$Z = 1$, $\rho_w = 62.4$ lb/ft^3. and taking M as 28.97

for dry air,

equation 33 reduces to :-

$$Q_S = 32.8 \ C_o \ A_o . \sqrt{\frac{\Delta h \ P_2}{T_1}} \ . \ . \ . \ . \ . \ . \ . \ . \ . \ . \ . \ . \ (34)$$

where Q_S = cu.ft./sec. measured at 60°F and 76 cm.Hg. pressure.

The procedure for calibrating the orifices was to connect one or more of the gas meters in place of the fluidization tube, record the atmospheric pressure, and then for a set flow of air to measure the differential pressure across the orifice plate (centimetres of water), the upstream temperature (°F), the downstream static pressure (millimetres of mercury.), and the time in seconds for the flow of a certain volume of air through the meters. This was repeated for different flow rates, and graphs of Q_S versus $\Delta h \ P_2 / T_1$ were plotted for each orifice. The constant C_o as given by equation 34 was also calculated from the slopes of the lines obtained, and these values, are shown on the graphs. The equations of these graphs are given in appendix A.

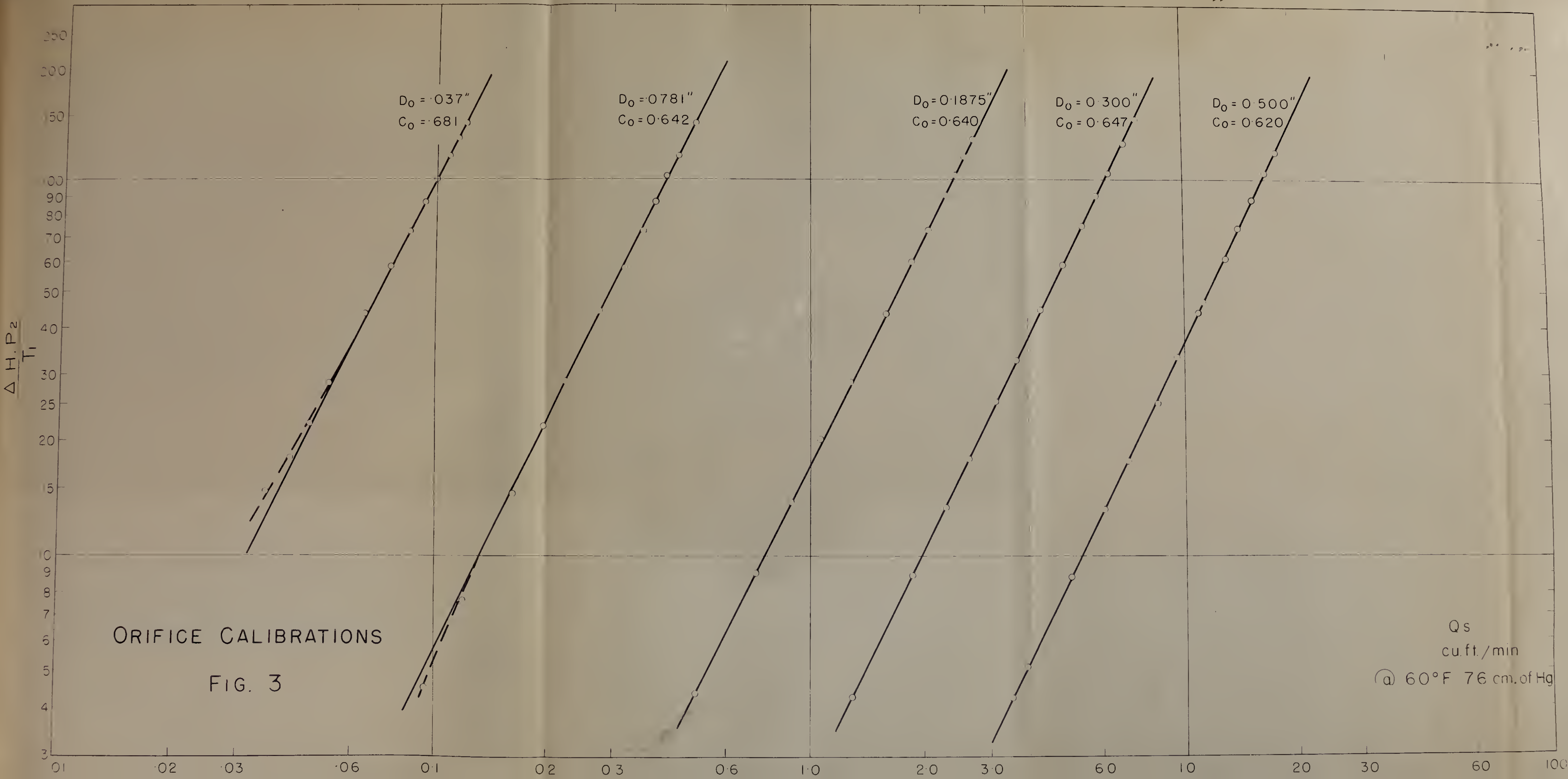
D_o = ·037"
C_o = ·681
D_o = ·0781"
C_o = 0·642
D_o = 0·1875"
C_o = 0·640
D_o = 0·300"
C_o = 0·647
D_o = 0·500"
C_o = 0·620
$\frac{\Delta H . P_2}{T_1}$
Qs
cu.ft./min
@ 60°F 76 cm. of Hg
ORIFICE CALIBRATIONS
FIG. 3

In all further work, flow rates were obtained from figure 3. The variation of air density with moisture content was calculated, and at a relative humidity of 100% was found to be of the order of 1%. Since the relative humidity of the air used varied between 30% and 70%, it was felt that this variation could be neglected within the accuracy of other measurements.

The deviations at low flow rates obtained for orifices 1 and 2 indicate a variation in the value of the constants C_o. All other data agree well with equation 34.

(b) Other calibrations.

The hygrometer was checked according to the manufacturers specifications against a sling psychrometer, and found to be within the quoted limits of accuracy ($\pm 1\frac{1}{2}\%$).

The dial-type thermometer used was also checked against a mercury-bulb thermometer, and appeared to be reading about two degrees low in the range of 70° - 100°F. Since the difference noted depended on the immersion length etc., and since all temperatures are converted to the absolute scale, this difference was neglected.

The fluidizing column diameter was measured with internal calipers, and an average internal diameter of 2.236 in. was obtained from 6 readings. This represents

a cross-sectional area of 0.0272 ft^2. Similarly, the internal diameter of the 2 in. column used in the fixed-bed experiments was measured as 2.012 in., representing a cross-sectional area of 0.0221 ft^2.

3. PREPARATION OF MATERIALS.

The glass beads used were supplied by Potters Brothers, Inc., Carlstadt, New Jersey, U.S.A. Samples were studied, and quantities of roughly sized beads were ordered according to the quantities of each size required, about 50 lb. of beads being obtained. These beads were then closely sized using successive Tyler standard sieves, batches being obtained for all sizes from 14/16 mesh down to -325 mesh Tyler.

The char particles were obtained from the low temperature carbonisation of Edmonton coal in a fluidized bed. The proximate analysis and size analysis of a typical sample of the char (as produced) are shown below in Table 1.

TABLE 1.

SIZE.		PROXIMATE ANALYSIS.	
Tyler mesh size.	%. by weight retained.		%. by wt.
+10	0.6	Moisture Content	0.4
10/14	7.3		

Table 1. continued.

SIZE.		PROXIMATE ANALYSIS	
Tyler mesh size.	%. by weight retained		%. by wt.
14/20	18.3	Volatile Matter	9.6
20/28	22.4		
28/35	16.0	Ash	14.0
35/48	10.8		
48/65	8.1	Fixed Carbon	76.0
65/100	6.2		
100/150	3.8		100.0
150/200	3.1		
-200	3.4		
	100.0		

Closely sized fractions of the char were prepared using successive Tyler standard sieves. For the smaller sizes, further grinding of some of the coarser fractions in a ball mill was necessary to obtain the quantities required.

Samples of Canmore coal were also prepared for fixed bed and terminal velocity experiments.

All the sized fractions were stored in sealed containers. Plates 111 and IV show photomicrographs of various samples of char and glass beads.

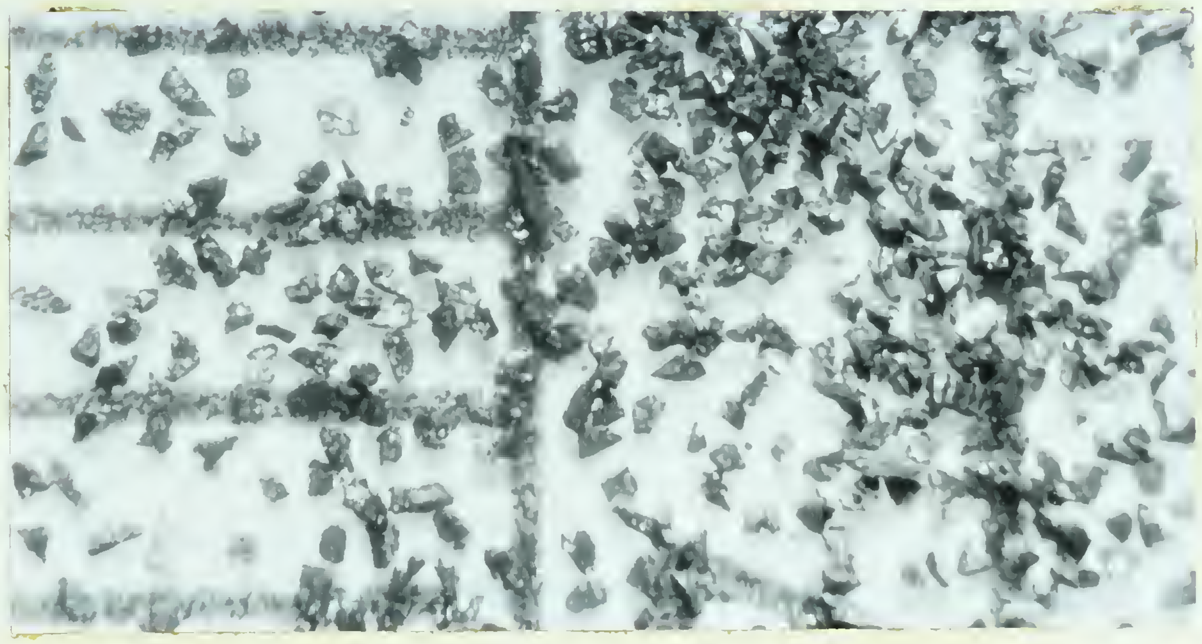

100/115 mesh.

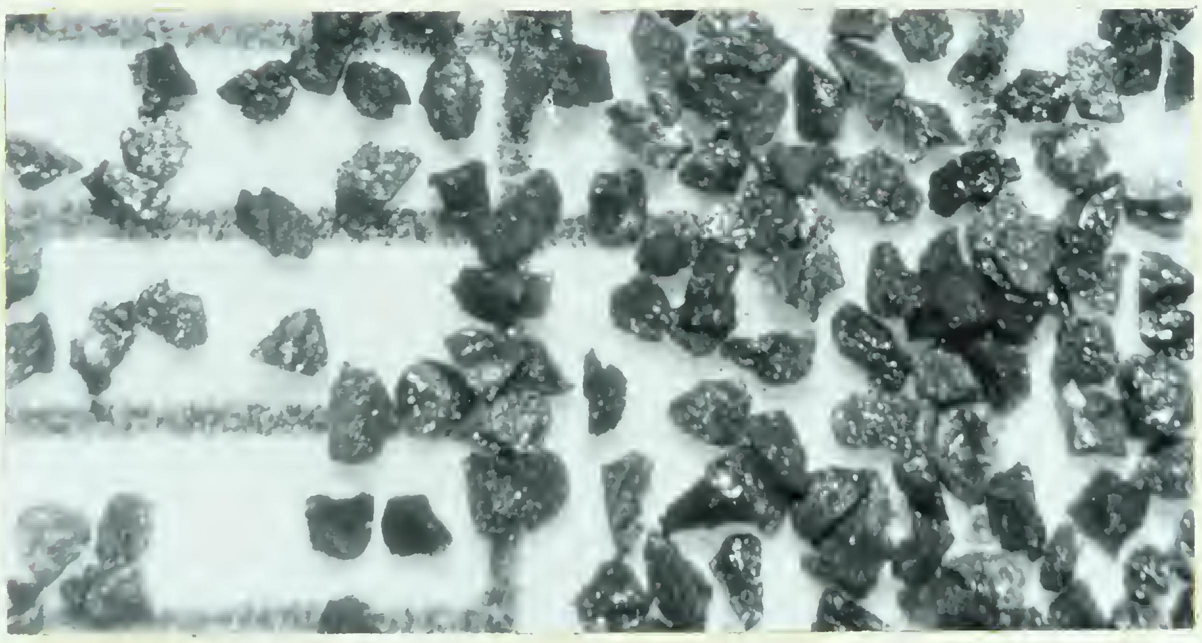

48/60 mesh.

24/28 mesh.

PLATE 111. PHOTOMICROGRAPHS OF CHAR PARTICLES.

(1 scale division = 1 millimetre.)

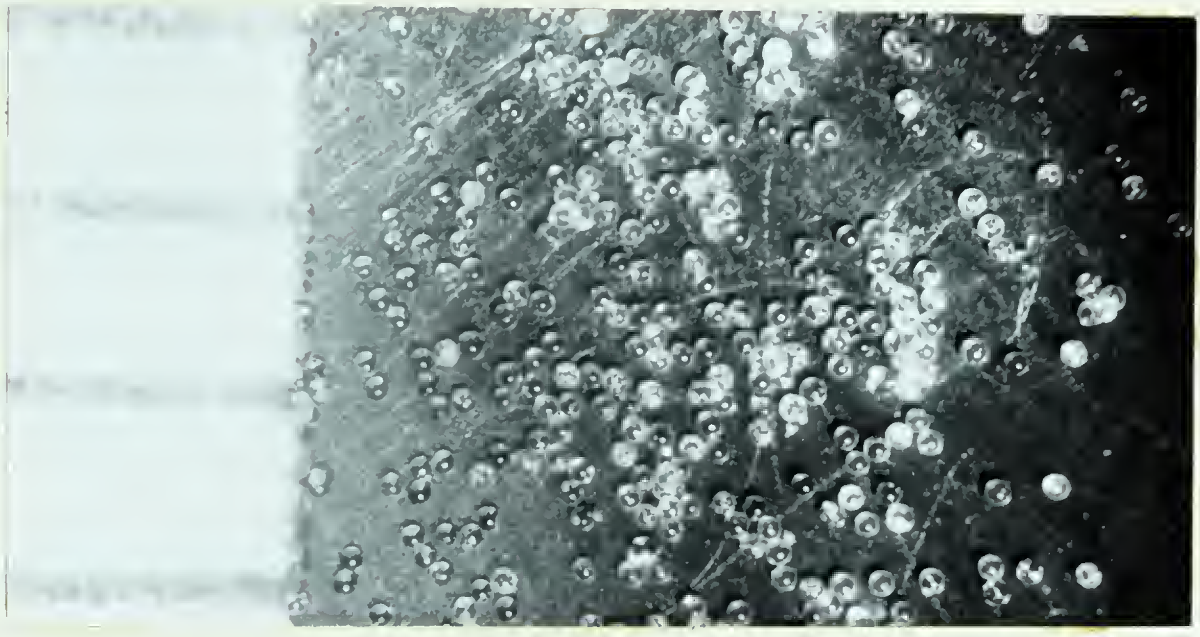

100/115 mesh.

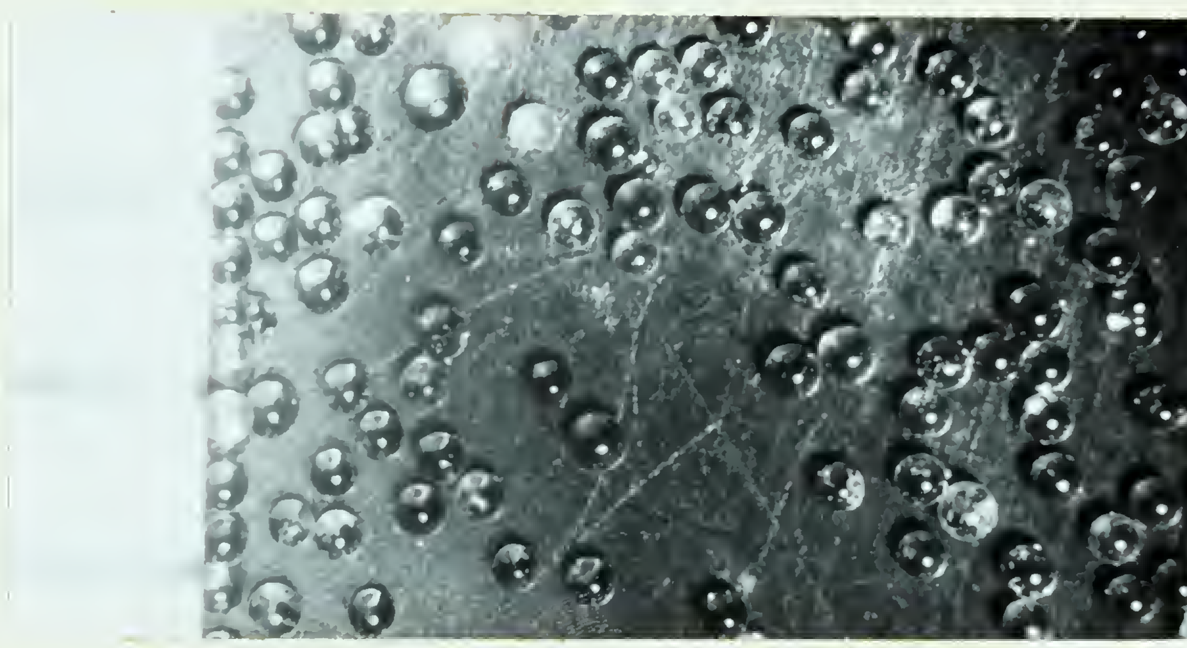

48/60 mesh.

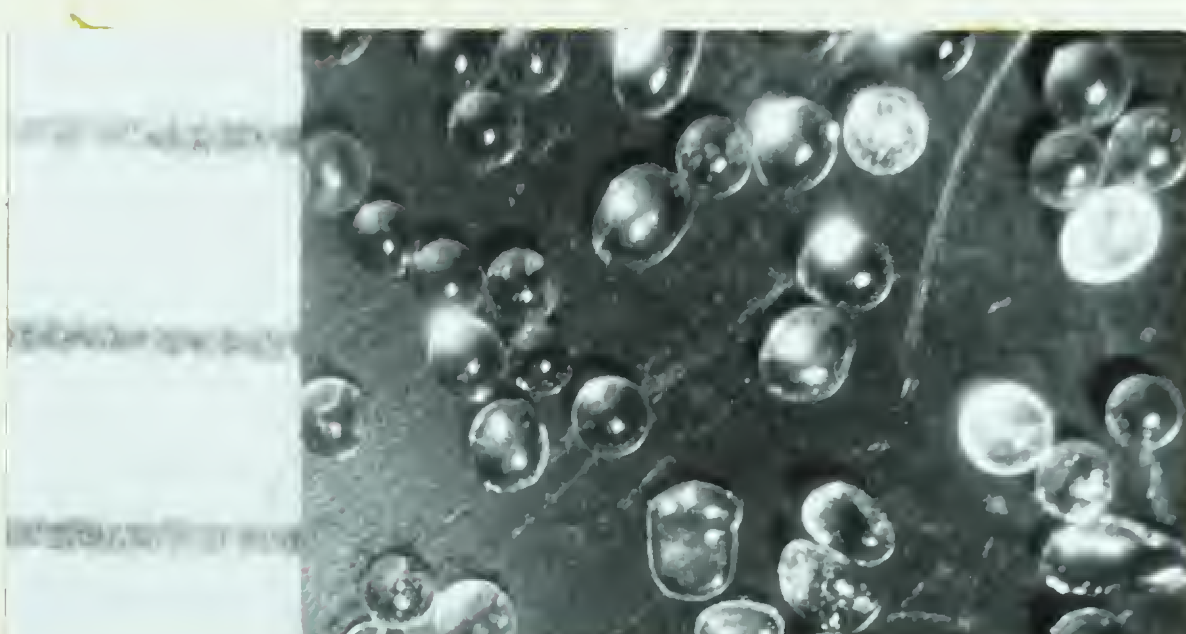

35/42 mesh.

PLATE IV. PHOTOMICROGRAPHS OF GLASS BEADS.

(1 scale division ≏ 1 millimetre.)

4. PROPERTIES OF THE MATERIALS.

(a) Particle diameter.

The average sieve diameter (d_m) was obtained in all cases as the arithmetic mean of the adjacent sieve openings. (based on the Tyler series.)

In the case of the glass beads, a microscopic determination was also carried out, and the average diameter (d_A) was obtained by taking the mean of 50 or more particle measurements.

(b) The number of particles/gram of material.

A large number of particles were counted and weighed on an accurate analytical balance. The number counted depended on the size of the particle (increased as the particle diameter decreased) and several determinations were made for each size. These determinations were a preliminary step in the determination of the spherical diameter (d_s) and the equivalent diameter (d_e).

(c) Particle density.

The density of the glass beads was found by the standard water-displacement method using a 25 ml. specific gravity bottle and an accurate analytical balance.

Due to the internal porosity of the coal and char particles, the conventional methods of density determination were found to be unsuitable when using such

liquids as water, toluene or glycerin. It was therefore decided that the mercury-density should be used, since it seemed most suited to the present study (cf. p. 46). A modified mercury-displacement method was therefore adopted, similar to that used by Sherlock (67).

(d) Determination of bed porosity at the point of fluidization.

The bed porosity was plotted against the gas velocity as the velocity was being decreased, and from the break point in this graph, the critical bed porosity was determined.

(e) Determination of terminal velocities.

A sample of the particles to be tested was charged to an elutriating column, and the air velocity was increased slowly as elutriation progressed. Graphs of the percentage (by weight) removed at a given velocity versus the superficial air velocity were plotted in each case, and the terminal velocity was taken as the velocity required to remove 50% of the particles. For very small particles (< 200mesh) a Roller particle size analyser was used. For medium size particles (200m-28m) the fluidizing column was adopted, and for particles greater than 28 mesh, a long glass tube (2.18 cm dia. 80 in. long.) was used. (due to the high flow rates

required). The data obtained in the small tube were corrected to the same conditions used in the other tests. Wall effects were found to be negligible and all tests were carried out in the turbulent range of flow so that velocity profiles were approximately constant across the tube.

(f) Shape factors.

Direct determinations of shape factors were not attempted. The number of particles per gram was used to define certain shape effects, and experiments on the flow through packed beds of the particles also gave an indirect method of shape-factor approximation. (See Appendix B.)

(g) Air density.

This was calculated assuming the air to be dry, and that the ideal gas law was valid. Errors introduced in so doing were negligible.

5. EXPERIMENTAL PROCEDURE.

The procedure when dealing with closely-sized batches was relatively simple, and will be considered first.

After checking the apparatus, a weighed batch of particles was charged to the fluidization tube, the

correct orifice plate to cover the lowest range of air rates anticipated was put in position, and the apparatus was closed up ready for the test. The air rate was then increased until the bed was well fluidized, after which step-increases in the air rate were used, and readings were taken at each 'step' when conditions were observed to be steady. A set of readings consisted of :-

1. Pressure differential across the orifice plate (cm. of water).

2. Pressure differential across the fluidized bed (cm. of water).

3. The height of the bed. (in.)

4. Temperature upstream of the orifice (°F).

5. Static pressure downstream of the orifice (mm. of mercury).

6. Static pressure at the bottom of the bed (mm. of mercury).

7. Relative humidity (%.).

8. Notes on the appearance of the bed.

These readings were taken after each change in air flow with the exception of temperature and relative humidity which were taken every two or three readings. The batch weight, particle size and type, orifice number, atmospheric pressure, date and test number were also listed for each complete run.

In a typical run, readings were taken with increasing

flow rate until the operation became too violent to allow bed height readings to be made. The orifice plate was changed during each run, to allow sufficient increases in the flow rate. Readings were also taken as the velocity was decreased, and some readings were usually repeated as a check. With decreasing velocity, readings were taken down to, and below the point of fluidization, and the point at which the bed settled was carefully noted. Extreme caution was exercised in this region since a slight vibration would cause serious error. Each settling reading was repeated two or more times, and readings were discarded if any vibration effects were noticed.

After fluidization the bed action became increasingly violent with increasing flow rate, and readings of the bed height and pressure drop were determined by eye, taking the average of the maximum and minimum values recorded. A small correction factor was also applied to the bed height readings to allow for the positioning of the graduations on the column. Readings were terminated when the upper boundary of the bed ceased to have any definite significance.

The relative humidity of the air was only controlled in tests using glass beads, and was usually maintained in the order of 60 - 70%. Static charges were not important

in the case of char, and the relative humidity of the air used in these tests varied between 20 - 40%.

With wider size distributions, the procedure was as follows. The proportions of the individual closely-sized fractions required were determined from figure 9, weighed out on a gravimetric balance, and thoroughly mixed together in a double-cone mixer, previously built for this purpose. Care was taken during the handling of the mixture to prevent segregation, and the material was charged to the column in small batches to minimise segregation on pouring. The air rate was then increased until the bed was completely fluidized, and readings were taken as the velocity was decreased, allowing time for complete equilibrium to be established at each step. With these wider size distributions, segregation took place as the velocity was decreased, and very small step-changes were used to allow the process to continue as smoothly as possible. These readings were repeated several times, and then the velocity was slowly increased and further readings were taken. When elutriation started (ie. particles were observed in the cyclone.) readings were terminated, and the air-rate was increased to give the desired elutriation velocity. The test was continued until virtually no further elutriation of particles could be detected (usually after 3-4 hrs.) and the

particles removed from the bed were then carefully weighed, and sized on Tyler sieves. The unelutriated part of the bed was further tested as described under the procedure for single sizes, and it was finally removed from the column, weighed and sized on Tyler sieves. By this method, the composition of the original charge could be checked and any losses detected. These experiments were repeated using different elutriation velocities, and complete tests were carried out on 5,10,25 and 100 fold size distributions for both char and glass beads. All other details of these runs were essentially the same as in the tests on uniformly sized particles.

C. RESULTS.

The experimental results, together with examples of calculations based directly on them, are tabulated in Appendix C.

The important properties of the beads and char are shown in figures 4 - 8 (inclusive) and in tables 2 and 3. Some data for Canmore coal is also included for comparison.

The various size-distributions used in the experiments are shown in figure 9 on log-probability co-ordinates. The results of these experiments for glass beads are shown in figures 10 - 19 (incl.), and for char in figures 20 - 27 (incl.). These graphs show the variation in bed porosity and pressure drop with superficial velocity for each run, and also show the changes in the "average particle size" as the elutriation velocity is increased.

Figure 28 shows the ε-V characteristic for 35/42 mesh glass beads. (designated: 35/42-1.) Due to its irregular form, further tests were carried out to study the effect of particle diameter on the shape of the ε-V curves. The results of these tests are shown in figures 29 and 30 for beads and char respectively. The pressure drop characteristics for the same tests are shown in figure 31.

Other properties and results of all the fluidization tests are shown in tables 4 - 7 (incl.) and some typical flow conditions obtained in the fluidized bed are shown in plates V and Vl. The zones of operation indicated in figures 29 and 30 are based on visual observations of the action within the fluidized bed.

TABLE 2.

Particle Diameters in microns.

BEADS.

Tyler mesh size	Mean sieve dia. (d_m)	Equivalent dia. (d_e)	Spherical dia. (d_s)	Microscopic dia. (d_A)
10/12	1524			
16/20	912	930	925	936
24/28	645	650	654	645
35/42	384	410	389	425
48/60	271	276	275	279
65/80	192	198	195	202
100/115	136	140	138	144
170/200	81	83.5	82	84

$d_s = 1.012\ d_m.$

CHAR.

Tyler mesh size	Mean sieve dia. (d_m)	Equivalent dia. (d_e)	Spherical dia. (d_s)
10/12	1524	1775	1584
16/20	912	1020	947
24/28	645	725	670
35/42	384	430	399
48/60	271	310	282
65/80	192	220	199
100/115	136	156	141
170/200	81	93	84

$d_s = 1.04.d_m.$

TABLE 3.

Particle densities. (gm/cc.). (ρ_s).

TYLER MESH SIZE.	CHAR.	BEADS.
10/12	1.075	-
14/16	1.075	2.520
16/20	1.080	2.555
20/24	1.075	2.515
24/28	1.075	2.545
28/32	-	2.525
32/35	1.080	2.470
35/42	1.085	2.465
42/48	-	2.550
48/60	1.085	2.550
60/65	-	2.500
65/80	1.085	2.520
80/100	-	2.505
100/115	1.085	2.470

Table 3. continued.

TYLER MESH SIZE.	CHAR.	BEADS.
115/150	1.095	-
150/170	-	2.430
170/200	1.100	2.400
270/325	-	2.333
-200	1.100	2.030

TABLE 4.

Results of Fluidization tests: Glass beads, mixed sizes.

Run N°	Distribution	Ave.dia. $(d_m)(\mu)$	Ave.density (ρ_s)(g /cc)	$\varepsilon_{v\to 0}$	ρ_s/μ (hr.ft^{-2})
1	48/60-1	271	2.55	0.410	1.62
4	48/60-5	271	2.54	0.392	1.63
4c′	†E.V.=287	295	2.53	0.396	1.625
4c″	E.V.=360	320	2.53	0.402	1.62
7	48/60-10	271	2.52	(0.383)*	1.66
7a′	E.V = 210	295	2.52	(0.384)	1.67
7b′	E.V =370	360	2.51	0.398*	1.625
7c′	E.V =410	385	2.48	0.400	1.630
8	48/60-25	271	2.52	(0.381)	1.625
8a′	E.V =250	320	2.53	(0.386)	1.61
8b′	E.V =260	320	2.53	(0.386)	1.60
8a″	E.V.=350	365	2.52	0.400*	1,60
8b″	E.V =425	405	2.50	0.384	1.62
9	48/60-100	271	2.50	(0.350)*	1.63
9a′	E.V = 158	310	2.52	(0.370)	1.62
9a″	E.V = 262	370	2.52	0.380	1.625
9a‴	E.V = 382	450	2.53	0.383	1.61
9b′	E.V = 395	450	2.53	0.383	1.61

( ) variable due to segregation effects.

* humidity too high in test.

† E.V. = elutriation velocity. (ft./min.)

Table 4. continued.

CRITICAL CONDITIONS.

Run N^{o}	ε_o (seg)	ε_o (obs)	ε_o (graph)	V_o (seg)	V_o (obs)	V_o (graph)
1	-	0.410	0.410	-	14.0	14.0
4	-	0.400	0.399	-	12.0	11.8
4c′	-	0.405	0.405	-	17.5	16.8
4c″	-	0.405	0.405	-	20.0	19.2
7	0.419	(0.400)	(0.397)	18.0	(11.0)	(9.9)
7a′	0.400	(0.391)	(0.387)	17.5	(16.0)	(14.5)
7b′	-	0.408*	0.403*	-	26.0*	24.7*
7c′	-	0.400	0.399	-	31.0	29.5
8	0.452	(0.387)	(0.390)	20.0	(7.5)	(8.6)
8a′	0.395	(0.391)	(0.395)	18.0	(16.0)	(18.0)
8b′	0.395	(0.391)	(0.399)	18.0	(16.5)	(19.0)
8a″	-	0.402	0.400	-	25.0	24.0
8b″	-	0.385*	0.388*	-	28.0*	29.0*
9	0.453	-	-	23.0	-	-
9a′	0.404	-	(0.390)	20.0	-	(16.0)
9a″	-	0.390	0.405	-	23.0	27.0
9a‴	-	0.385	0.409	-	33.0	40.0
9b′	-	0.385	0.399	-	33.0	37.0

TABLE 5.

Results of Fluidization tests: Char, mixed sizes.

Run N°	Distribution	Ave.dia. (d_m)(μ)	Ave.density (ρ_s)(g /cc)	$\varepsilon_{V\to 0}$	ρ_f/μ. (hr.ft.$^{-2}$)
2	48/60-1	271	1.086	0.510	1.61
3	48/60-5	271	1.086	0.498	1.61
3b′	E.V.=150	300	1.085	0.484	1.60
3c′	E.V.=222	360	1.085	0.460	1.60
10	48/60-10	271	1.085	0.495	1.64
11	48/60-25	271	1.085	0.498	1.64
11a′	E.V.=116	300	1.085	0.484	1.63
12	48/60-100	271	1.080	0.490	1.66
12a′	E.V.=117	350	1.085	0.485	1.63

CRITICAL CONDITIONS.

Run N°	ε_0 (seg)	ε_0 (obs)	ε_0 (graph)	V_0 (seg)	V_0 (obs)	V_0 (graph)
2	-	0.519	0.517	-	9.5	9.0
3	-	0.510	0.508	-	8.2	7.5
3b′	-	0.490	0.490	-	10.2	10.0
3c′	-	0.462	0.461	-	15.4	14.4
10	0.516	(0.505)	(0.506)	9.6	(6.9)	(7.1)
11	0.565	-	-	17.0	-	-
11a′	0.530	(0.493)	-	16.2	(8.5)	-
12	0.592	-	-	23.0	-	-
12a′	0.539	-	-	23.0	-	-

TABLE 6.

Results of Fluidization tests: Glass beads, single sizes.

Run N°	Mesh size	ε_o (obs.)	ε_o (graph)	ε_c	$\varepsilon_{v\to o}$
22	16/20	0,408	0.410	0.421	0.400
21	24/28	0.400	0.402	0.415	0.395
6	35/42	0.396	0.396	0.408	0.392
1	48/60	0.410	0.410	0.430	0.410
20	65/80	0.404	0.403	0.414	0.403
19	100/115	0.409	0.409	0.416	0.406
18	170/200	0.432	0.432	0.437	0.424

Run N°	V_o (obs.)	V_o (graph)	V_c (ft/min.)	ρ_f / μ (hr.ft^{-2})
22	106	105	114	1.65
21	61.0	64.0	70.0	1.65
6	29.5	29.0	34.0	1.65
1	14.0	14.0	17.5	1.62
20	6.80	6.70	8.20	1.65
19	3.65	3.60	4.55	1.67
18	1.60	1.65	2.20	1.65

TABLE 7.

Results of Fluidization tests: Char, single sizes.

Run N°	Mesh size.	ε_o (obs.)	ε_o (graph)	ε_c	$\varepsilon_{V\to o}$
23	10/12	0.502	0.520	0.538	0.488
17	16/20	0.518	0.520	0.525	0.504
16	24/28	0.509	0.512	0.525	0.495
5	35/42	0.505	0.505	0.521	0.499
2	48/60	0.519	0.519	0.530	0.510
13	65/80	0.517	0.517	0.524	0.509
15	100/115	0.533	0.533	0.540	0.522
14	170/200	0.554	-	0.574	-

Run N°	V_o (obs.)	V_o (graph)	V_c	ρ_f/μ (hr.ft^{-2})
23	108	118	124	1.63
17	62	65	67	1.65
16	40	41	44	1.62
5	15	15	19.5	1.605
2	9.5	9.0	11.0	1.61
13	4.5	4.5	5.35	1.62
15	2.5	2.6	3.6	1.635
14	0.8	-	1.8	1.62

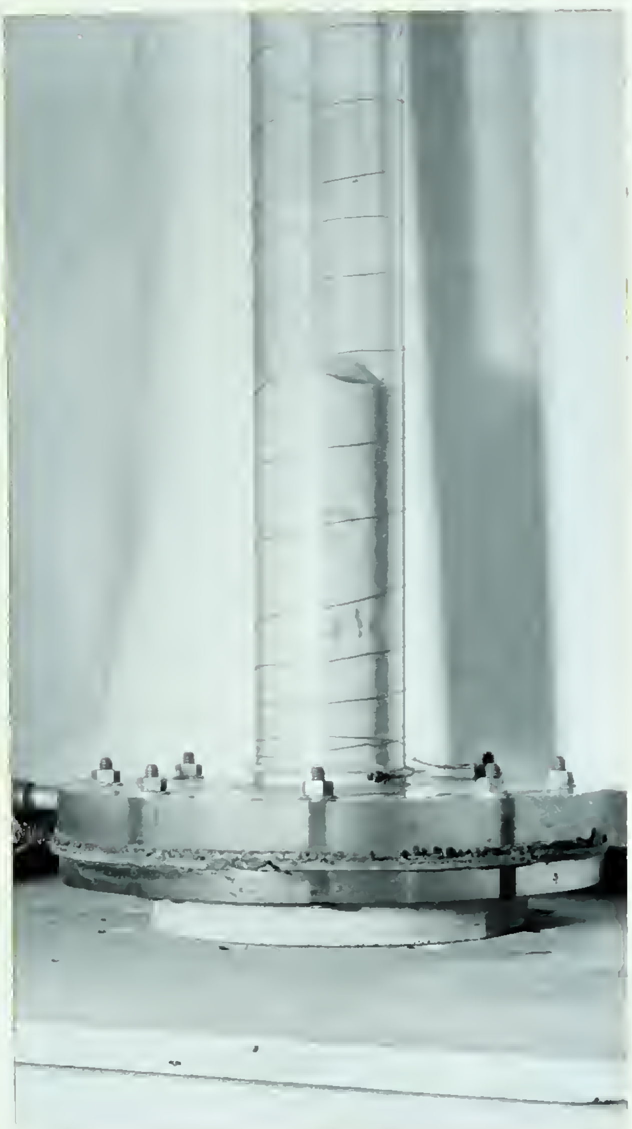

1.

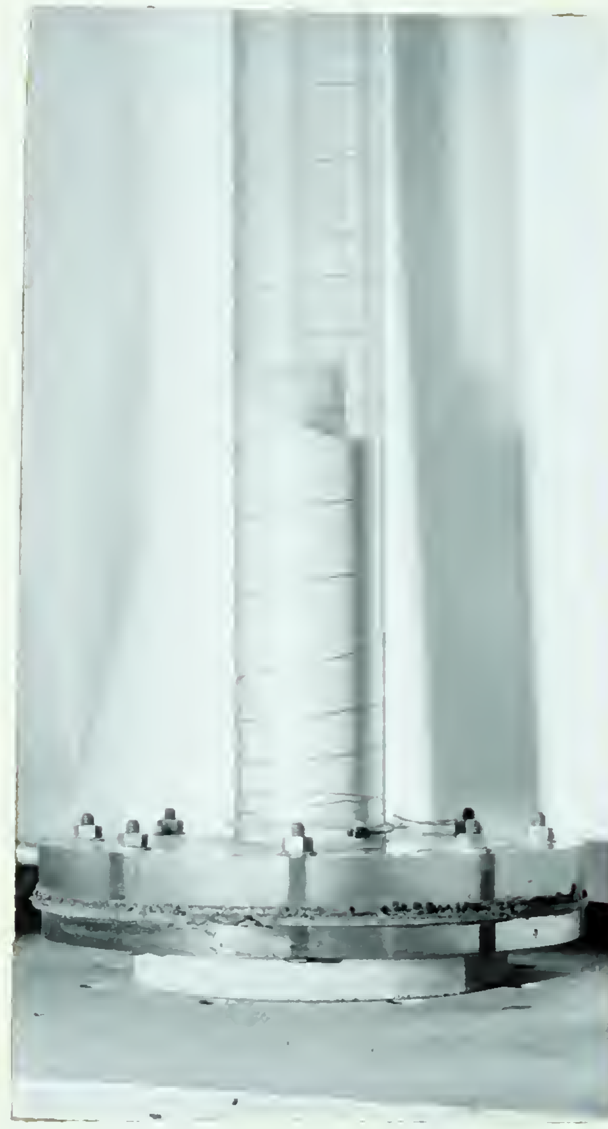

2.

PLATE V. BUBBLING ACTION IN BEDS OF GLASS BEADS FLUIDIZED WITH AIR.

1. Bubbles rising through the bed.

2. Bubbles breaking at the surface of the bed.

(48/60-1 w=600gm.)

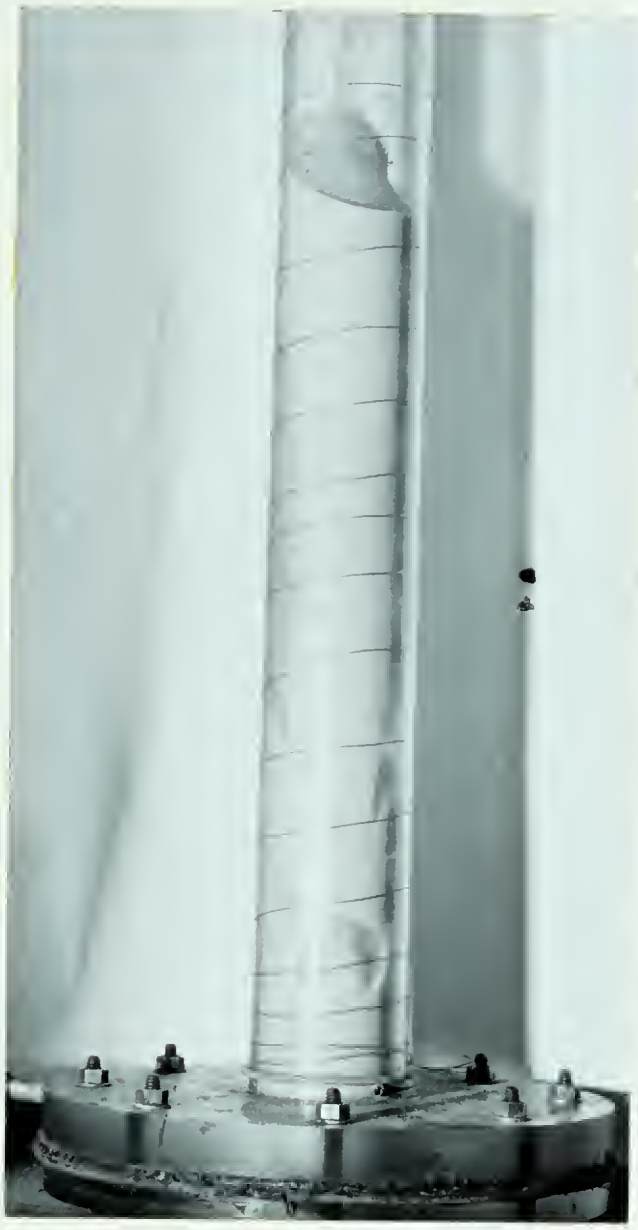

1.

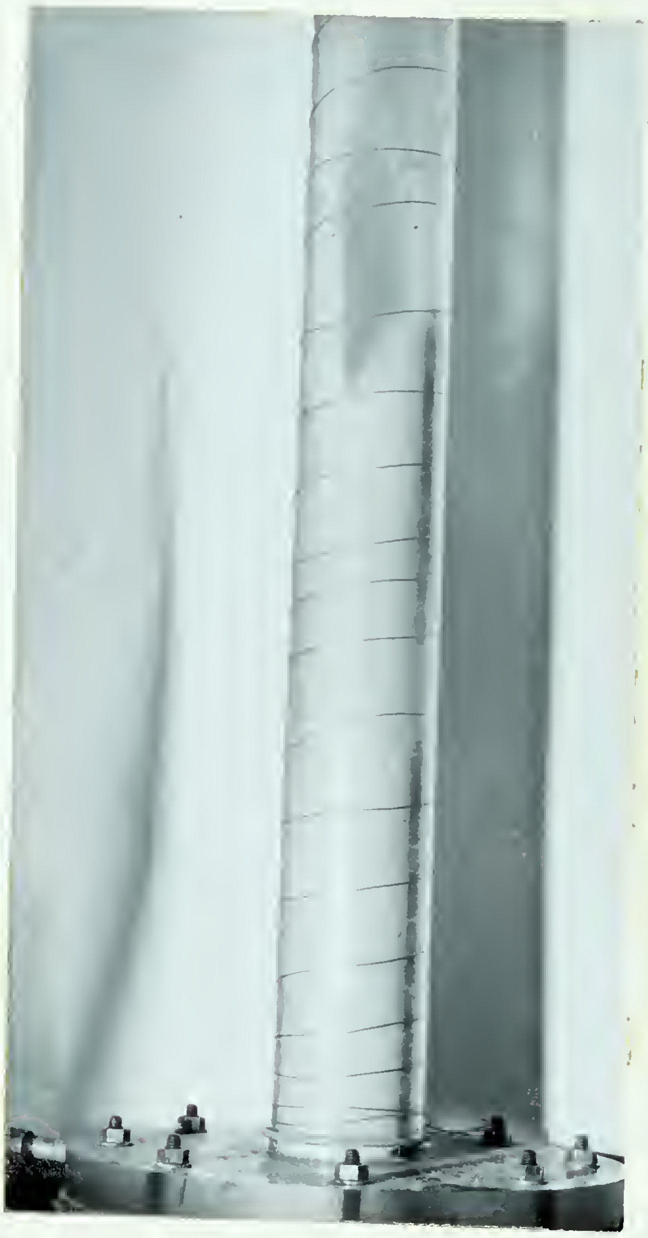

2.

PLATE V1. SLUGGING ACTION IN BEDS OF GLASS BEADS FLUIDIZED WITH AIR.

1. Slugs forming in the bed.

2. Slugs breaking at the surface of the bed.

(48/60-1 w = 600gm.)

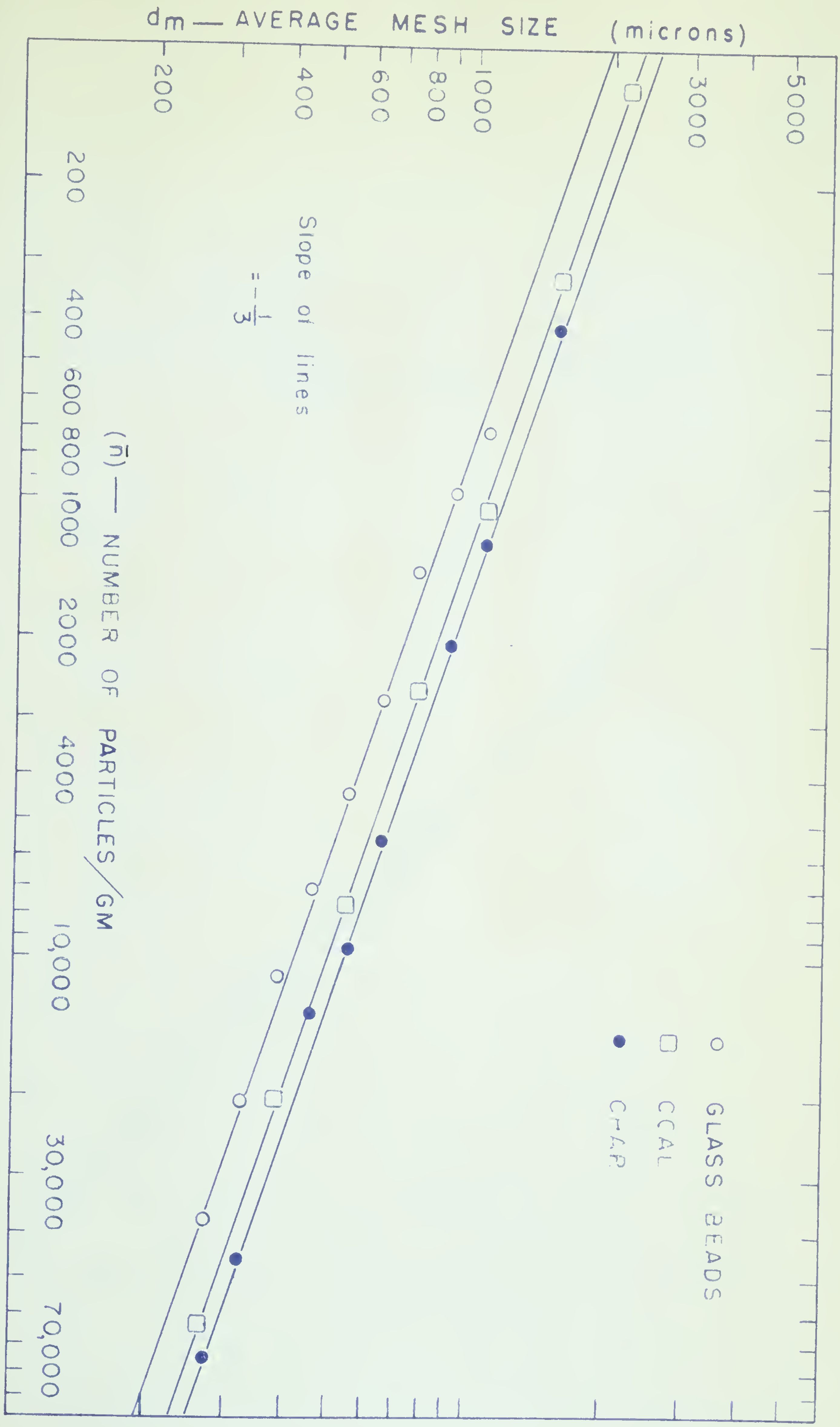
dm — AVERAGE MESH SIZE (microns)
200
400
600
800
1000
3000
5000
Slope of lines
$= -\frac{1}{3}$
GLASS BEADS
CCAL
($\bar{n}$) — NUMBER OF PARTICLES/GM
200
400
600
800
1000
2000
4000
10,000
30,000
70,000

FIG. 4

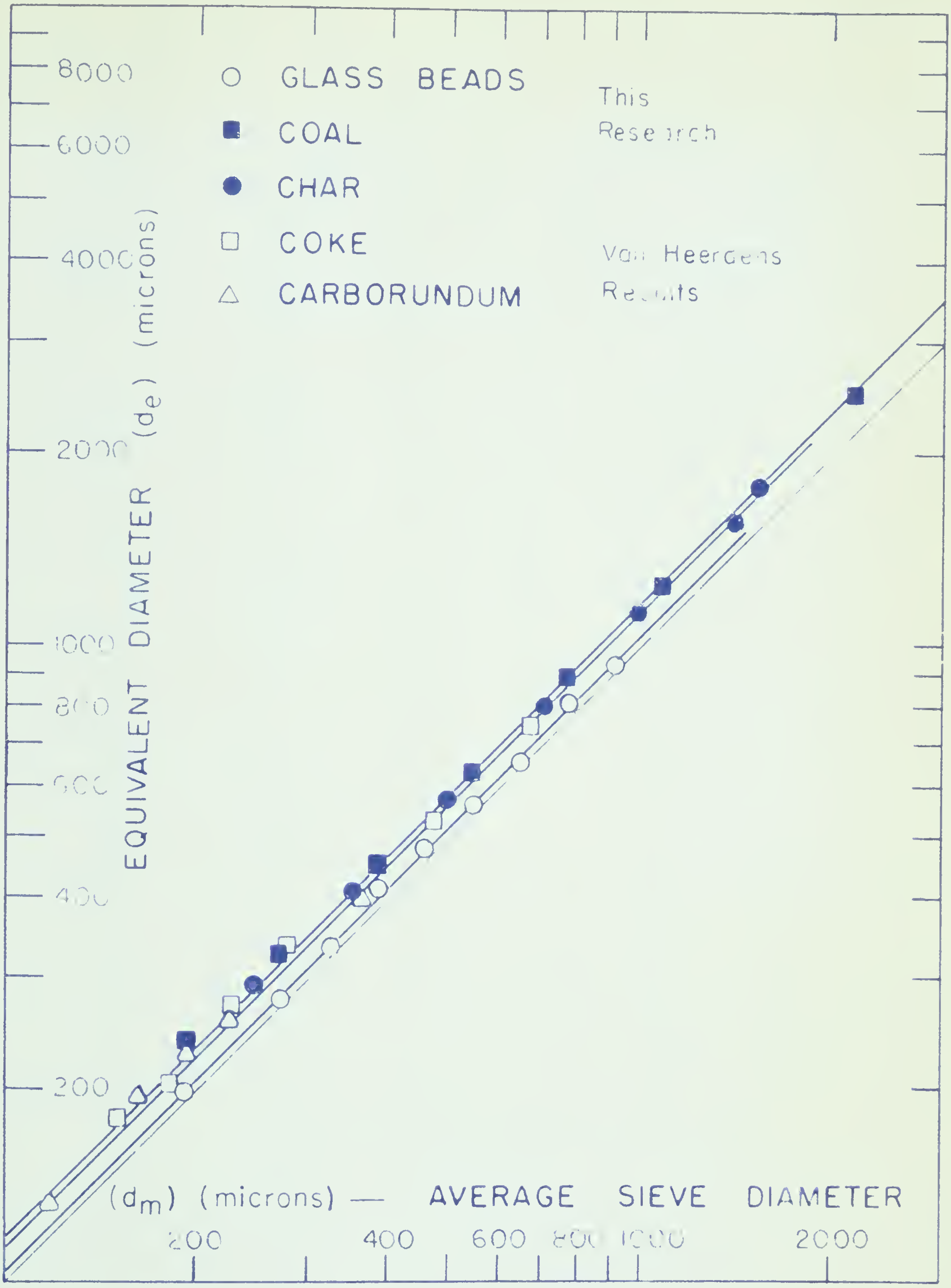
GLASS BEADS
COAL
CHAR
COKE
CARBORUNDUM
This Research
Van Heerdens Results
EQUIVALENT DIAMETER (d_e) (microns)
8000
6000
4000
2000
1000
800
600
400
200
(d_m) (microns) — AVERAGE SIEVE DIAMETER
200
400
600
800
1000
2000

FIG. 5

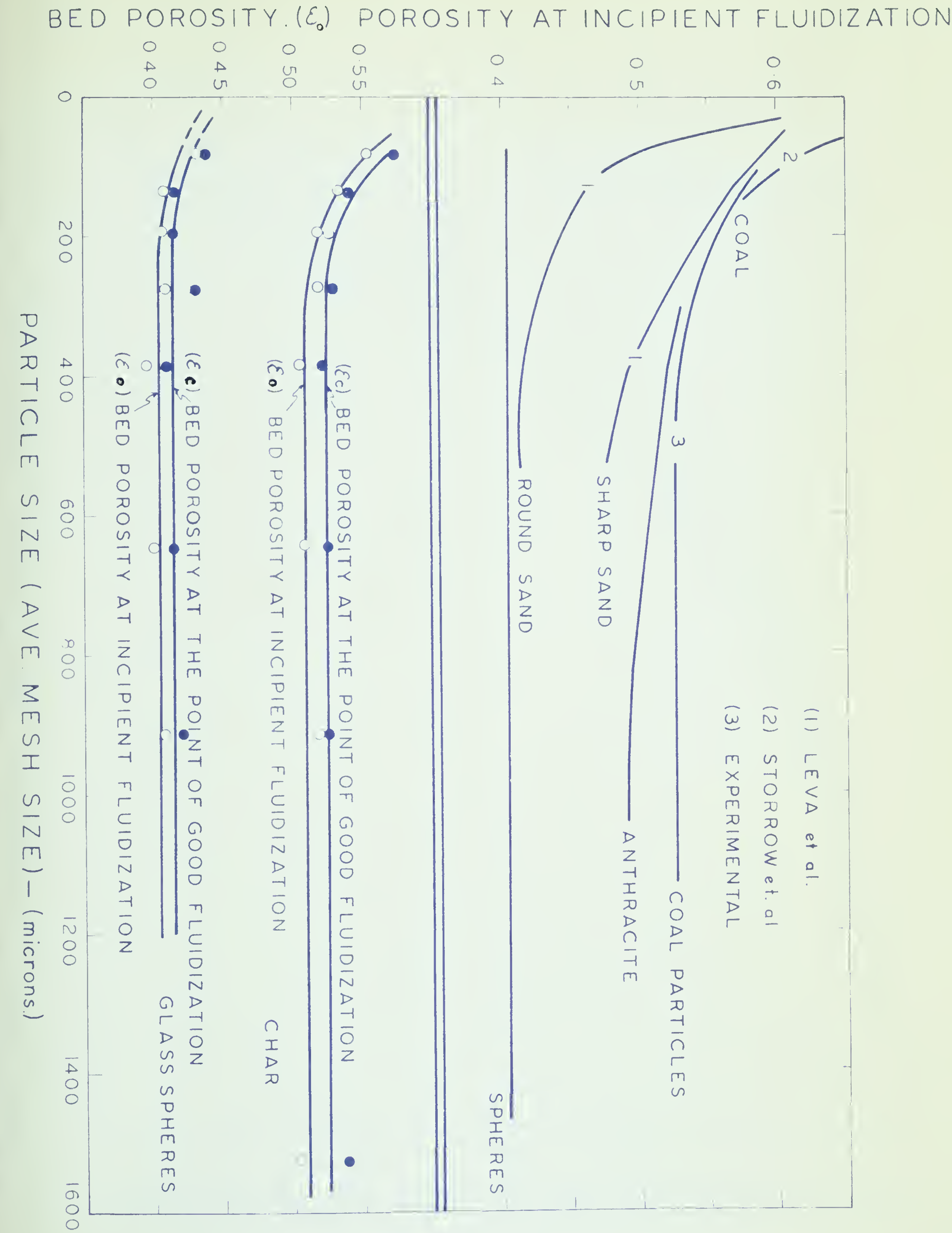
BED POROSITY.($\mathcal{E}_o$) POROSITY AT INCIPIENT FLUIDIZATION
0.6
0.5
0.4
0.55
0.50
0.45
0.40
(1) LEVA et al.
(2) STORROW et. al
(3) EXPERIMENTAL
COAL
COAL PARTICLES
ANTHRACITE
SHARP SAND
ROUND SAND
SPHERES
($\mathcal{E}$c) BED POROSITY AT THE POINT OF GOOD FLUIDIZATION
($\mathcal{E}$o) BED POROSITY AT INCIPIENT FLUIDIZATION
CHAR
GLASS SPHERES
0
200
400
600
800
1000
1200
1400
1600
PARTICLE SIZE (AVE. MESH SIZE)–(microns.)

FIG. 6

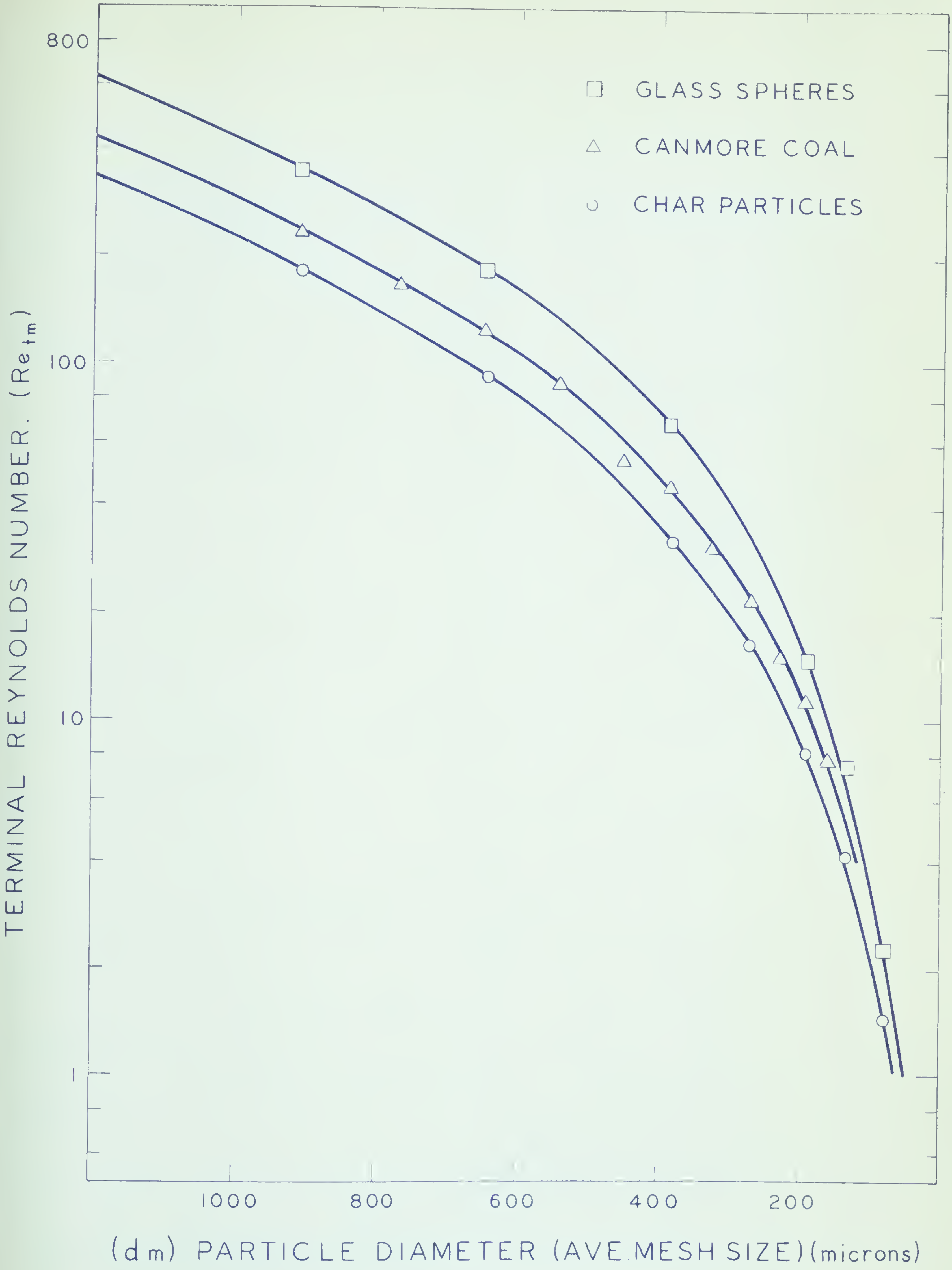
800
100
10
1
1000
800
600
400
200
GLASS SPHERES
CANMORE COAL
CHAR PARTICLES
TERMINAL REYNOLDS NUMBER. (Re_{tm})
(dm) PARTICLE DIAMETER (AVE. MESH SIZE) (microns)

FIG 7

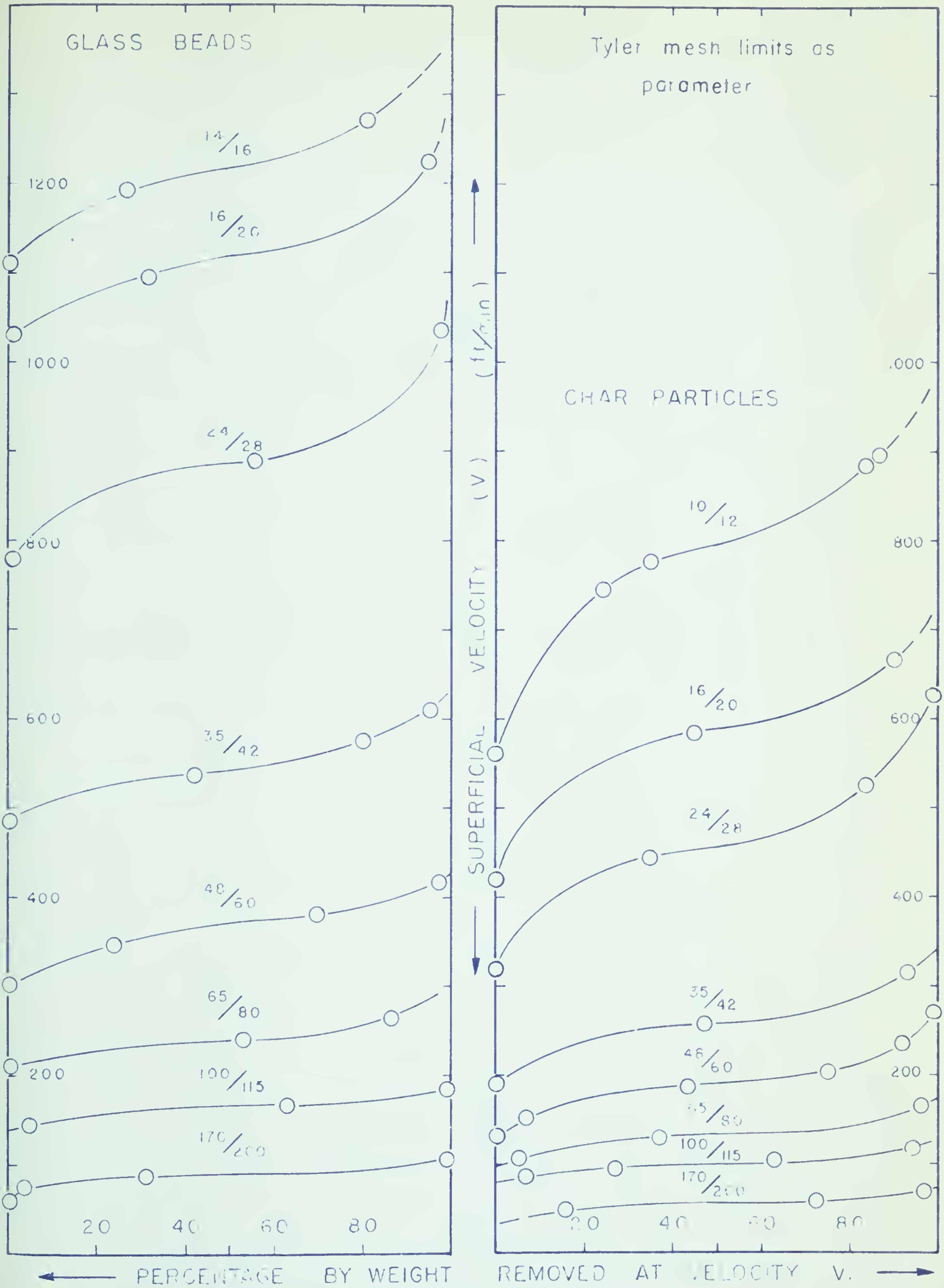
GLASS BEADS
Tyler mesh limits as parameter
CHAR PARTICLES
SUPERFICIAL VELOCITY (V) (ft/min)
14/16
16/20
24/28
35/42
48/60
65/80
100/115
170/200
10/12
1200
1000
800
600
400
200
20
40
60
80
← PERCENTAGE BY WEIGHT REMOVED AT VELOCITY V. →

FIG. 8

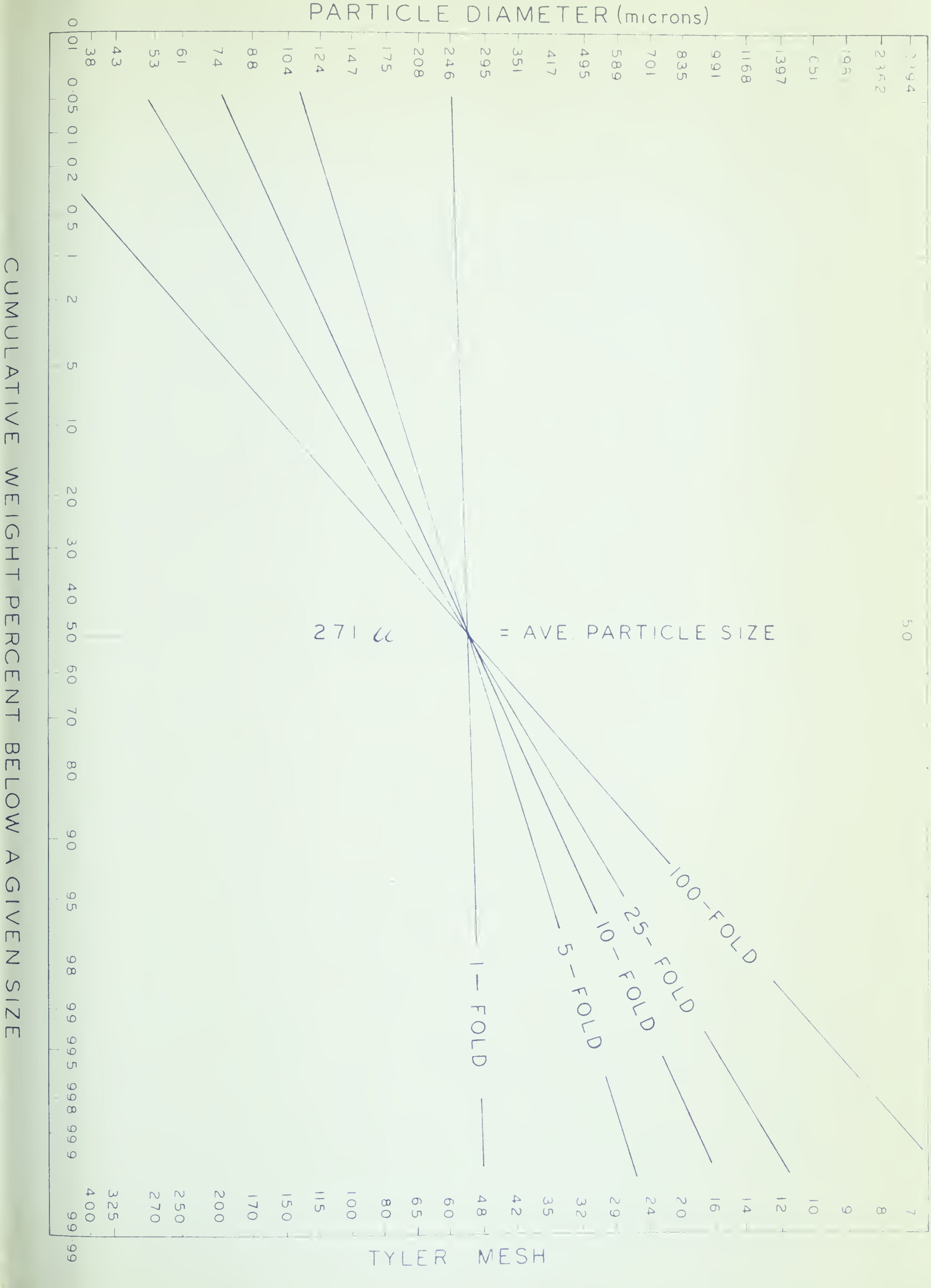
PARTICLE DIAMETER (microns)
38 43 53 61 74 88 104 124 147 175 208 246 295 351 417 495 589 701 835 991 1168 1397 2362
CUMULATIVE WEIGHT PERCENT BELOW A GIVEN SIZE
0.01 0.05 0.1 0.2 0.5 1 2 5 10 20 30 40 50 60 70 80 90 95 98 99 99.5 99.8 99.9 99.99
271 μ = AVE. PARTICLE SIZE
100-FOLD
25-FOLD
10-FOLD
5-FOLD
1-FOLD
400 325 270 250 200 170 150 115 100 80 65 60 48 42 35 32 29 24 20 16 14 12 10 9 8 7
TYLER MESH

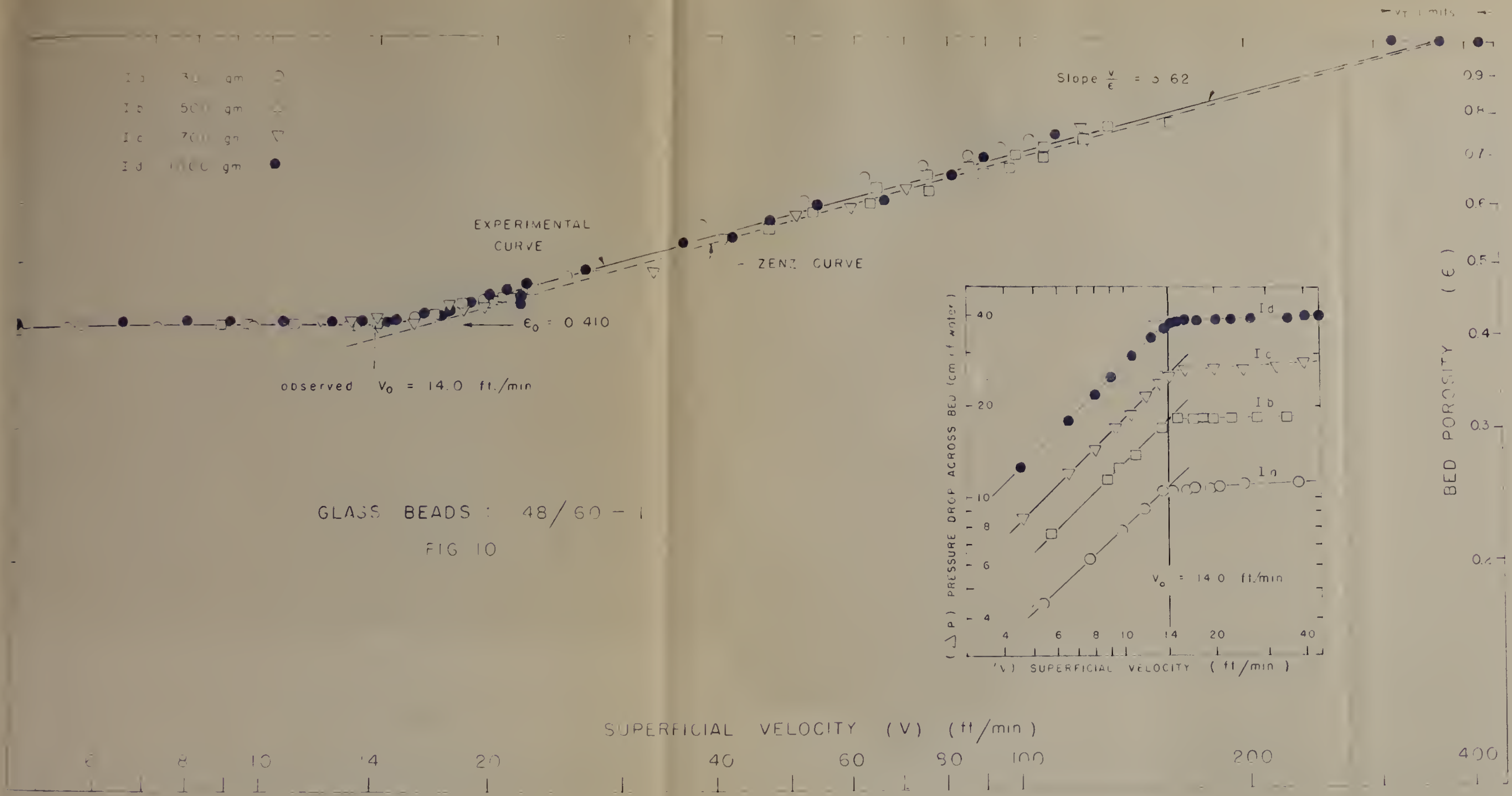

GLASS BEADS : 48/60 - I

FIG 10

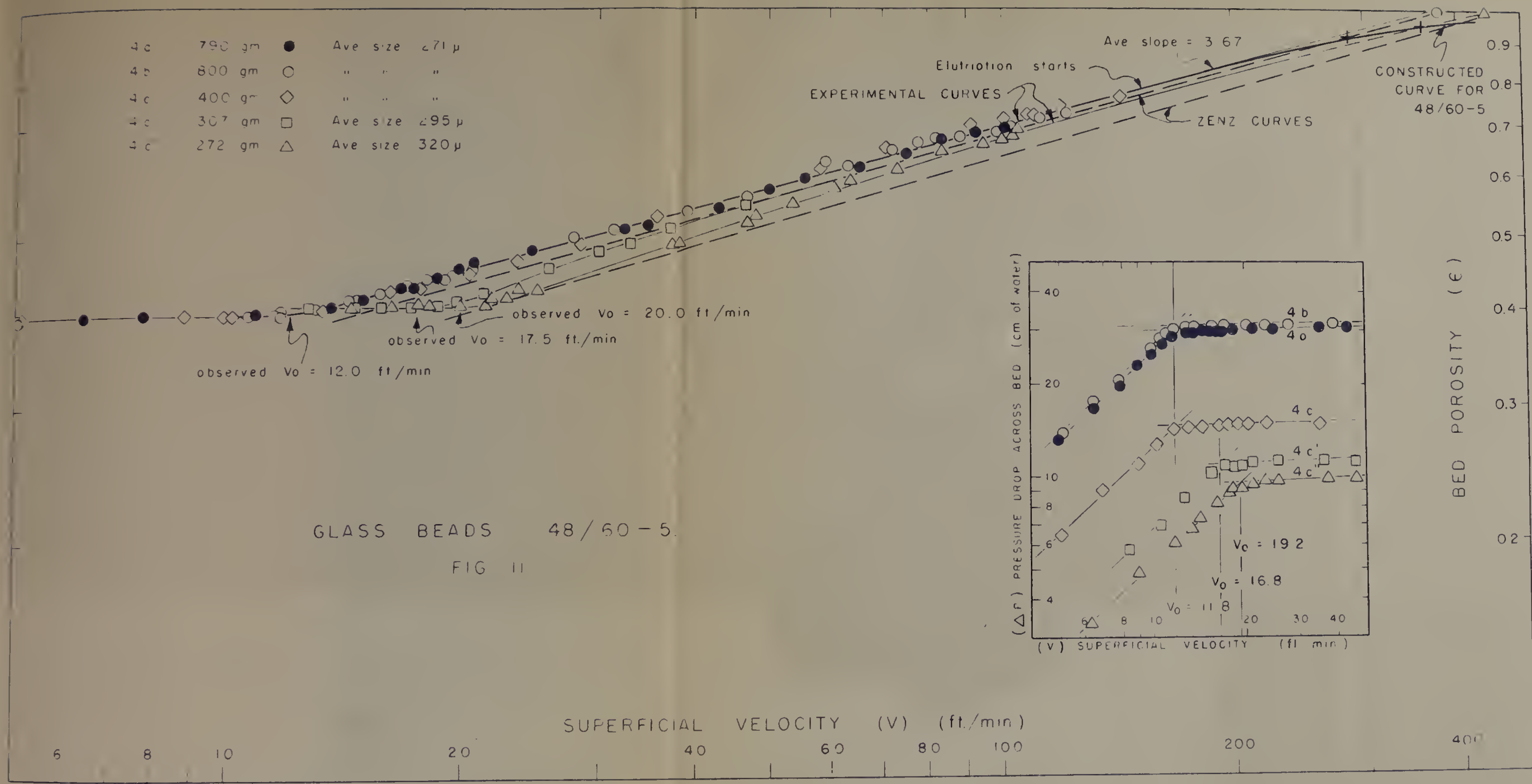

4 c 790 gm ● Ave size 271 μ
4 b 800 gm ○ " " "
4 c 400 gm ◇ " " "
4 c 307 gm □ Ave size 295 μ
4 c 272 gm △ Ave size 320 μ
Ave slope = 3.67
Elutriation starts
EXPERIMENTAL CURVES
ZENZ CURVES
CONSTRUCTED CURVE FOR 48/60-5
observed Vo = 20.0 ft/min
observed Vo = 17.5 ft./min
observed Vo = 12.0 ft/min
GLASS BEADS 48/60-5
FIG II
(Δp) PRESSURE DROP ACROSS BED (cm of water)
4 b
4 a
4 c
4 c'
4 c"
Vo = 19.2
Vo = 16.8
Vo = 11.8
(V) SUPERFICIAL VELOCITY (ft/min)
BED POROSITY (ε)
SUPERFICIAL VELOCITY (V) (ft./min)

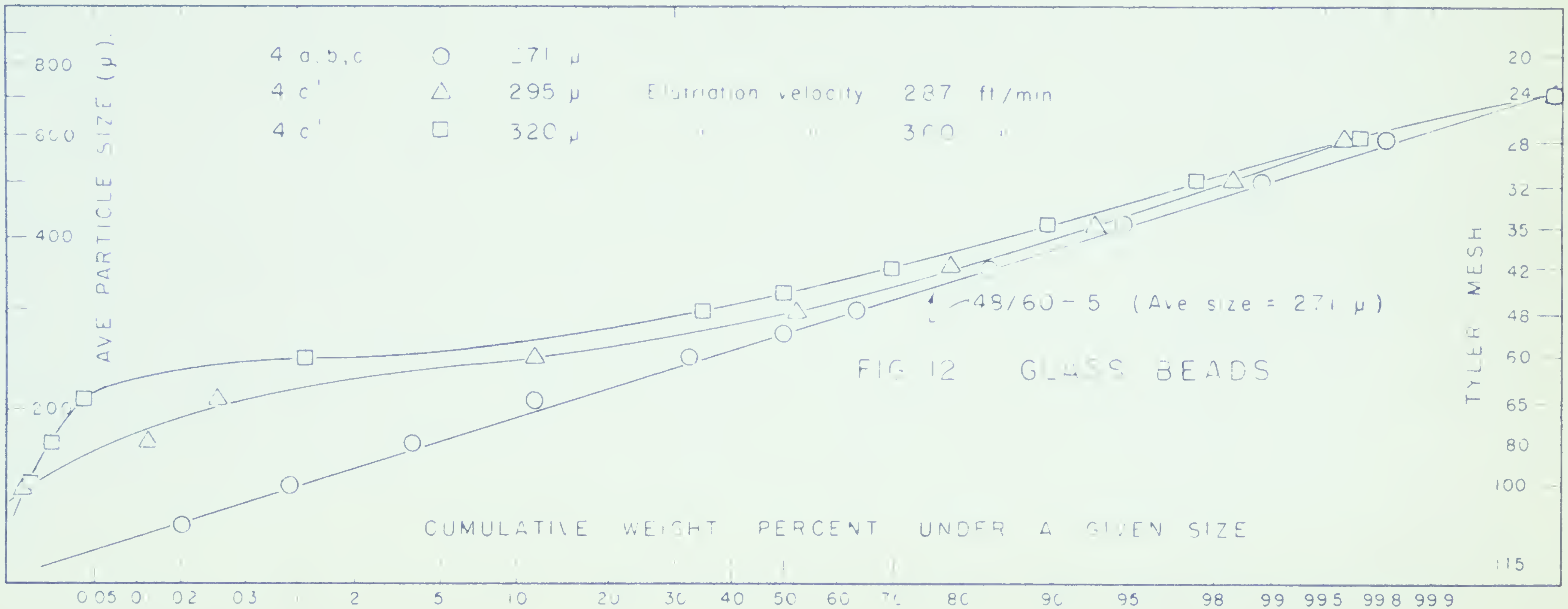

FIG 12 GLASS BEADS

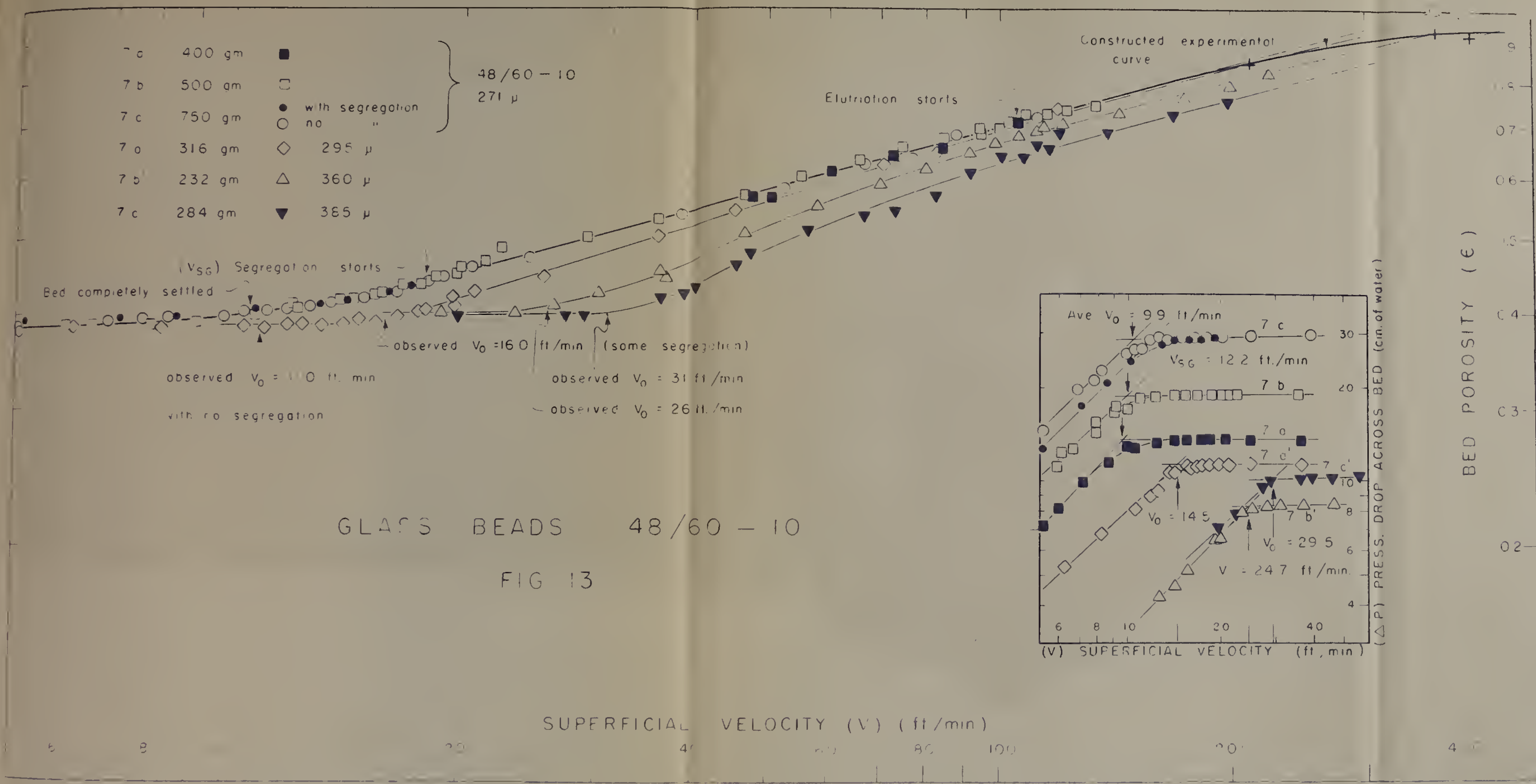

GLASS BEADS 48/60 – 10

FIG 13

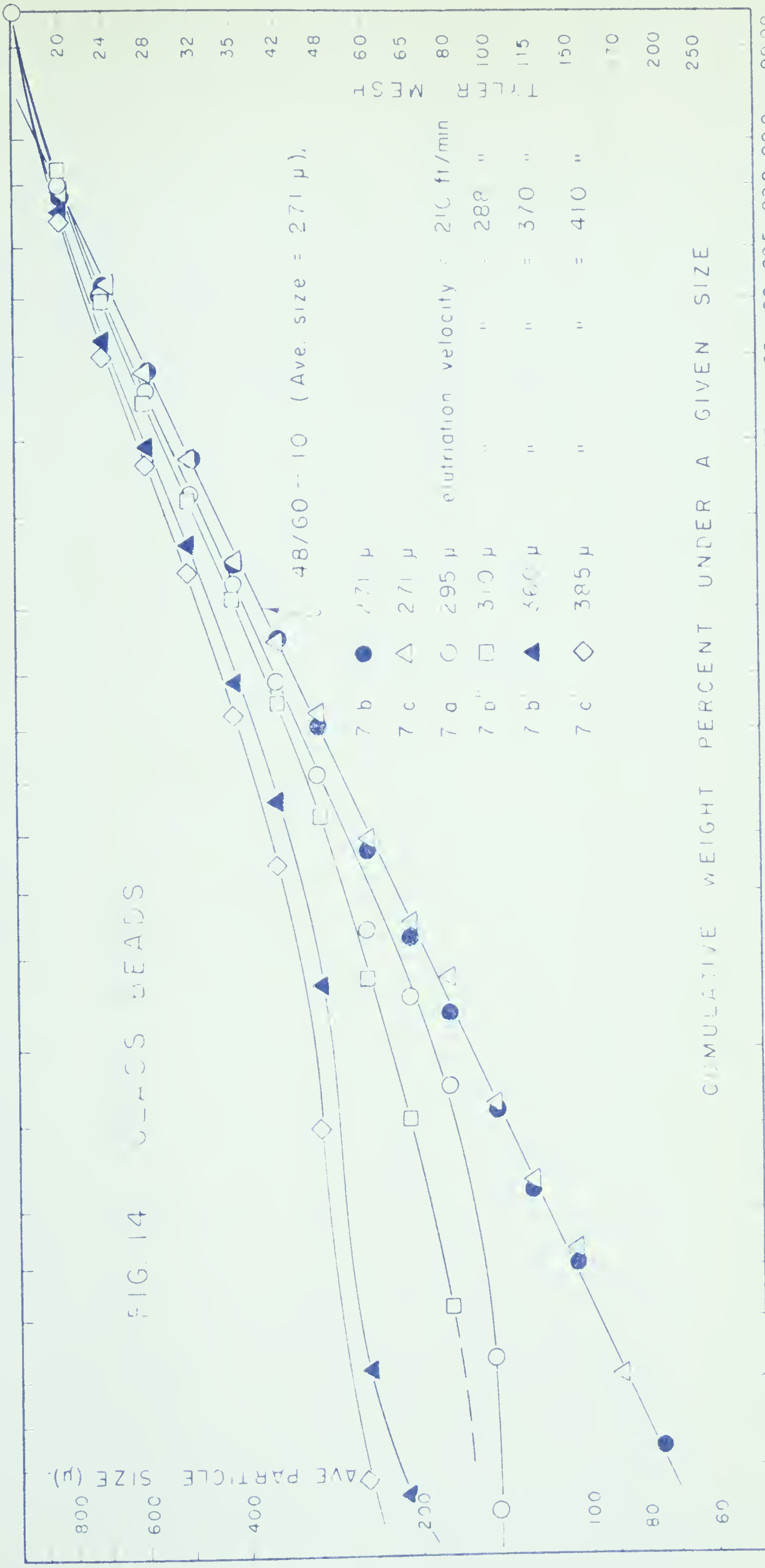

FIG. 14 GLASS BEADS

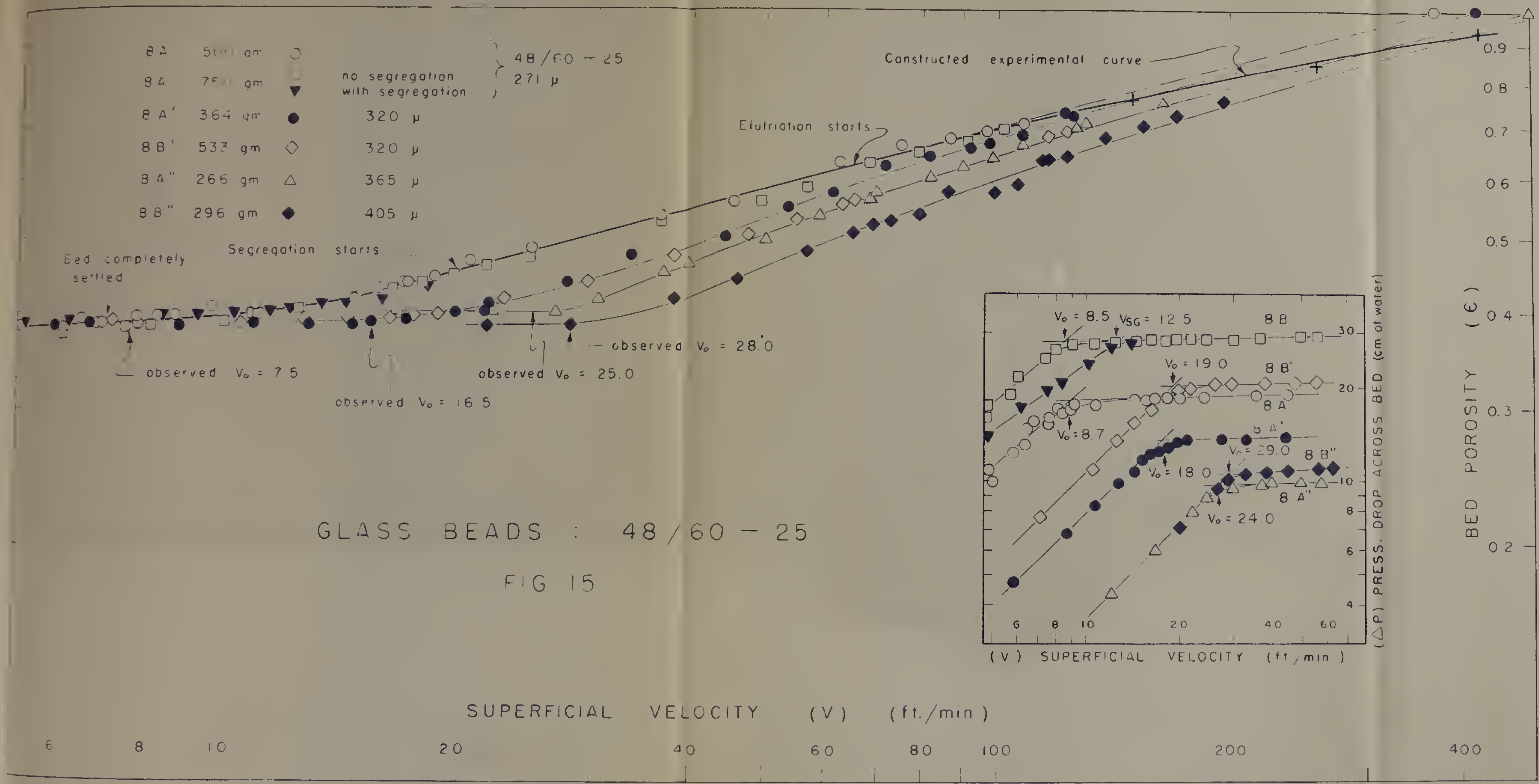

GLASS BEADS : 48/60 – 25

FIG 15

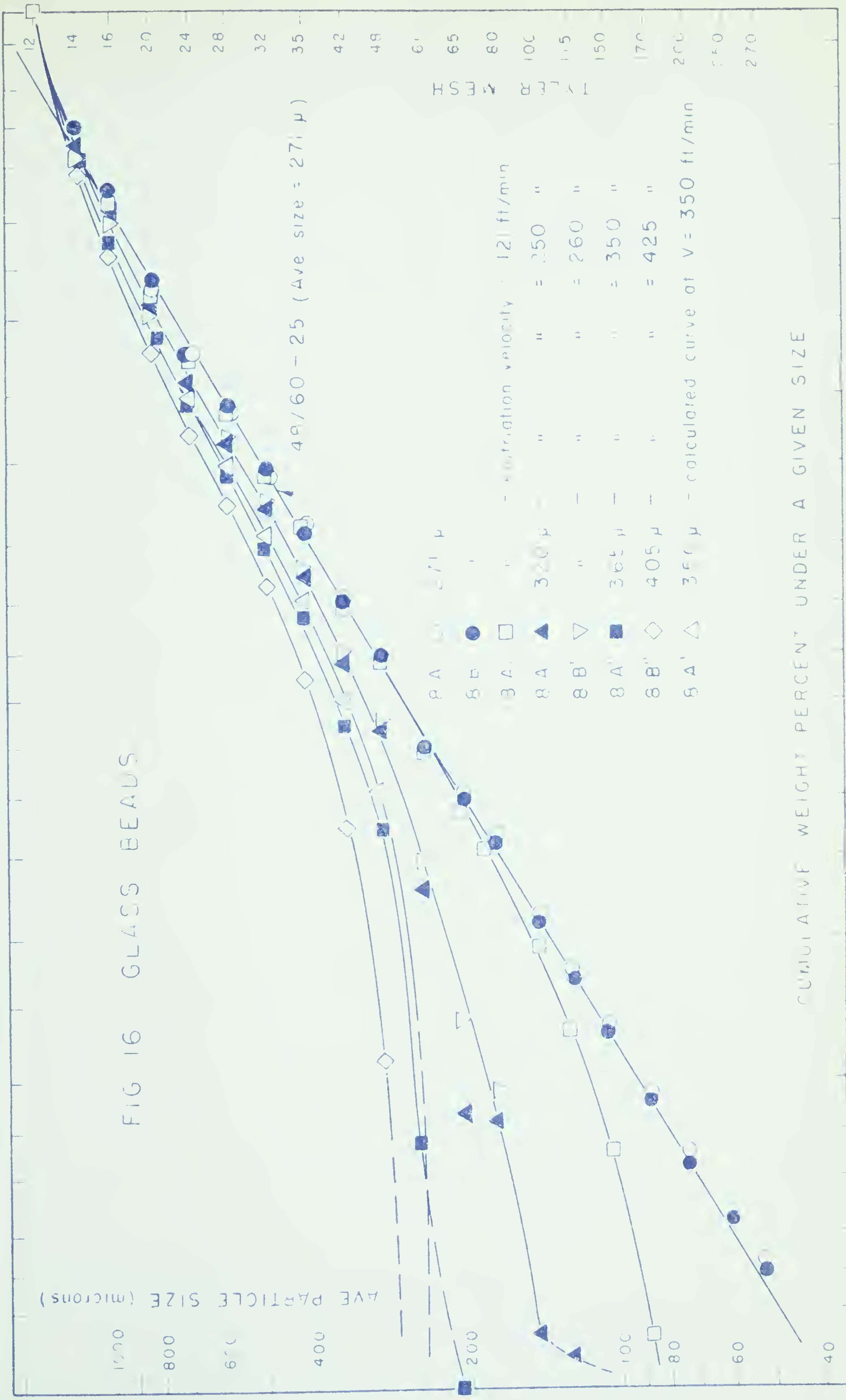

FIG 16 GLASS BEADS

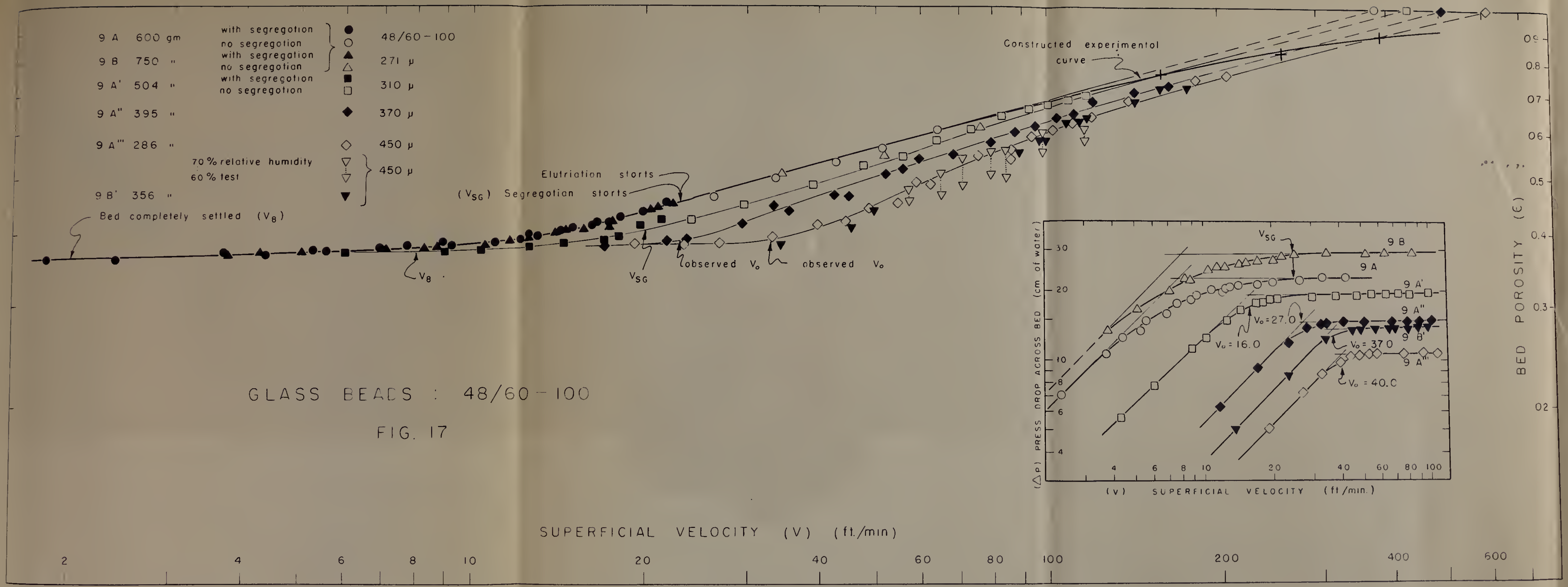

GLASS BEADS : 48/60 - 100

FIG. 17

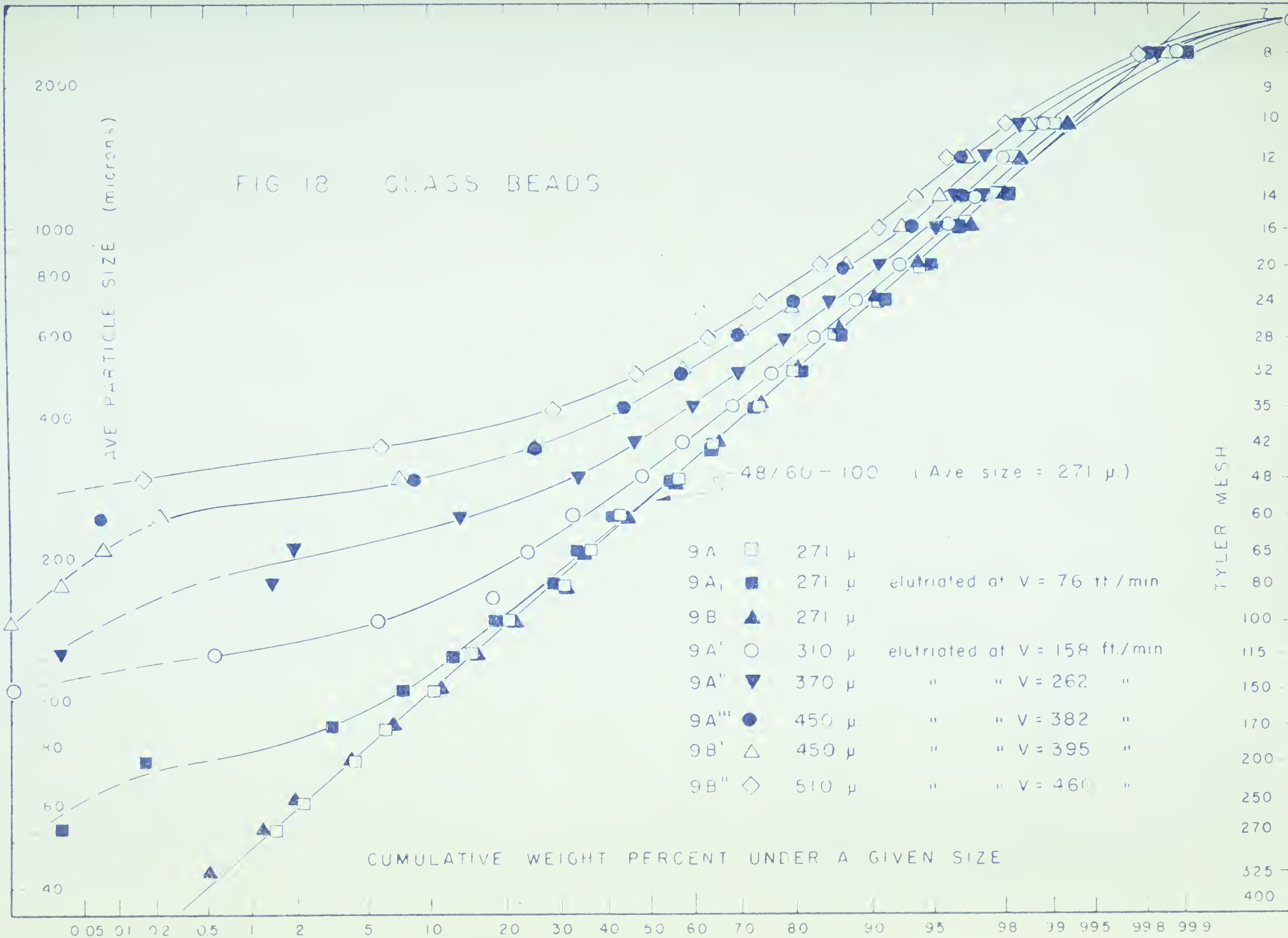

FIG 18 GLASS BEADS

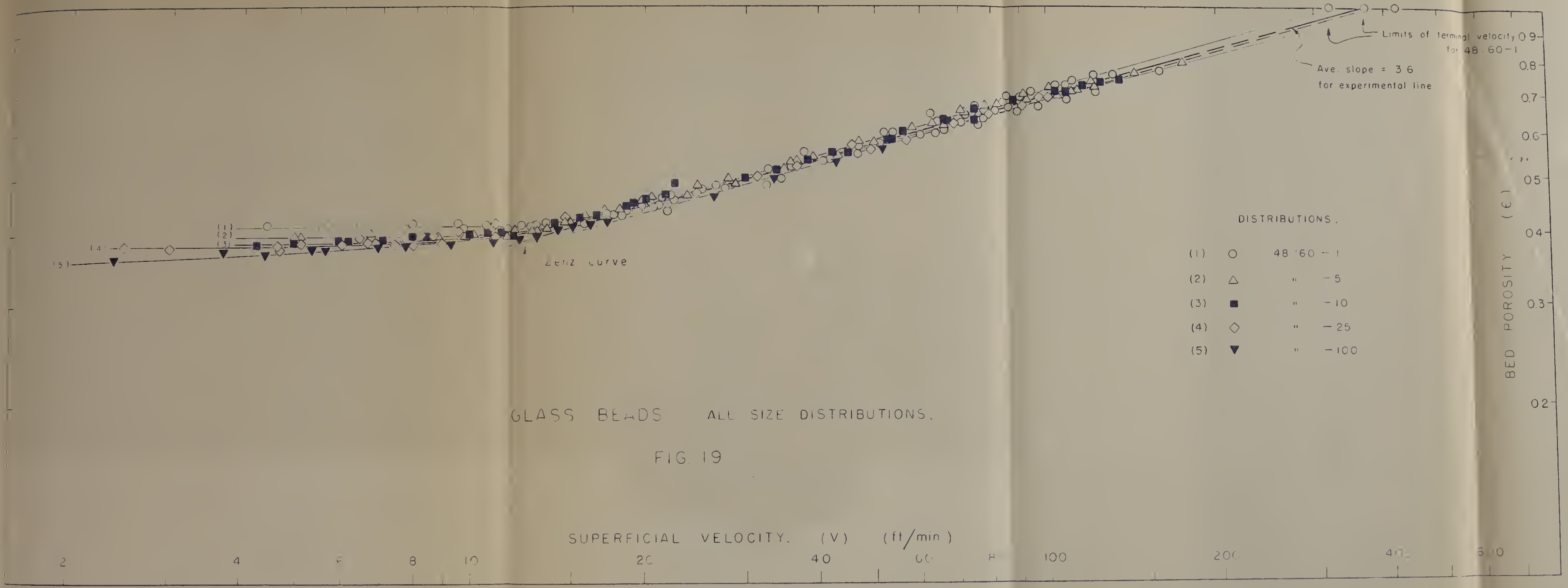

GLASS BEADS ALL SIZE DISTRIBUTIONS.

FIG. 19

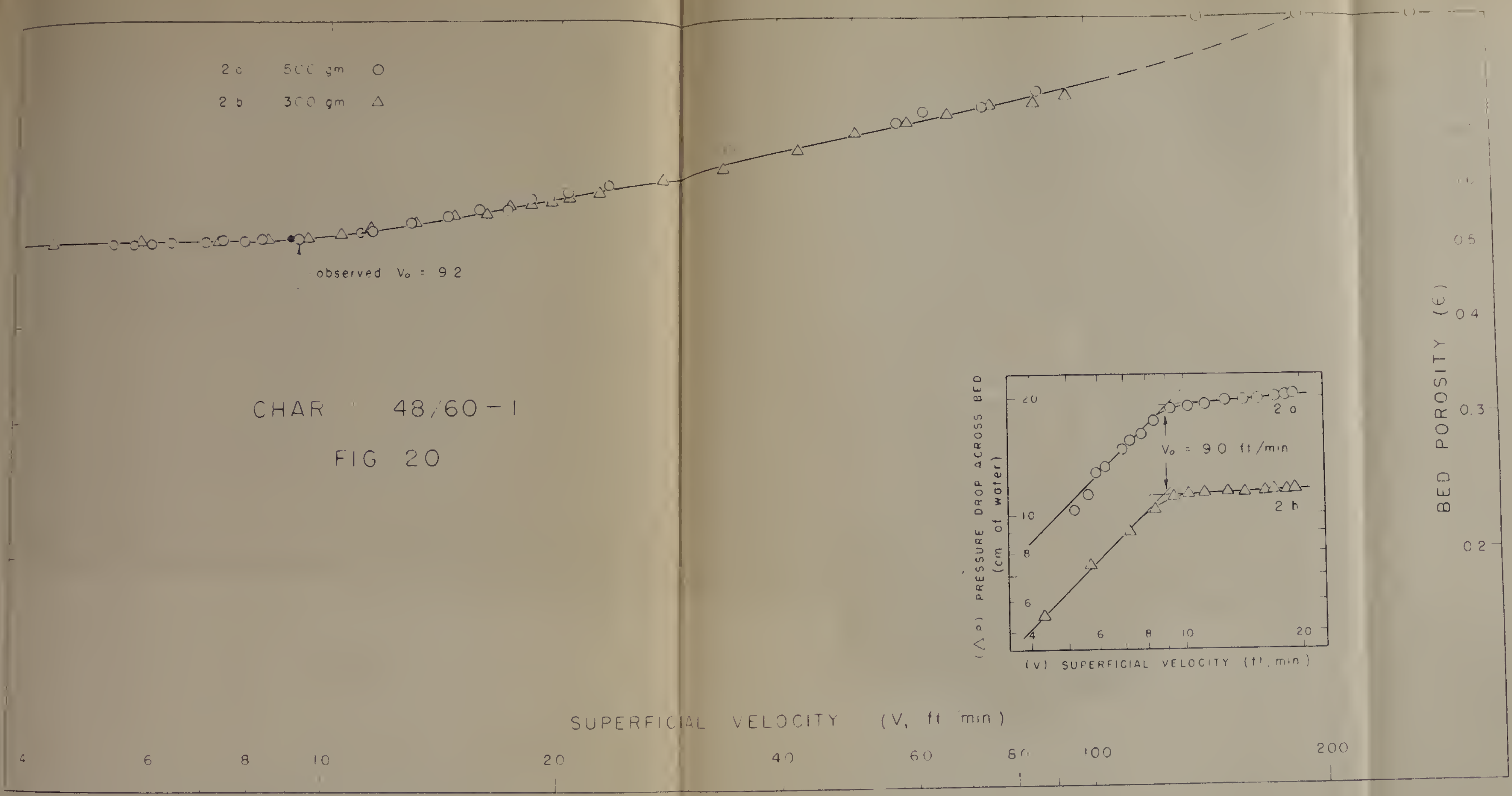

2 a 500 gm ○
2 b 300 gm △
observed V_o = 9.2
CHAR 48/60-1
FIG 20
BED POROSITY (ε)
0.5
0.4
0.3
0.2
SUPERFICIAL VELOCITY (V, ft/min)
4
6
8
10
20
40
60
80
100
200
(ΔP) PRESSURE DROP ACROSS BED (cm of water)
(V) SUPERFICIAL VELOCITY (ft/min)
V_o = 9.0 ft/min
2 a
2 b

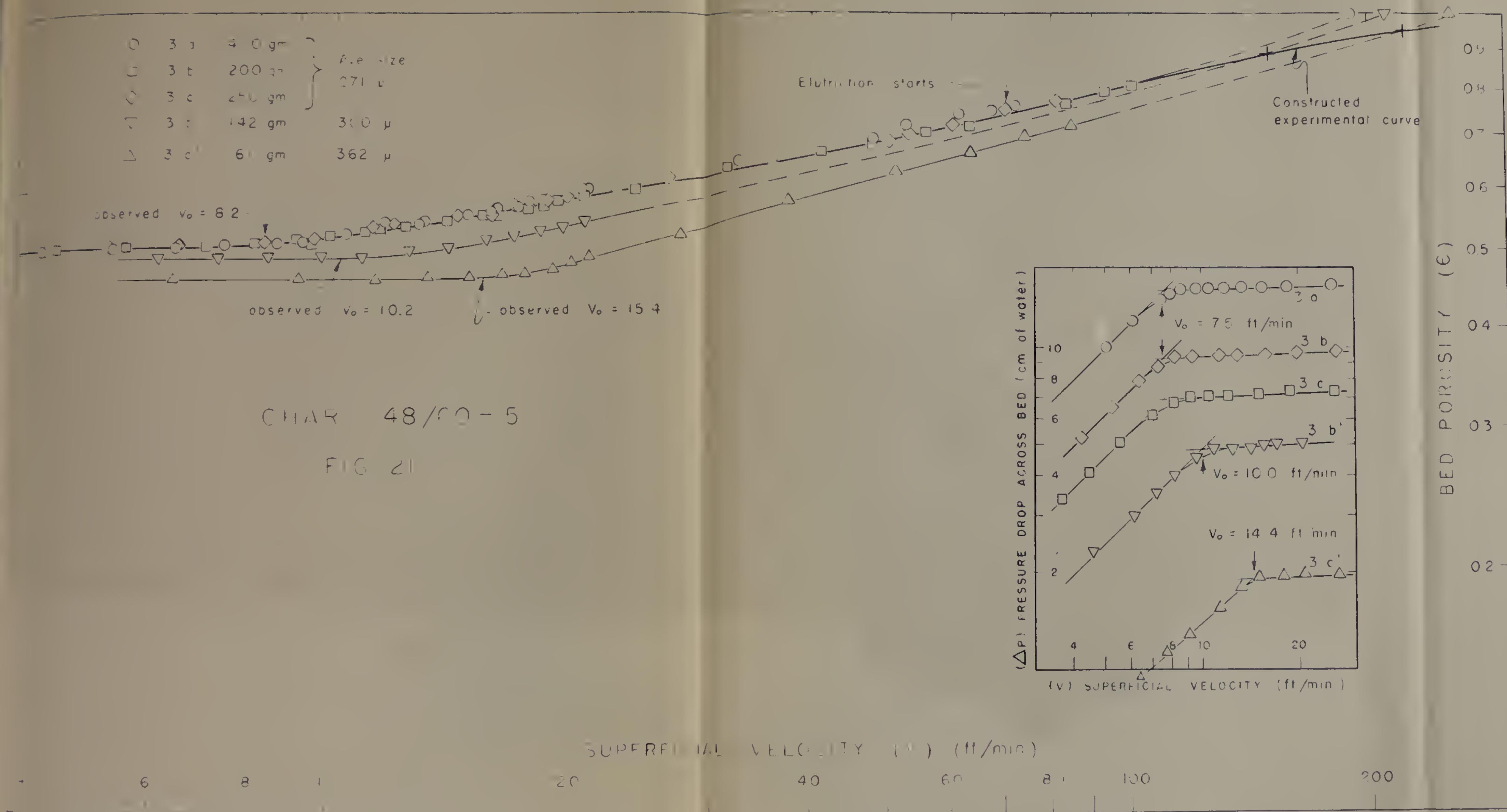

CHAR 48/60 - 5

FIG 21

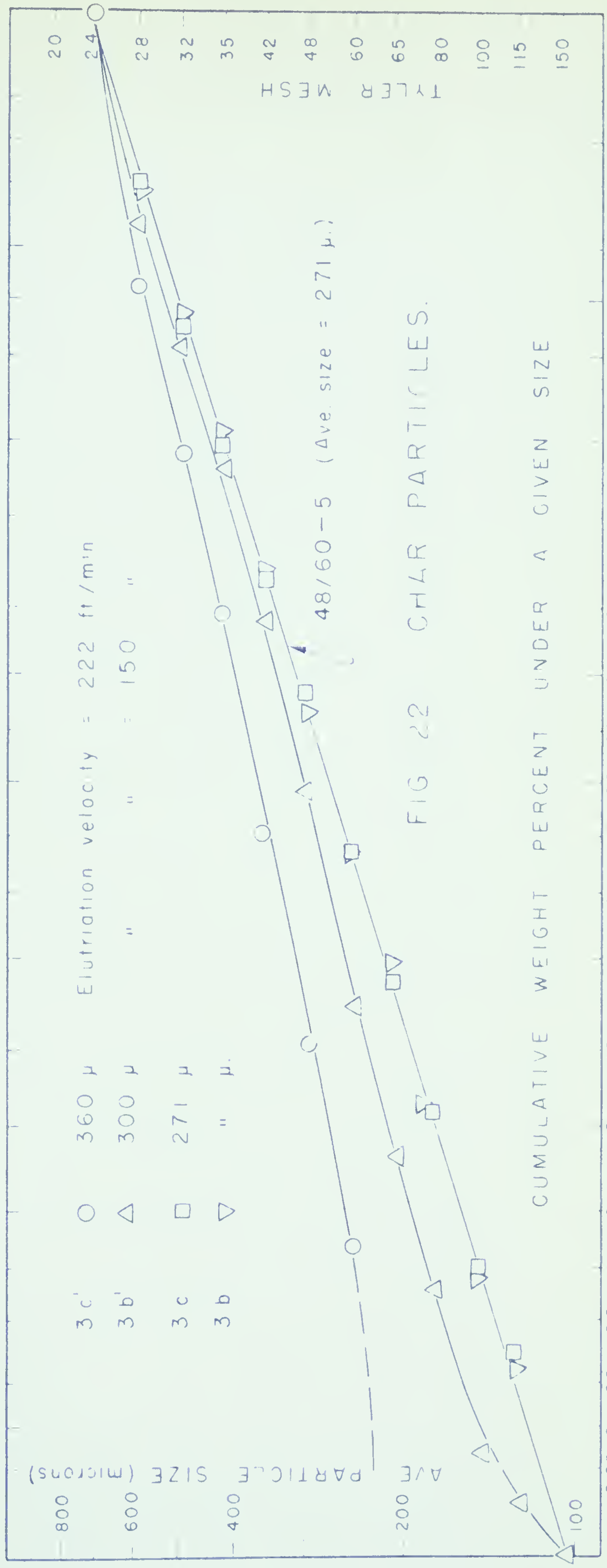

3c' ○ 360 µ Elutriation velocity = 222 ft/min
3b' △ 300 µ " " = 150 "
3c □ 271 µ
3b ▽ " µ
48/60-5 (Ave. size = 271 µ.)
FIG 22 CHAR PARTICLES.
TYLER MESH
20 24 28 32 35 42 48 60 65 80 100 115 150
AVE PARTICLE SIZE (microns)
800 600 400 200
CUMULATIVE WEIGHT PERCENT UNDER A GIVEN SIZE
0.05 0.1 0.2 0.5 1 2 5 10 20 30 40 50 60 70 80 90 95 98 99 99.5 99.8 99.9
100

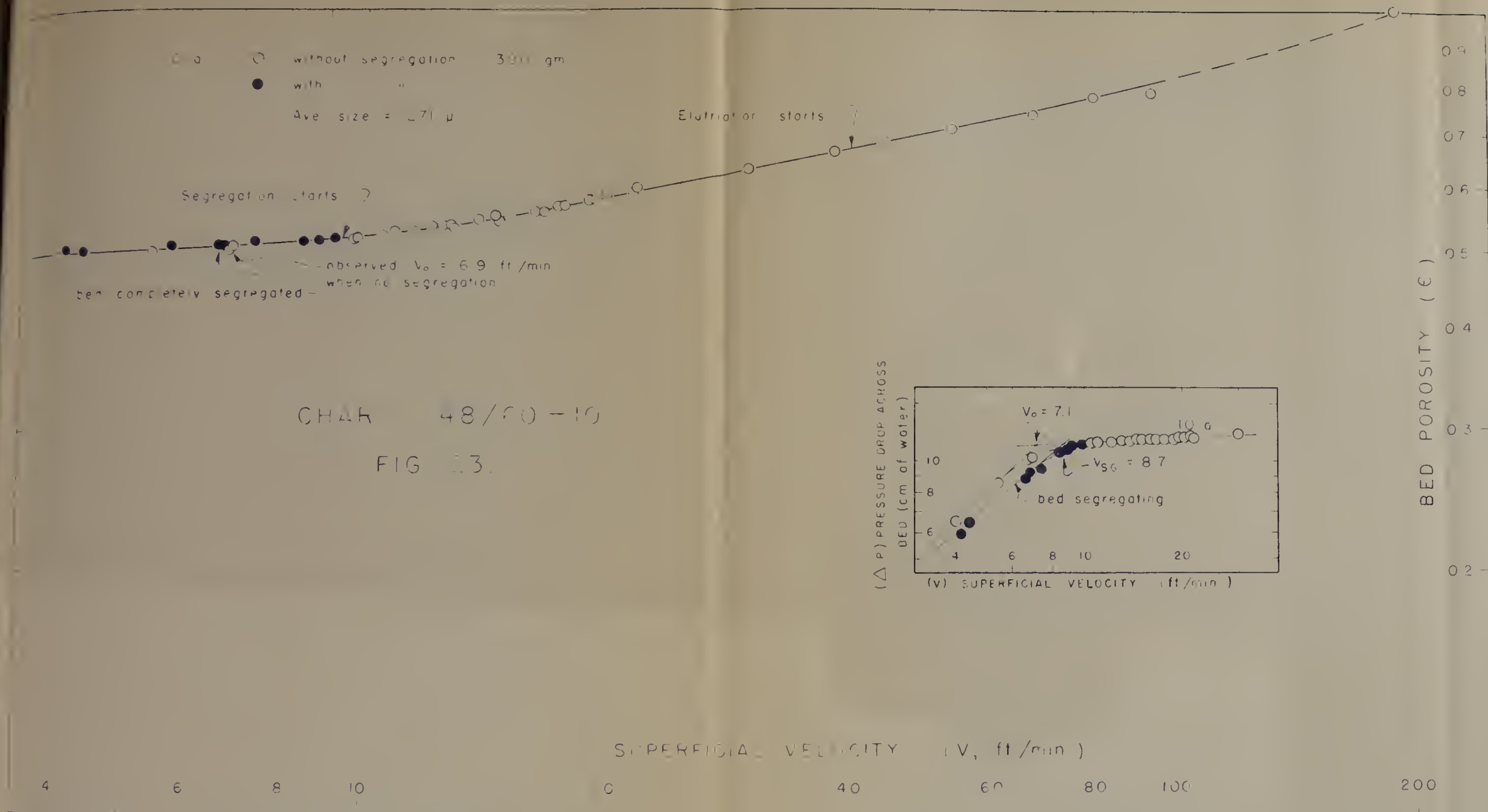

○ without segregation 300 gm
● with
Ave size = 71 μ
Elutriation starts
Segregation starts
observed V_o = 6.9 ft/min when no segregation
bed completely segregated
CHAR 48/60 - 10
FIG 13
V_o = 7.1
V_{SG} = 8.7
bed segregating
(Δ P) PRESSURE DROP ACROSS BED (cm of water)
(V) SUPERFICIAL VELOCITY (ft/min)
BED POROSITY (ϵ)
SUPERFICIAL VELOCITY (V, ft/min)

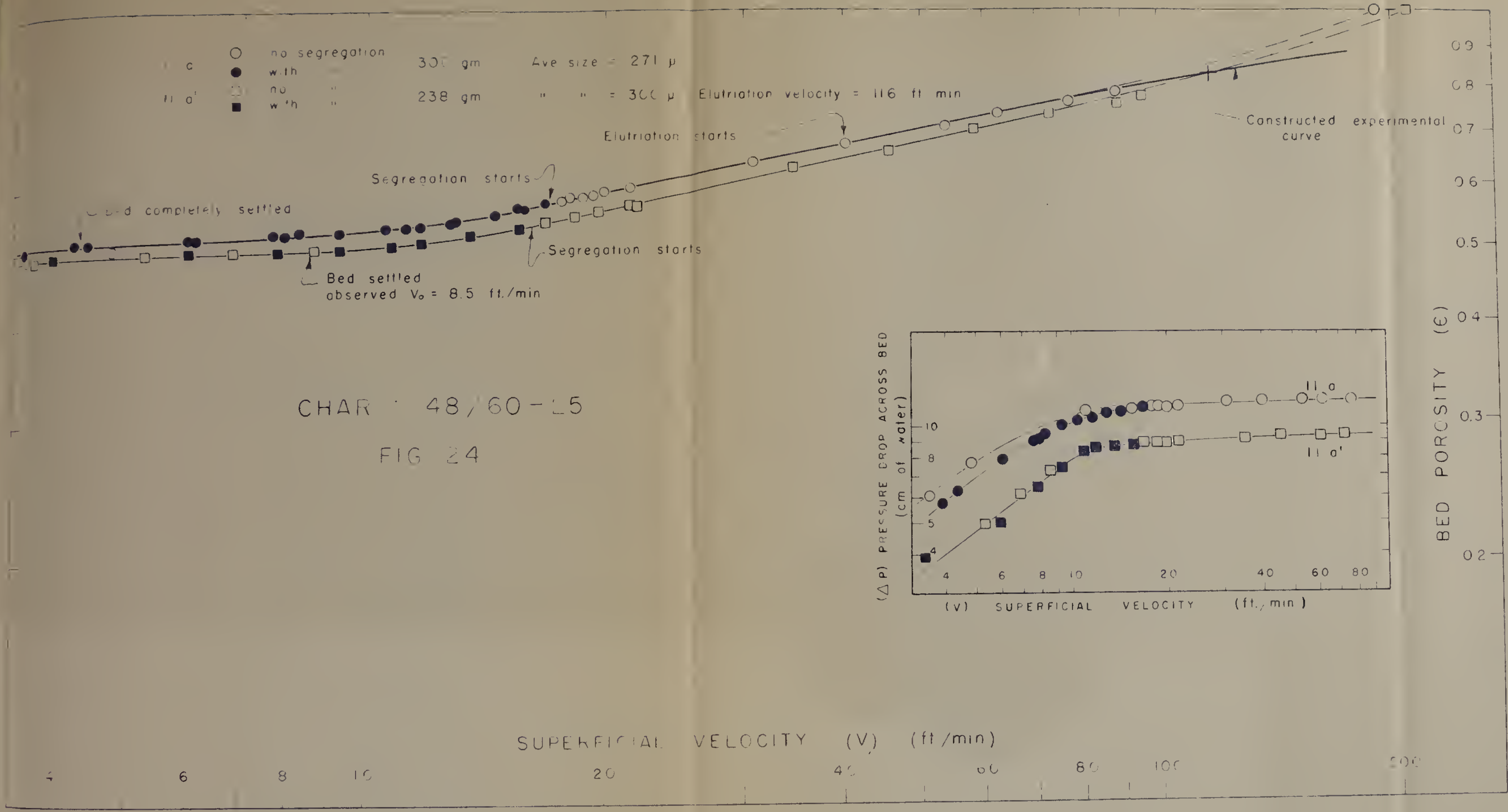

CHAR 48/60-L5

FIG 24

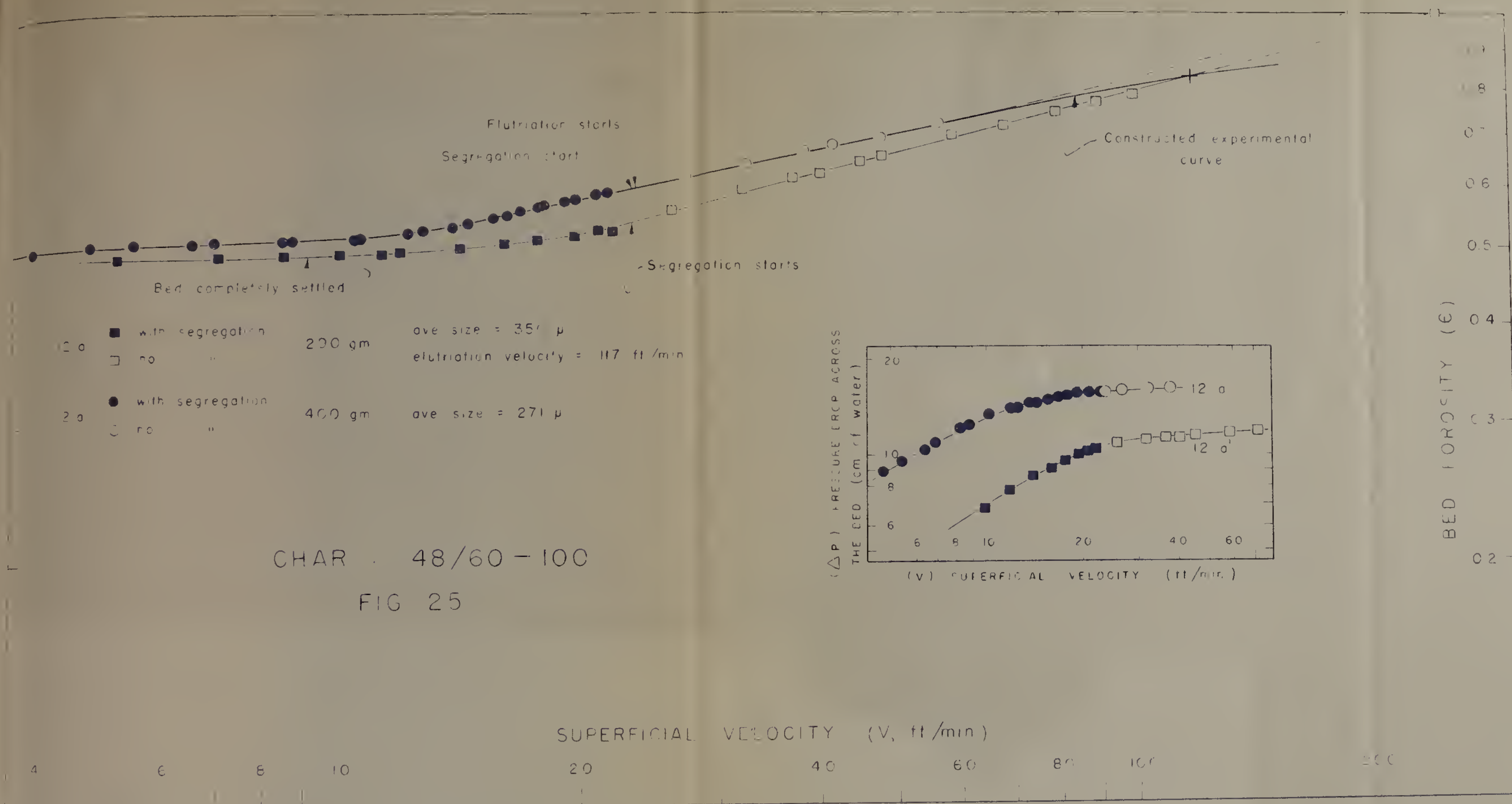

CHAR 48/60 - 100

FIG 25

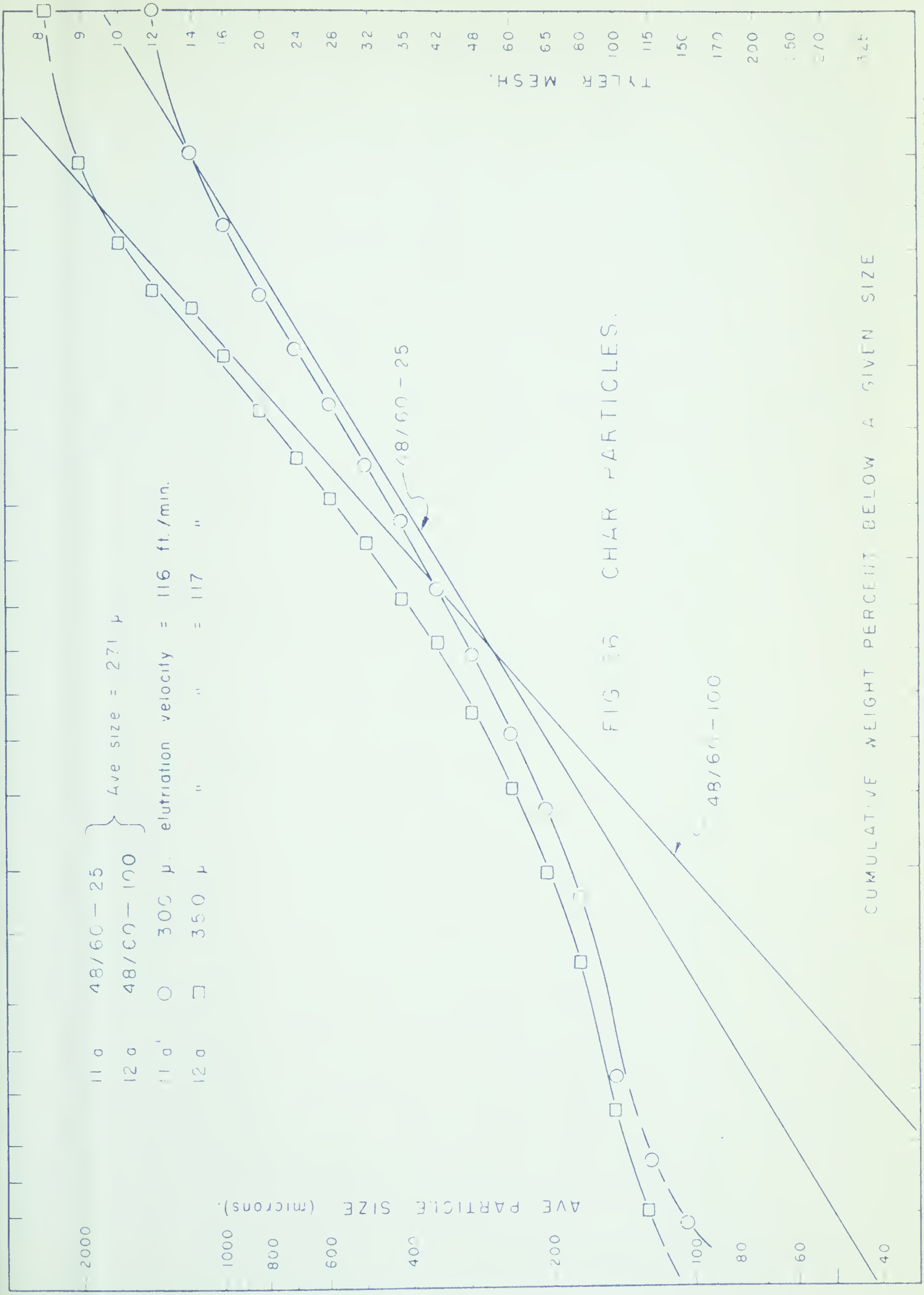

FIG 15 CHAR PARTICLES.

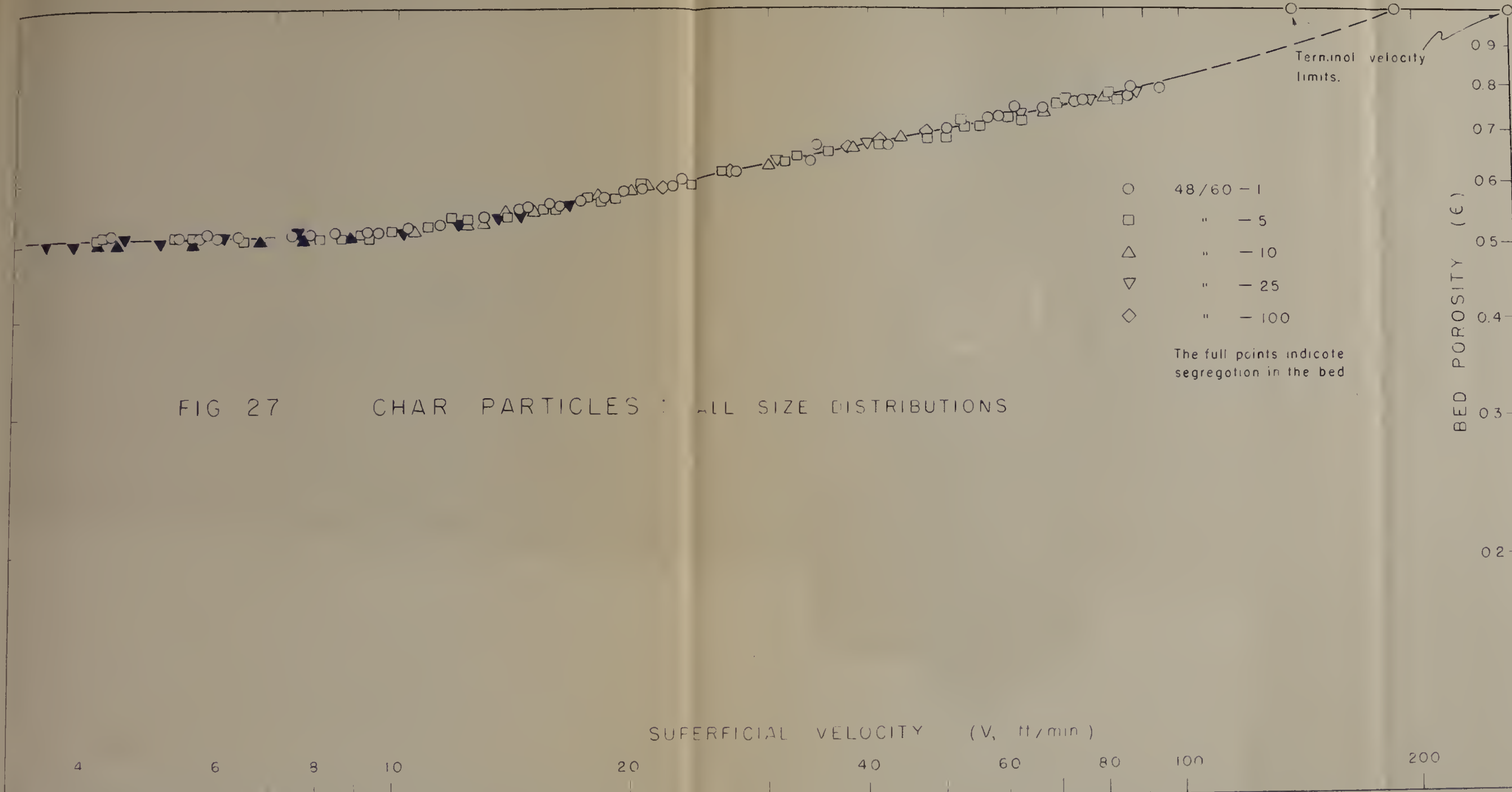

FIG 27 CHAR PARTICLES : ALL SIZE DISTRIBUTIONS

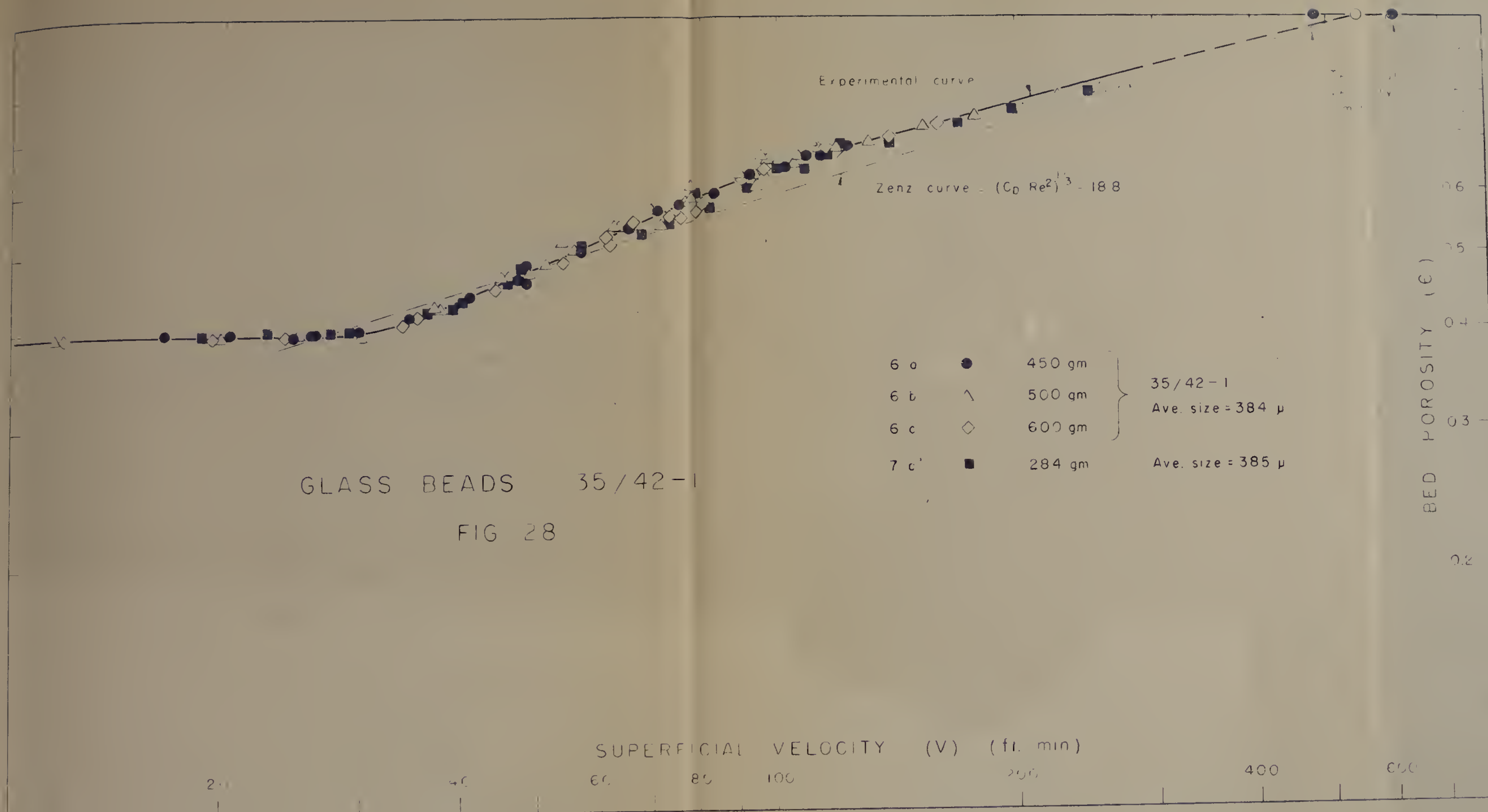

GLASS BEADS 35/42-1

FIG 28

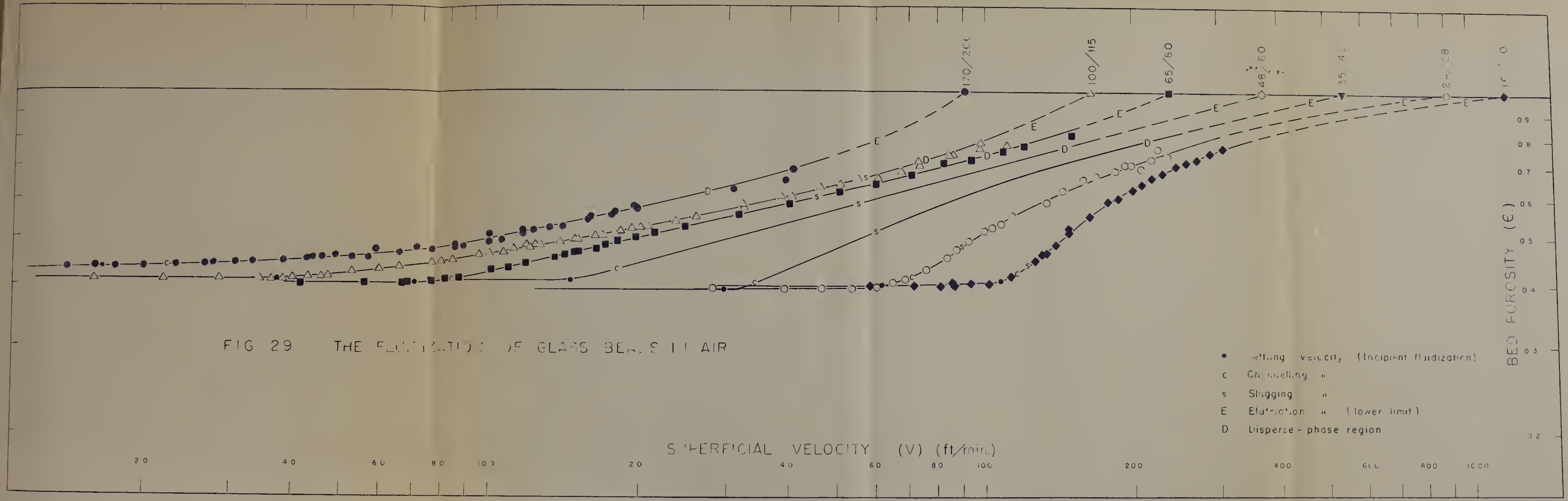

FIG 29 THE FLUIDIZATION OF GLASS BEADS IN AIR

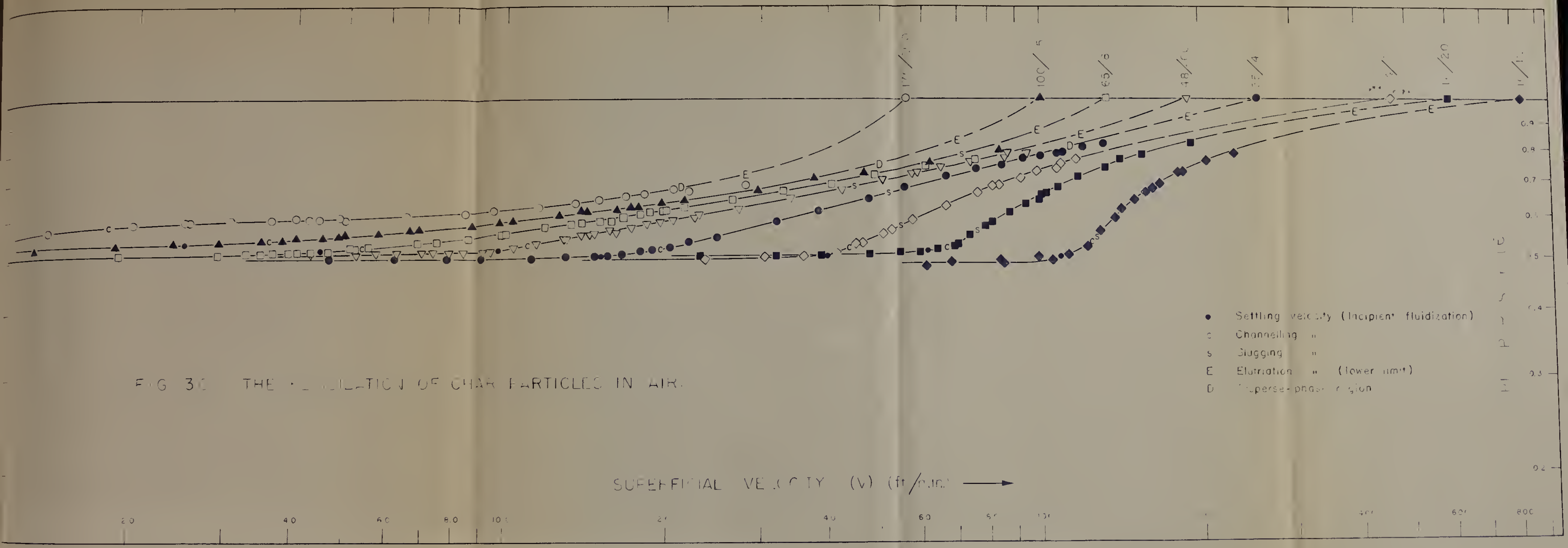

FIG. 30 THE FLUIDIZATION OF CHAR PARTICLES IN AIR.

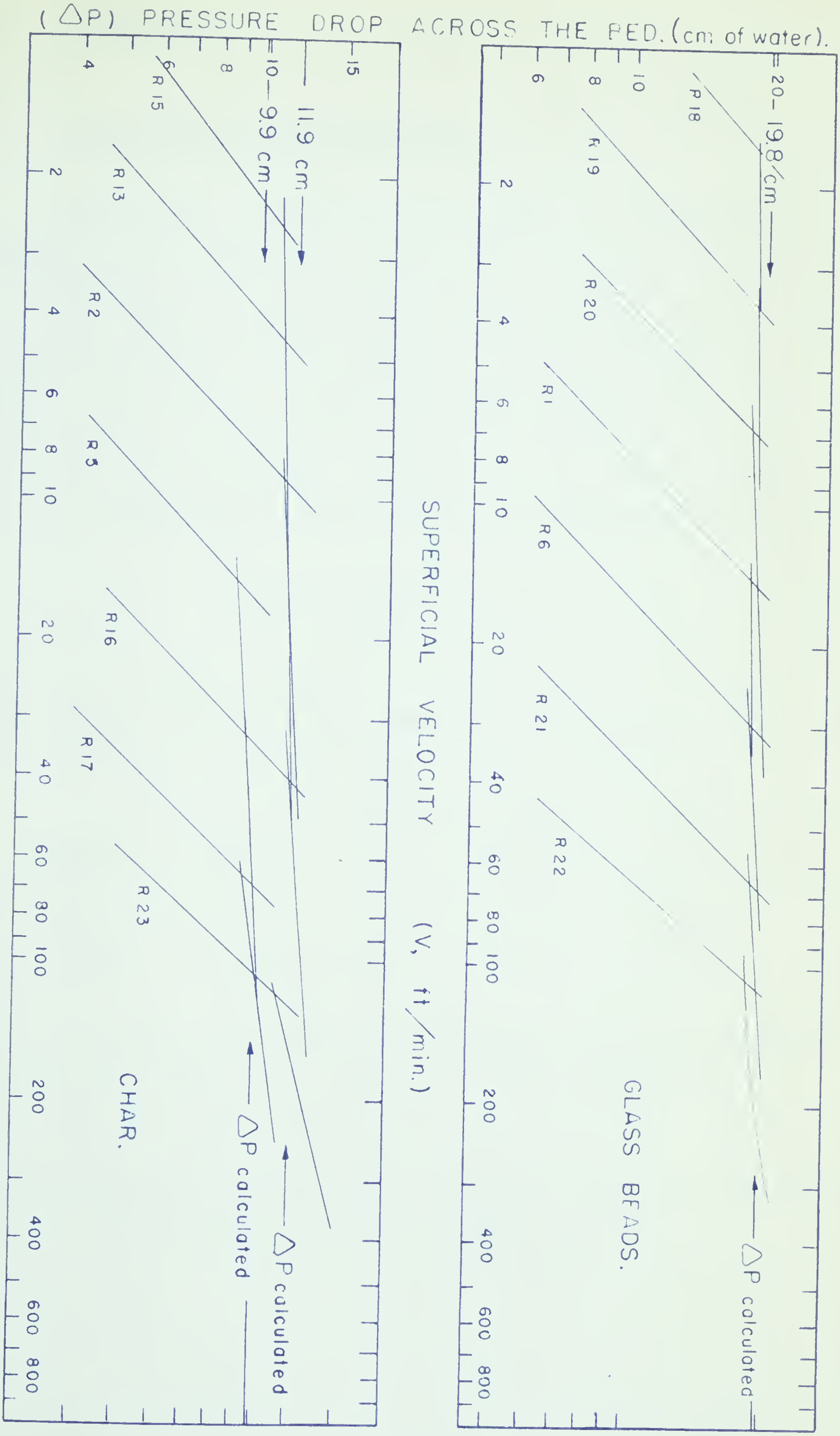

(△P) PRESSURE DROP ACROSS THE BED. (cm of water).
SUPERFICIAL VELOCITY (V, ft/min.)
CHAR.
GLASS BEADS.
11.9 cm
9.9 cm
19.8 cm
△P calculated
△P calculated
△P calculated
R 15
R 13
R 2
R 5
R 16
R 17
R 23
R 18
R 19
R 20
R 1
R 6
R 21
R 22

FIG. 31

D. DISCUSSION.

1. PROPERTIES OF THE MATERIALS.

The number of particles per gram for the various sizes of coal, char and glass beads are shown in figure 4. The results show a linear relationship in each case, of the form $d_m = C\,\bar{n}^{-1/3}$, where $-\frac{1}{3}$ is the slope of the lines, and C is a constant depending on the density and shape of the particles. Since $\bar{n} = 1/\,K\,d_M^3\,\rho_s$, where K is a volume shape factor ($K = \pi/6$ for spheres.), then:

$$d_m = C\,(K\,d_M^3\,\rho_s)^{1/3}$$

or $$K = 1/C^3\rho_s \quad \ldots\ldots\ldots\ldots (35)$$

The values of C and K obtained are shown below:

		C.	K.	K′
COAL	1.360	1.06	0.617	1.050
CHAR	1.085	1.16	0.590	1.040
BEADS	2.530	0.90	0.545	1.012

By definition, the spherical diameter (d_s) of a particle is given by: $\pi/6\; d_s^3 = K\,d_M^3$, or more simply by: $d_s = K'\,d_M$. The values of K' are tabulated. This diameter d_s is commonly used in conjunction with sphericity in correlating terminal velocity data.

Figure 5 shows a graph of the equivalent diameter, (d_e)(23) for coal, char and beads, compared with the average sieve diameter (d_M). In this graph, density effects are accounted for, and the relative position of the lines with respect to the line $d_e = d_M$ is a measure of the variation in shape of the particle. The deviation shown by the glass beads can be explained by plotting the d_e values against the microscopic diameter d_A ; the resulting line has the equation $d_e = d_A$. The data for coal and char agree well with the data for coke and carborundum obtained by Van Heerden et.al. (23). The bed porosity at the point of fluidization is shown in figure 6 plotted against the particle diameter d_M. The curve for char agrees well with similar data for coal particles; here again, the relative position of the $\varepsilon_0 - d_M$ curve is an indication of the particle shape. The curve for beads is slightly higher than the curve for true spheres (ε_0 = constant = 0.406.), and there is also a definite variation of ε_0 with d_M for sizes less than 200 μ, indicating that these beads contained a certain proportion of irregular particles. This was verified under the microscope. The critical conditions for all the tests are listed in tables 4 to 7, and will be discussed later.

The terminal velocities of the particles are shown in figures 7 and 8. Figure 8 shows the original data plotted systematically for all the sizes considered, and the terminal velocity is read at the 50% point. The main problem in obtaining these results was due to static electricity, which tended to hold the beads in the column, resulting in a low 'percent removed' reading at any given velocity. By careful control of the humidity, this effect could be greatly reduced. Figure 7 shows the terminal Reynold's number Re plotted against the particle diameter d_M, and once again the particle shape and density define the relative positions of the curves. It should be noted that the terminal velocities described here are only average values for a sample of particles. The terminal velocities measured for any closely sized fraction varied by 30 - 40%, due to the very wide range of particle weights retained between adjacent sieves, and the terminal velocity as quoted represents the velocity at which half of a closely sized fluidized bed would be elutriated.

Whilst dealing with the properties of the particles, it is convenient to briefly consider the results of the fixed bed tests described in Appendix B. The results are treated by the method proposed by Leva et.al. (2), and excellent correlations are obtained as shown in figures 41 and 42. The results for glass beads plotted

against a modified Reynolds number (based on d_A) show excellent agreement, and for the laminar region, $f = 95/Re$. This agrees well with Leva's value of $f = 100/Re$, but is higher than $f = 77/Re$ obtained by Lewis et.al. (16). There is still some doubt as to the exact value of the constant in the above equation: Leva in a recent publication (68) claims that the value 100 is correct, whilst others (23) favour the value 77. The general form of the above equation is $f = C\lambda/Re$, where C is a constant in the laminar region. By comparing the values of the friction factor for various materials at $Re = 1$, λ may be calculated. By definition $\lambda = 1/\phi$.

The values of λ and ϕ, assuming $C = 95$ and $\lambda = 1$ for the glass beads, are shown below.

	λ	ϕ
COAL	1.61	0.622
CHAR	1.38	0.725
BEADS	1	1

These figures agree well with values for similar materials presented in the literature.

Fixed bed tests were also carried out with loosely packed beds obtained after fluidization. In the case of the beads, the results obtained agreed well with the other tests, but for char, the results for loose packings

were all 15 - 30% lower. Extensive checks of the apparatus revealed nothing to account for these deviations. It seems likely that this decrease in pressure drop is due to some orientation effect of the particles, since variations in other bed properties are accounted for in the correlation used.

2. FLUIDIZATION TESTS: MIXED SIZES.

The size distributions used are shown in figure 9 on log-probability co-ordinates, and the results of the tests are shown in figures 10-27 inclusive. An average size of 271 microns was chosen since this allowed wide size distributions to be made up with particles which could be handled on standard Tyler sieves. The initial tests on mixed sizes were to study the effects of size distribution on the expansion characteristics of the beds.

(a) Glass beads.

Figure 10 shows the results obtained for 48/60-1 fluidization tests. (The designation used throughout this work gives the mesh limits based on the Tyler standard series followed by the size distribution as defined by figure 9.) The test was repeated using four different bed weights, and the results show that bed weight has no effect on the shape of the ε-V plot. The incipient fluidization point also remained constant

as shown by the break-point in the pressure-drop curves. The only major effect of bed weight was on the point at which slugging was observed as shown below:

Bed weight. (gm)	300	500	700	1000
Slugging velocity (ft./min.)	None observed	60	45	40

In general, as the bed expanded beyond the point of fluidization, channelling was observed for a short range after which smooth bubbling was obtained. Depending on the bed weight, this gave way to either "boiling" or "slugging", or both, as the velocity was further increased. Towards the terminal velocity, a disperse phase developed above the bed, and at this point, bed height reading ceased to be significant and runs were terminated: This is usually shown by a deviation in the expansion curve (ε-V) due to low porosity values.

For the 48/60-1 tests, a linear log-log ε-V plot was obtained which extrapolated directly to the average terminal velocity at $\varepsilon = 1$. The dotted line in figure 10 is obtained from the particulate correlation (figure 34) for $(C_D Re^2)^{1/3} = 13.3$, and shows excellent agreement with the experimental line. However, this linear expansion curve and the apparent correlation with the particulate curve is later shown to be a coincidence, since the shape

of the ε -V curve is dependent on the particle diameter.

Expansion curves are plotted in figures 11,13,15 and 17 for the 5,10,25 and 100 fold size distributions, and all the results are compared with the 48/60-1 curve in figure 19. Between the point of fluidization and the start of elutriation, the experimental points can all be represented by the 48/60-1 expansion curve, and size distribution has no effect. The magnitude of these limits however, depends on the size distribution. The wider distributions contain smaller particles and hence the elutriation velocity at which fines are removed decreases as size distribution increases. In the 48/60-100 tests, fines were removed from the bed before fluidization was really established, although this had little effect on the shape of the expansion curve until larger fractions were removed, as can be seen in figure 17. The effect of size distribution on incipient fluidization is more complex. For 48/60-5 tests, the critical velocity was found to be lower, and the porosity ε_o was also reduced due to the interpacking of the finer particles amongst the larger ones. (The porosity obtained as the velocity was reduced to zero ($\varepsilon_{V \to 0}$) was found to decrease with increasing size distribution due to this interpacking effect.) In the tests with 10,25 and 100-fold distributions, segregation took place as the velocity was decreased, and the point of fluidization

ceased to have any significance. For the 10 and 25 fold distributions a pseudo-critical velocity could be obtained by rapidly reducing the velocity so that the bed settled before segregation could take place, but this has little practical value. Care must be taken when interpreting results obtained during segregation since the bed height and pressure drop become dependent on the rate of decrease of velocity: The amount of fines trapped in the segregated part of the bed obviously depends on the magnitude and frequency of the velocity changes. Segregation also occurs in these beds if the velocity is increased slowly. The small particles block the pore spaces in the bed and give rise to pockets of air which grow in size until they can break through the bed, and rise to the surface. The fines are carried upwards in these bubbles, and fluidize smoothly on the surface. The effect of segregation on the ε -V and pressure drop curves is clearly shown in figure 17. (ie. segregation causes a gradual change in the slope of the curves rather than a break-point.) A detailed study of segregation was not made in these tests, but from a study of the results obtained, it would seem that the segregation velocity (the velocity at which particles first segregate as the velocity is reduced.) increases as the size distribution increases. Segregation was not observed for distributions less than 5 - 6 fold.

The effects of static electricity were observed in all tests with glass beads. By careful control of the humidity of the fluidizing air, these effects could be minimised, but it is possible that the humidity had a separate effect on bed expansion as described below. In general static tended to maintain a denser bed due to inter-particle and particle-wall attractions. This latter effect became evident if the relative humidity fell below about 40%, when regular patterns of beads were observed on the column wall. It is believed that charged particles are attracted to the wall, discharge, and then pass back into the bed; some particles are therefore supported by the wall at any instant, and this could account for the reduction in pressure drop observed in these tests. In some tests with the wider size distributions, a rythmical bouncing motion of the bed was obtained; the amplitude of the fluctuations varied with velocity, but the period remained constant. By increasing the humidity of the air, the normal action of the bed was always resumed.

The humidity of the air had very marked effects on the action of the fluidized bed. Excessive moisture in the bed caused the particles to adhere very strongly, and always resulted in either severe channelling or severe slugging, depending on the superficial velocity in the

bed. The effect of humidity is readily seen in figure 17, Run 9b. Readings were taken for both 60% and 70% relative humidity, and it can be seen that in all cases, different bed densities were obtained. At lower velocities, readings for 70% R.H. could not be obtained since the bed settled, but good fluidization was obtained at the same velocities using 60% R.H. In fluidization tests the humidity was controlled such that static effects were minimised and humidity effects were also negligible; reproducible results could be obtained within the range 55 - 70 % R.H. in most tests.

(b) Char particles.

The expansion curves for the tests on char mixtures are shown in figures 20,21,23,24,25, and 27, and the results are essentially similar to those obtained for the glass beads. The closer agreement of the experimental data shown in figure 27 is probably due to the absence of static and humidity effects; dry air (30 - 50% R.H.) was used in these tests. Minimum fluidization porosities are much higher in the case of char, and the porosities obtained as the velocity was reduced to zero show only a small variation due to size distribution. Both these differences can be attributed to the irregular shape of the char particles. The slope V/ε is much

larger than the corresponding slope obtained from Zenz's particulate correlation for 48/60-1 char tests, and as will be seen later, this too is probably a shape effect. Segregation and elutriation limits are shown on the graphs, and bed behaviour in most cases was the same as that described for the glass beads.

Figure 27 again shows that size distribution has no effect on the shape of the ε-V curve for distributions of the same average size. The ε-V plot for the 48/60-1 char shows a definite curvature at higher porosities, and indicates that the shape of the expansion curve depends on the particle properties. It also indicates that the expansion curves for size distributions of any average diameter can be correlated by expansion curves for the single sizes of the same average diameter. This is further illustrated in a later section by a comparison of the expansion curves obtained from elutriation tests with the expansion curves obtained for single sizes, and it can be concluded that the average size of any distribution as defined by the log-probability scale can be used to describe the expansion curve for the bed by reference to the expansion curve for the same average sized particle. It should be noted however, that simple mixtures (ie. mixtures of only two or three different sizes in various proportions.)

cannot be represented on the log-probability scale as a continuous curve, and the reciprocal mean diameter as previously described must be used.

In general, the wider size distributions resulted in smoother fluidization, with channelling and slugging tendencies somewhat reduced, but little difference could be observed between the fluidization of the 10,25 and 100-fold distributions. Explanations of these observations are given by Matheson et.al.(32) who have shown that the addition of fines to closely sized beds results in better fluidization, and by Zenz (27) who has extended this to show that the maximum improvement of fluidization quality is obtained with about an eleven-fold size distribution.

3. CHANGES IN AVERAGE PARTICLE DIAMETER DUE TO ELUTRIATION.

It has been suggested (27) that an explanation of the differences between aggregative and particulate fluidization might lie in the interpretation of the particle diameter when dealing with beds of widely sized particles. Zenz found that he could apparently correlate his data for the fluidization of cracking catalyst by allowing for the changes in particle diameter

accompanying elutriation; the tests described here were designed to test this proposal.

Preliminary experiments showed that it was not possible, by direct observation, to follow the changes in the expansion characteristics of the bed as elutriation took place, since at the velocities involved the action of the bed was too violent to allow readings of the bed height to be taken. An indirect method was therefore developed, which consisted of :-

(a) the elutriation of the original charge at a chosen velocity.

(b) the determination of the expansion curve (ε-V) for the unelutriated part of the original bed.

(c) the analysis of the unelutriated part of the original bed.

This series of tests was repeated for various elutriation velocities and the expansion curves are shown on the graphs for the original mixtures. The analysis of the unelutriated portions were plotted as log-probability curves (figures 12,14,16,18,22 and 26.), and the average particle diameters were determined. These diameters were used with figure 7 to obtain the terminal velocities, and the expansion curves were then extrapolated through these points (ie. $\varepsilon = 1$, $V = V_T$.) The elutriation velocity was marked on each of these expansion curves

and the locus of the points represented the constructed expansion curve of the original bed, allowing for the changes in diameter due to elutriation. (See figures 11,13,15,17 and 21.) These curves show that a considerable amount of fines can be removed from a fluidized bed before any appreciable change in the expansion curve can be detected. This is especially true when dealing with pulverised materials, which usually contain a larger percentage of fines than predicted by a skew-normal distribution. They also show that changes in diameter will not be significant under normal fluidizing conditions even with the widest distributions of the skew-normal type.

Figure 32 shows the change in average diameter with increasing velocity for the four distributions of glass beads. The vertical line at $d_m = 271\ \mu$. represents 48/60-1 tests, and ends at the terminal velocity $V_T = 374$ ft./min. The results can be represented closely by straight lines, breaking from the $d_m = 271\ \mu$ line at velocities which decrease with increasing size distribution. The dotted lines on figure 32 show results calculated as follows:

(a) From figure 36 or 37, the diameter of the particle having a terminal velocity equal to the elutriation velocity used is calculated. (Any other graph of terminal velocities could be used here.)

(b) The size analysis of the original bed is modified to exclude all particles below this calculated diameter.

(c) The new distribution is plotted on log-probability co-ordinates and the average particle diameter is obtained.

An example of the calculated size analysis curve is shown in figure 16, and the results of the calculations for char and beads are summarised in table 8. Excellent agreement is shown, with the calculated values being from 1-4% lower than the experimental results.

The expansion curves for the elutriated beds show an increasing curvature as the average particle diameter increases, and these curves were found to deviate considerably from the curves obtained from the particulate correlation. To study these deviations further, tests on closely sized fractions were made, and showed that the shape of the expansion curve was dependent on the particle diameter (see later.) The curves presented for the unelutriated beds were drawn in after the single-size tests had been made and the nature of the deviations established.

4. <u>FLUIDIZATION TESTS</u>: <u>SINGLE SIZES</u>.

(a) Glass beads.

The results of the first test carried out (35/42-1)

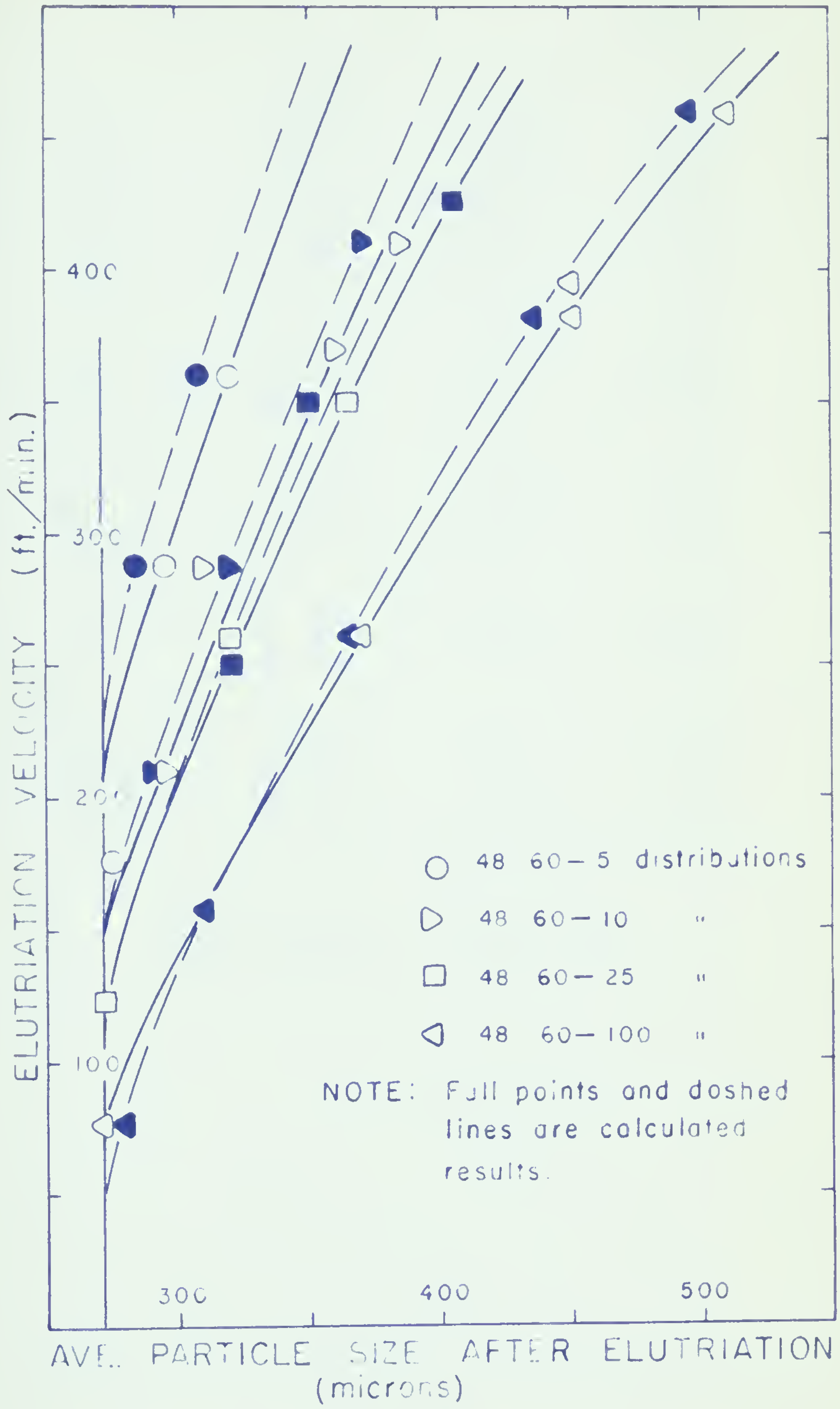
400
300
200
100
ELUTRIATION VELOCITY (ft./min.)
300
400
500
48 60 – 5 distributions
48 60 – 10 "
48 60 – 25 "
48 60 – 100 "
NOTE: Full points and dashed lines are calculated results.
AVE. PARTICLE SIZE AFTER ELUTRIATION (microns)

FIG. 32

TABLE 8.

Run No.	Expl. Ave. Dia.	E.V. ft/min	$\frac{(Re)^{1/3}}{(C_D)}$	$(C_D Re^2)^{1/3}$	Max.* Size Elutd.	Calcd. Ave. Dia.
9a	271	76	0.496	3.82	78.5	280
9a′	310	158	1.03	6.50	134	310
9a″	370	262	1.71	9.40	194	365
9a‴	450	382	2.50	13.0	268	435
9b′	450	395	2.58	13.2	272	435
9b″	510	460	3.00	15.8	326	495
8a′	320	250	1.63	9.0	185	320
8a″	365	350	2.27	11.9	243	350
8b″	405	425	2.76	14.2	291	405
7a′	295	210	1.38	7.85	161	290
7b″	310	288	1.90	10.10	207	300
7c′	385	410	2.70	14.0	287	370
4c′	295	287	1.86	9.95	195	283
4c″	320	360	2.34	12.2	250	308
3b′	300	150	1.29	7.8	213	290
3c′	360	222	1.90	11.6	317	360
11a′	302	116	1.01	6.25	167	305
12a′	350	117	1.02	6.30	169	350

* diameters in microns.

are shown in figure 28. This graph shows a definite deviation from the straight "particulate" line, and gave the first indication that the curvature obtained in the previous tests was a particle size effect. The results of run 7c′ are also plotted in figure 28 since this mixture had the same average size (385 μ), and good agreement is obtained. This suggests that the type of size distribution also has no effect on the shape of expansion (ε-V) curve, since mixture 7c′ was not of the skew-normal type as in former comparisons, and it indicates that the average size as defined by the log-probability scale will give satisfactory results for the size-distributions met in practice.

The results of the many tests on single sized glass beads are shown in figure 29. Bed weights of 500 gm. were used in most tests, and visual observations of the action in the beds are recorded on these expansion curves. Static and humidity effects were minimised as previously described, and the tests were terminated when a disperse-phase region formed above the bed. In general, good fluidization was established at some point C (ie. the end of the channelling zone) and slugging began at the point S. Channelling tendencies were observed to increase sharply with decreasing particle diameter (see figure 6), and this was characterised by a very slow increase in the porosity with increasing

velocity. This effect was so pronounced in tests with 250/325 mesh beads that reproducible results could not be obtained, since the slightest vibration of the equipment caused a change in the bed voidage at low velocities. Slugging tendencies increased as particle diameter increased; the smaller sizes did not show slugging, whereas the larger beads gave slugging and channelling points which were almost the same. (It should be noted that the slugging characteristics are also dependent on bed geometry and comparison here is only justified for similar bed heights.)

The most important observation shown in figure 29, and later in figure 30, is the considerable variation in the shape of the expansion curve for various particle diameters. The porosity increases rapidly at low velocities and slowly at high velocities for the larger sizes, whilst for sizes below about 48/60 mesh the opposite is true. Sizes close to 48/60 mesh seem unique in that their expansion curves represent a change-over in shape, and a linear ε-V graph results. This curve was discussed previously, and the correlation shown with the particulate "line" now seems coincidental. These systematic variations in the shape of the expansion curve account for the variations previously mentioned in the literature, and this work shows quite clearly

one of the reasons for the lack of correlation of expansion data for gas-solid systems. At the present time, no satisfactory explanation for the shape of these curves has been found, but it is felt that the variation in the "bubbling" action of the bed is a major factor: Further studies on the nature of bubble rise and growth will be needed to solve this problem.

Pressure drop curves for the tests with both beads and char are shown in figure 31: The calculated values of pressure drop were obtained by use of equation 5a.

(b) Char particles.

The results for the char tests are shown in figure 30, and in general the curves obtained are similar in shape to those for the beads; (the relative displacement is due to the differences in shape and particle density). Static and humidity effects were absent in these tests, and visual observations are recorded as before, and show the same trends. The change-over linear expansion curves for char seem to be obtained with sizes just greater than 35/42 mesh, as compared to 48/60 mesh for the glass beads: This difference is again probably due to differences in particle properties, since increasing particle density is known to favour slugging action, and at the same nominal diameter, this might well affect the shape of the expansion curve. As

previously mentioned, the slopes (ε/V) of the expansion curves for char are always less than the corresponding slopes for glass beads.

(c) General comments.

In all the tests reported here, the data were found to be reproducible within experimental limits of about $\pm 5\%$, irrespective of bed weight or motion: Smooth curves were extrapolated through the experimental points to cut the $\varepsilon = 1$ axis at the terminal velocity, as obtained from figure 7, and are shown dotted in the extrapolated regions. A close study of the data shows that the porosity values fall off rapidly as soon as disperse-phase conditions are established; this is due to the fact that readings of bed height do not include particles supported above the bed in the dispersed region, and hence a low average porosity value is obtained. Principles of disperse phase fluidization are not yet fully understood, but in general, the disperse-phase grows at the expense of the denser fluidized bed until all the particles in the bed have been dispersed and removed from the column; this region is shown by the dotted extrapolations of the expansion curves.

The expansion curves for aggregative fluidization are obviously non-linear, and the expansion process is so unlike particulate expansion that it would seem

certain that the two types could not be correlated by the same method. This is shown to be the case in figures 36 and 37, which are discussed in a later section.

5. THE POINT OF INCIPIENT FLUIDIZATION.

Defined by the co-ordinates (V_o, ε_o) this point is reasonably well defined for closely sized particles. The critical point is determined either by visual inspection of the bed or by the graphical construction method outlined on page 13: The critical porosity obtained by reducing the velocity to zero after fluidization ($\varepsilon_{V\to 0}$) is also used. The results obtained by these methods are shown in figure 6 and in tables 6 and 7. In most cases, excellent agreement is shown between the observed and calculated results, but $\varepsilon_{V\to 0}$ is always lower than ε_o by about 1 - 7%. It has already been mentioned that the settling point of a fluidized bed is very sensitive to static electricity, excessive moisture and vibrations, and caution is therefore advised in using data quoted in literature for conditions other than those specified.

The channelling porosities (ε_c), (obtained by visual observation of the column as the velocity was reduced) are also shown in figure 6, and range from 10 - 30% higher than the corresponding critical porosities

(ie. the percentage increases with decreasing size). These points represent the start of good fluidization.

The critical velocities for the char and beads are plotted (as Re_o) against the particle diameter (d_M) in figure 33, and show smooth curves embracing both the laminar ($Re < 1$) and transition regions. Values calculated by the methods of Van Heerden (23) and Leva (2) are also shown on this graph, and the results of the calculations are listed in table 9. The calculations based on the method of Leva use the fixed bed data shown in Appendix B. Calculations based on his original method (ie. using $f = 100/Re$ and an estimated shape factor λ.) give values of Re_o from 20 - 30% low, whereas the results based on actual fixed bed tests give much closer agreement. In general, the calculated results fall within the limits $\pm$ 30% of the experimental results.

The point of incipient fluidization for beds containing widely-sized particles is not clearly defined, and in most cases, does not exist. The results of tests with mixed sizes of beads and char are shown in tables 3 and 4. For distributions with less than a 5 or 6 fold variation in size, a critical point was observed, and good agreement is again obtained for both methods of observation. For wider size distributions, segregation was evident in all cases, and a list of segregation

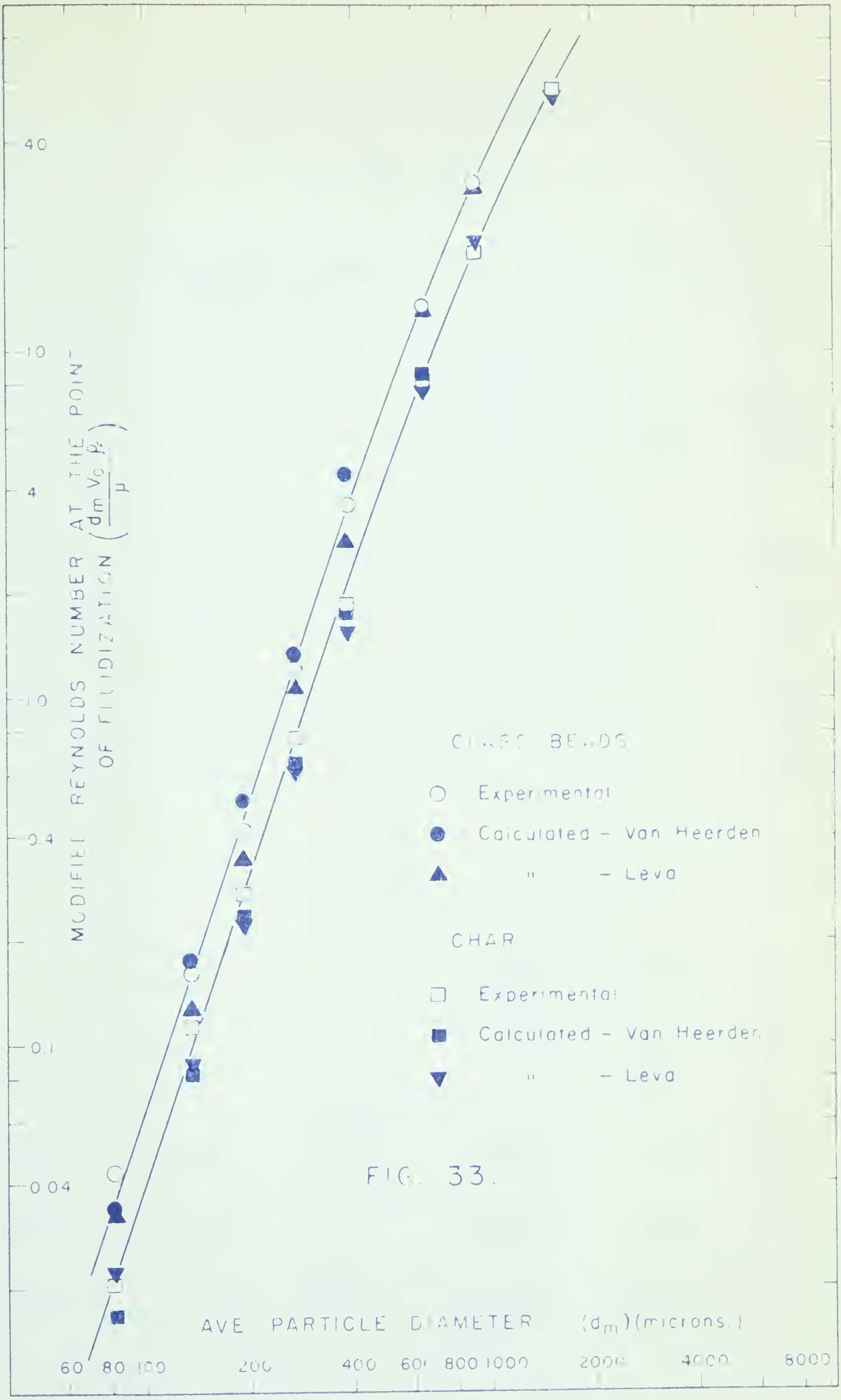
MODIFIED REYNOLDS NUMBER AT THE POINT OF FLUIDIZATION $\left(\frac{d_m V_0 \rho_f}{\mu}\right)$
40
10
4
1.0
0.4
0.1
0.04
GLASS BEADS
Experimental
Calculated - Van Heerden
" - Leva
CHAR
Experimental
Calculated - Van Heerden
" - Leva
AVE PARTICLE DIAMETER (dm)(microns.)
60
80
100
200
400
600
800
1000
2000
4000
8000

FIG. 33.

TABLE 9.

CRITICAL CONDITIONS.

Beads:

Size	EXPERIMENTAL Re_o (graphical) based on d_M	based on d_A	CALCULATED Re_o Van Heerden. based on d_e	Leva. based on d_M	Leva. based on d_A
16/20	31.1	31.9	-	31.0	32.0
24/28	13.4	13.4	-	14.0	13.5
35/42	3.62	4.00	4.47	3.20	3.62
48/60	1.21	1.25	1.35	1.20	1.18
65/80	0.42	0.44	0.51	0.39	0.40
100/115	0.16	0.17	0.178	0.144	0.15
170/200	0.0435	0.045	0.35	0.37	0.37

Char:

	based on d_M	based on d_e	based on d_m
10/12	57.8	-	57.0
16/20	19.3	-	20.4
24/28	8.44	8.56	7.74
35/42	1.82	1.80	1.55
48/60	0.78	0.06	0.61
65/80	0.28	0.24	0.22
100/115	0.11	0.084	0.088
170/200	0.021	0.017	0.022

velocities is therefore given. These are higher than the critical velocities for the same average particle size, although the point at which the whole bed was settled is of course lower depending on the minimum size present. A critical zone is therefore obtained in the case of wide size distributions, and this is clearly shown by the gradual change in the pressure drop obtained with decreasing velocity. None of the methods of calculating the critical velocity can be used in these cases to predict the segregation velocity, and the porosity of the bed depends entirely on the type of distribution (due to the variations in the inter-packing of the particles caused by various velocity changes), as is shown by the variation in the values of $\varepsilon_{v \to o}$ for distributions of the same average diameter. A method of calculating the critical porosity of any given size distribution has not been, and due to the number of complications, is not likely to be developed, and a direct experimental method must be used.

6. CORRELATION.

A brief review of the methods of correlation of fluidization data is given in part A of this thesis. The correlation to be tested here is that proposed by Zenz (27), and a smoothed plot of $(C_D Re^2)^{1/3}$ versus

SMOOTHED CORRELATION
FOR PARTICULATE FLUIDIZATION

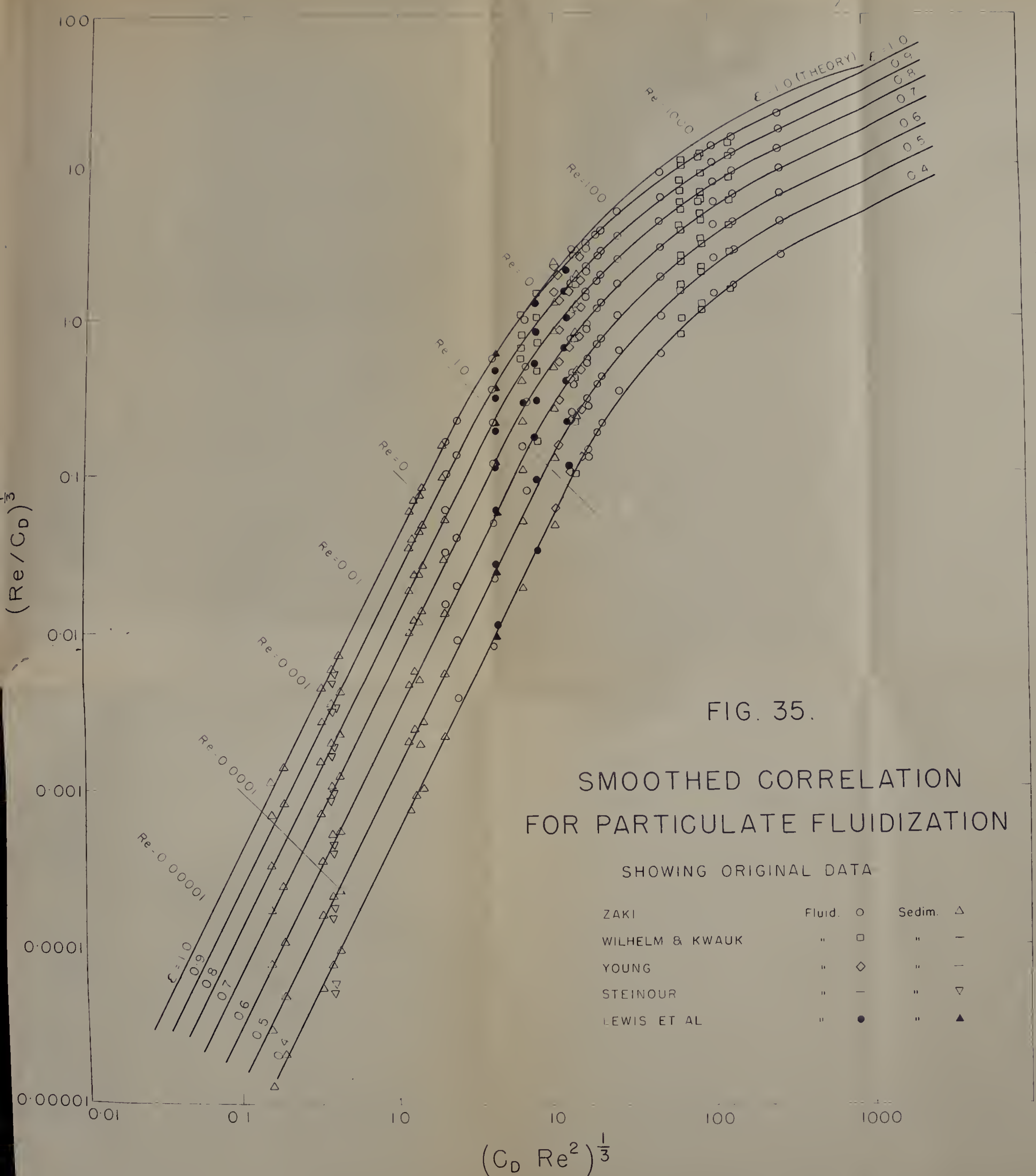

FIG. 35.

SMOOTHED CORRELATION FOR PARTICULATE FLUIDIZATION

SHOWING ORIGINAL DATA

$(Re/C_D)^{1/3}$ with bed porosity as parameter is shown for particulate fluidization in figure 34. This graph is exactly similar to that given by Zenz, but a more extensive range of data was used in obtaining these curves, the original data being shown in figure 35. (See also tabulated data in Appendix C.) It can be seen that the data used was obtained for both fluidization and hindered settling, and the correlation shows that these two processes are essentially the same. It should also be noted that the correlation shown in figure 34 is developed for particulate fluidization, and is only applicable to spherical particles. The dimensionless groups of the correlation are such that the product of the co-ordinates at any point gives the Reynolds number, and lines of constant Reynolds number are shown on the graphs. The line marked $\varepsilon = 1$ represents the standard drag coefficient for spheres, and the deviation shown between the fluidization data and this curve at high Reynolds numbers is discussed later.

Zenz used this particulate correlation as a basis for correlating the data obtained from the batch fluidization of cracking catalyst. He suggested that by allowing for the change in average diameter due to elutriation of the finer particles, and by introducing a shape factor, the data for a wide size distribution could be correlated on the particulate fluidization curves. (It should be

noted that the original paper (27) was in error in its method of shape factor adjustment. The shape factor J should be used as 1/0.52 rather than as reported (ie. $J = 0.52$) to give the desired effect.) Fluidization tests have shown that particle size distribution has no effect on the shape of the expansion curve until elutriation begins, after which the average diameter of the particles increases (ie. $(C_D Re^2)^{1/3}$ increases), and a correction must be applied as suggested by Zenz. However, tests on single sizes showed that the shape of the expansion curve for aggregative fluidization was dependent on the particle diameter, and was not linear as in the case of particulate fluidization. The results of these tests are compared with Zenz'z correlation in figures 36 and 37, and it can again be seen that considerable deviations exist. These graphs emphasise the rapid increase in bed porosity at low velocities for large particles, and show the very small changes of porosity at low velocities for the smaller sizes. The very large value of the slope V/ε for these small sizes is also shown, as would be expected, if the data of Zenz for a 60 micron catalyst are considered, and the spread of the data obtained is clearly due to both the size distribution (ie. elutriation) and to the small average diameter. The results shown in figures 36 and 37 show that the particulate correlation

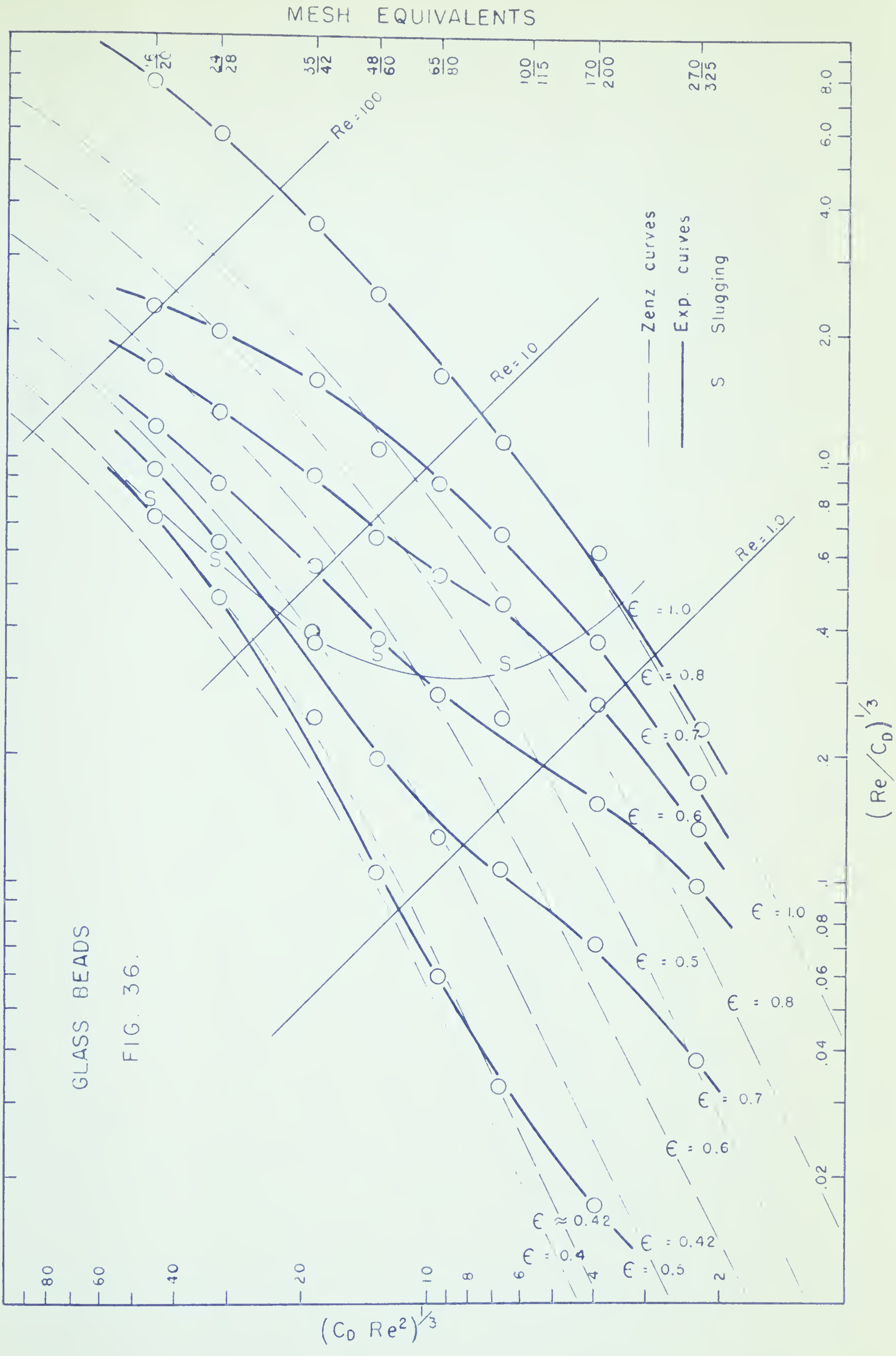
MESH EQUIVALENTS
16/20
24/28
35/42
48/60
65/80
100/115
170/200
270/325
Re = 100
Re = 10
Re = 1.0
Zenz curves
Exp. curves
S Slugging
ε = 1.0
ε = 0.8
ε = 0.7
ε = 0.6
ε = 0.5
ε = 0.42
ε ≈ 0.42
ε = 0.4
GLASS BEADS
FIG. 36.
(Re/C_D)^1/3
(C_D Re^2)^1/3

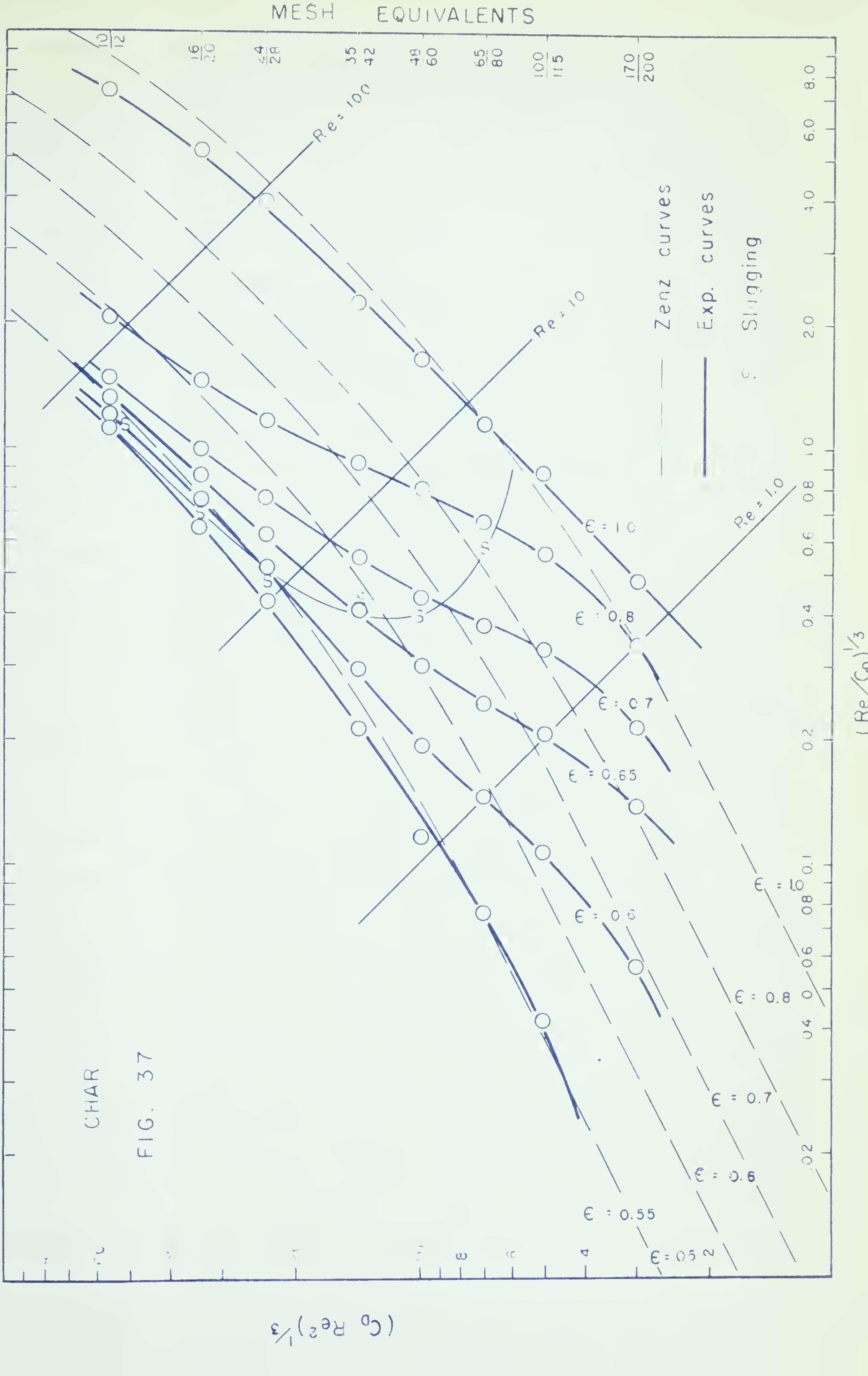
MESH EQUIVALENTS
10/12
16/20
24/28
35/42
48/60
65/80
100/115
170/200
Re = 100
Re = 10
Re = 1.0
Zenz curves
Exp. curves
Slugging
ε = 1.0
ε = 0.8
ε = 0.7
ε = 0.65
ε = 0.6
ε = 0.55
ε = 0.5
$(Re/C_D)^{1/3}$
$(C_D\ Re^2)^{1/3}$

CHAR

FIG. 37

cannot be used for predicting the expansion in aggregative fluidization, but it is interesting to note that the pattern of the expansion curves are very similar for both char and beads, and it is possible that a seperate system of curves could be obtained for gas/solid systems. The onset of slugging is also marked on each expansion curve in figures 36 and 37 and as observed by Becker (30), slugging seems to be the stable form of bed action in the transition zone of flow. Figure 38 shows a graph of the slope $n = V/\varepsilon$ versus the group $(C_D Re^2)^{1/3}$ (obtained from figure 36 by plotting values of against V and measuring the slope.) and also shows the calculated values of n according to the equations of Richardson and Zaki (28), with d_M/D_t set equal to 0.005. The agreement is excellent in the completely laminar and turbulent regions, but the calculated values are slightly lower in the transition region. The data of Presler (69) for magnesite and galena fluidized in water have also been plotted as ε-V curves and the slopes n are shown in figure 38. The shape of the curves obtained are similar for the three materials, and the value of n increases as the particle sphericity decreases; no correlation of shape effects has been attempted, since only a few materials have been studied, but the same trends are shown by the tests with char and beads (ie. the slope n is greater

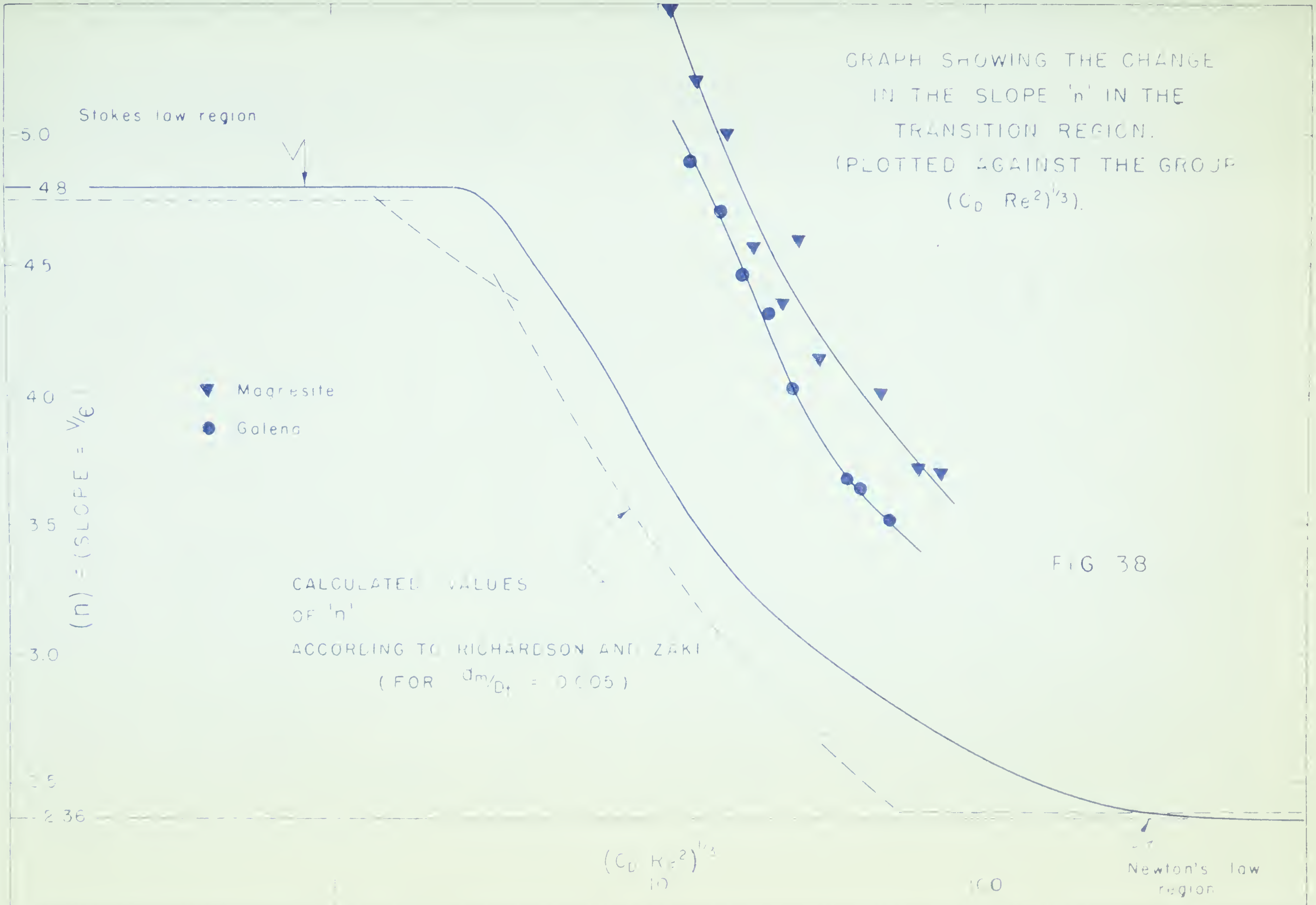

GRAPH SHOWING THE CHANGE IN THE SLOPE 'n' IN THE TRANSITION REGION. (PLOTTED AGAINST THE GROUP $(C_D\ Re^2)^{1/3}$).

FIG 38

for char than for beads.) even though the slope n is not a constant for aggregative fluidization. The effects of particle shape are also shown in figure 39, for high Reynold's numbers: The free-fall data of Hancock (35) and Needham and Hill (58) for mineral particles and of Pettyjohn and Christiansen (56) for regular non-spherical particles are plotted on the same co-ordinates as the particulate correlation, and it can be seen that the $\varepsilon = 1$ lines for non spherical particles fall below that for spheres, the deviation increasing with decreasing sphericity, and with increasing Reynolds number. The deviation between the standard drag curve for spheres and the $\varepsilon = 1$ line obtained from fluidization data for spheres is presumably due to these surface and shape effects as mentioned above.

Richardson and Zaki (28) are the only workers to have considered the effects of particle shape on the slope n, and considering only the turbulent region, they propose the equation:

$$n = 2.7\ k^{0.16} \quad \ldots\ldots\ldots\ldots (36)$$

where k is the volumetric shape factor of Heywood (55). Other workers have considered the effects of particle shape on the free-fall velocities (ie. $\varepsilon = 1$ line.) but no satisfactory correlation for irregular non-spherical

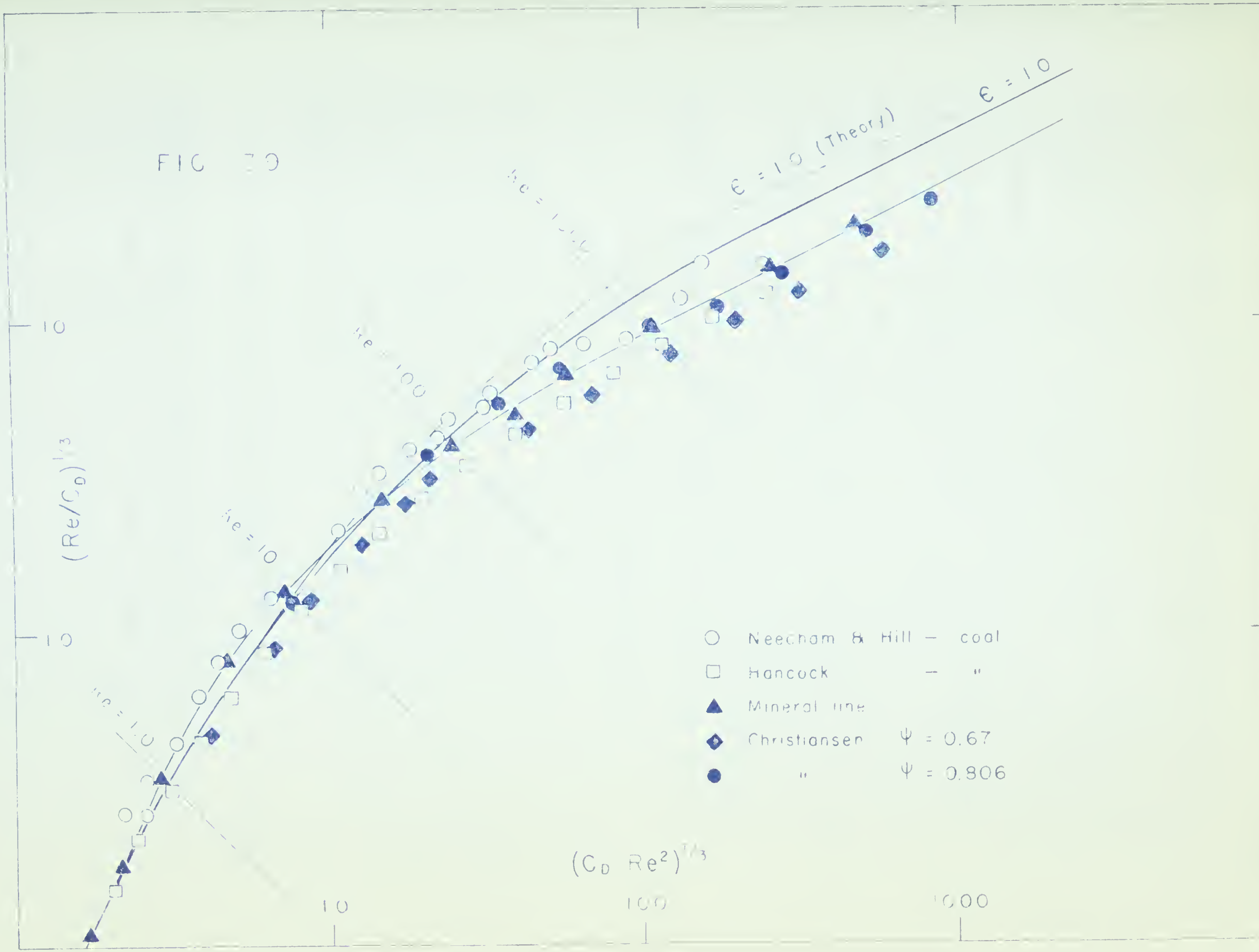

$\epsilon = 1.0$
$\epsilon = 1.0$ (Theory)
Re = 1000
Re = 100
Re = 10
Re = 1.0
$(Re/C_D)^{1/3}$
$(C_D\ Re^2)^{1/3}$
10
1.0
10
100
1000
Neecham & Hill – coal
Hancock – "
Mineral line
Christiansen ψ = 0.67
" ψ = 0.806

FIG 30

particles has yet been proposed.

From these considerations, it would seem that a simple shape factor could not be used to correlate the particulate fluidization of non-spherical particles on a system of curves as suggested by Zenz. A separate correlation would be necessary giving a shape correction factor versus the group $(C_D Re^2)^{1/3}$ with a simple shape factor such as sphericity as a parameter. This has been suggested by several workers, but at the present time, very little reliable data is available, and such a correlation cannot be made from a literature survey.

The correlation shown in figure 36 can be readily analysed in the laminar region, to give the equation:

$$(Re/C_D)^{1/3} = 0.041 \quad (C_D Re^2)^{2/3} \ \varepsilon^{4.75}$$

$$\text{or} \qquad C_D\,Re = 24\,\varepsilon^{-4.75} \qquad \ldots\ldots\ldots\ldots (37)$$

This agrees well with the standard equation for the free fall of spheres in the laminar region, (ie.) $C_D Re_T = 24$, and for spherical particles, this can be extended by the Schiller and Nauman equation to cover the transition region for $Re < 700$:

$$C_D\,Re = 24\,(1 + 0.15\,Re^{0.687})\ \varepsilon^{-n} \qquad \ldots (38)$$

where the index n is obtained either from figure 36 or is calculated from the equations of Zaki (28).

In the laminar region, a shape function (K) can be readily introduced as $C_D Re = 24/K$ and this can be obtained from the equations given by Pettyjohn and Christiansen (56) or others based on data for the free fall of isometric particles in a fluid, but in the transition zone, the shape function necessary is a complex function of particle shape and Reynolds number, and at the present time it must be determined from experimental results.

7. OTHER CORRELATIONS.

The data for single sizes of both glass beads and char have been considered by the methods of Leva et.al. (2) and of Lewis et.al. (16).

The method of Leva et.al. consists of plotting the group $60\ \mu V h/h_o = G\ \mu R/\rho_f$ against the porosity function $(1-\varepsilon)^2/\varepsilon^3$ on logarithmic co-ordinates, where R is the bed expansion ratio $= h/h_o$. From the resulting graphs, straight lines are drawn through the points and the slope m is measured; this is then plotted against the particle diameter as in figure 40. From this analysis, it was obvious that the graphs obtained tended to be increasingly curved as the particle diameter was decreased. The slopes m recorded in figure 40 are the slopes of the

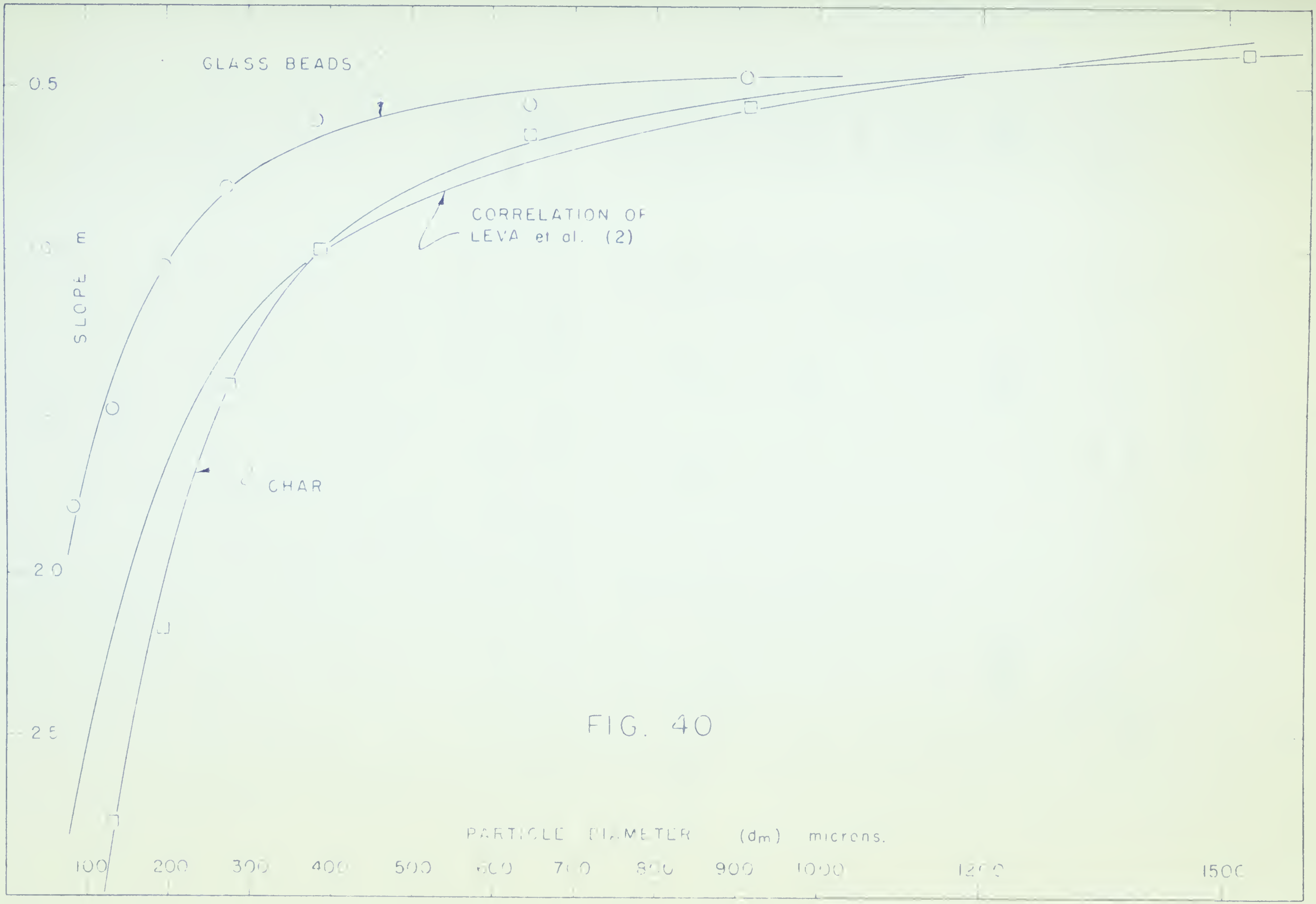
GLASS BEADS
CORRELATION OF
LEVA et al. (2)
CHAR
SLOPE m
0.5
2.0
2.5
100
200
300
400
500
600
700
800
900
1000
1200
1500
PARTICLE DIAMETER (dm) microns.

FIG. 40

TABLE 10.

Slope $|m|$ of the log-log graphs of $G \mu R/\rho_f$ versus $(1-\varepsilon)^2/\varepsilon^3$ for various sizes of char and beads.

SIZE	CHAR			BEADS		
10/12	0.392			-		
16/20	0.563			0.472		
24/28	0.650			0.552		
35/42	1.0	0.82		0.603		
48/60	1.42	0.88		0.805		
65/80	2.18	1.46	1.05	1.055	0.825	
100/115	2.78	1.59	1.08	1.50	1.086	0.83
170/200	5.54	1.81		1.80	1.067	

NOTE: For the smaller sizes, the curves obtained are approximated by straight lines, and the variation in $|m|$ is therefore shown.

lines drawn through the points of fluidization, and are only true for a very limited range of expansion. The curves were approximated by a series of straight lines, and the slopes are listed in table 10. For the larger sizes, the data showed some S-trends as described by Leva (2); this is readily explained by consideration of the ε-V curves, which also have the S-shape. Figure 40 shows that there is a difference between the data for beads and char, and this is probably a shape effect as described previouly. The line used by Leva is an average for many types of particles and does not take shape into consideration. A study of the original points on this line shows that the more irregular particles do give the higher negative slopes. In a recent publication (68), Leva explains the deviations $m < -1$ as being due to particle motion, (ie. kinetic energy at the expense of potential energy, therefore less bed expansion) and deviations $m > -1$ as being due to aggregation. These postulations are in agreement with the actions of the beds as observed in the present tests.

The correlation suggested by Lewis et.al. is similar to that used by Beranek (43) and both methods were tested. This involved log-log plots of $(V-V_o)/(V_T-V_o)$ against $(\varepsilon - \varepsilon_o)/(1- \varepsilon_o)$, where the subscript 'o' refers to the point of fluidization and the 'T' refers to terminal

conditions. The data plotted in this manner gave a series of lines passing through the point (1,1,), and tending to be parallel and straight at lower values of expansion. Some of the lines also crossed each other in these lower regions, and the data were therefore replotted using the channelling points in place of ε_o and V_o in the co-ordinates. The resulting curves were similar in shape, but the crossing of the lines was eliminated, and a consistent variation with particle diameter was obtained. This is not in agreement with the results of Beranek who found a single line correlation for particulate conditions. By introducing the term $d_M^{1/2}$ as a multiplier of $(V-V_o)/(V_T-V_o)$, the lines could be brought into much closer agreement. This is similar to the correlation of Lewis et.al., but its main drawback is that the lines cut the $\varepsilon = 1$ line at $d_M^{1/2}$, and above $\varepsilon = 0.8$, there is considerable divergence of the data to these limits. This method of correlation also expands the region of low porosity and compresses the region of high porosity, and since the experimental accuracy decreases as the porosity decreases, considerable scatter of the data is obtained; in general, it can be said that this method of correlation is not satisfactory. It seems likely that the multiplier $d_m^{1/2}$ should better be replaced by some function of the

characteristic velocities v_T and V_o . This was attempted, but since the data covers both laminar and turbulent regions, no reasonable alternative could be found.

Equation 3 as proposed by Ergun (8) was also tested, but the equation gave ε-V curves which were linear, and good agreement was obtained only for the 48/60 glass beads. It is likely that this equation could be used to predict bed expansion for liquid-solid fluidization since linear ε-V graphs are obtained in this case.

E. CONCLUSIONS.

(1). Equations for calculating critical velocities are only accurate within about ± 30%. Values of critical bed porosity should be obtained from direct experiment, visual observation of the settling point being a satisfactory method.

(2). Segregation occurs with size distributions greater than about 6-fold. No method of calculating this segregation velocity is known. The bed porosity for size mixtures depends on the type of distribution, and cannot be calculated.

(3). The shape of the expansion curve (log-log ε -V graph.) for aggregative fluidization is dependent on particle diameter, being in general non-linear.

(4). Size distribution has no effect on the shape of the expansion curve (ε -V) above the point of good fluidization and below the point of elutriation, for beds of the same average diameter as defined by the log-probability scale.

(5). The change in the average diameter of a bed of particles of wide size distribution due to elutriation can be calculated with better than 5% accuracy from a knowledge of the terminal velocity data for the material involved.

(6). Large quantities of fines can be removed from a fluidized bed of particles of wide size distribution before any change in the average diameter or expansion curve can be detected.

(7). Static electricity has a considerable effect on fluidization in some gas-solid systems. In general, a decrease in bed porosity results due to particle-wall attractions.

(8). Excessive moisture in a gas fluidized bed must be avoided. Slugging and channelling are both greatly increased by excessive humidity of the fluidizing gas.

(9). There are no really satisfactory correlations available at the present time for aggregative fluidization. The particulate correlation suggested by Zenz cannot be used to correlate the data from gas-solid systems.

(10). The particulate correlation suggested by Zenz gives good results for the fluidization and hindered settling of spherical particles in liquids.

(11). For non-spherical particles, the Zenz correlation must be modified. It cannot be used by the inclusion of a simple shape factor into the co-ordinates, since the shape function varies with Reynolds number and particle size.

(12). The correlation of Leva for fixed beds gives good

correlation of the data for pressure drop through beds of char and coal particles. Some evidence of a particle orientation effect is shown.

F. FUTURE WORK

From considerations of the present studies, it would seem that future work should be directed towards a study of the bubbling characteristics in aggregative fluidization. Some recent papers have briefly considered this, but no correlations have been proposed.

Further studies on the hindered settling and particulate fluidization of irregular particles are also needed to extend the present solid-liquid correlations to cover all types of solids.

TABLE OF NOMENCLATURE.

A	Cross-sectional area of the bed.	$ft.^2$
A_n	Projected area of the particle.	$ft.^2$
A_o	Cross-sectional area of the orifice.	$ft.^2$
A_p	Surface area of the particle.	$ft.^2$
A_s	Surface area of the sphere of the same. volume as the particle.	$ft.^2$
B	Generalised particle shape factor.(23)	-
C_D	Drag coefficient.	-
C_o	Orifice discharge coefficient.	-
d_p	Particle diameter.	ft.
d_s	Spherical diameter (ie. diameter of the sphere with the same volume as the particle)	ft.
d_e	Equivalent particle diameter.(23)	ft.
d_A	Microscopic particle diameter.	ft.
d_n	Diameter of the circle having the same projected area as the particle.	ft.
d_m	Average sieve diameter of the particle.	ft.
D_o	Orifice diameter.	ft.
D_t	Column diameter.	ft.
E	Fluidization efficiency.(2)	-
E.V.	Elutriation velocity.	ft./min.
f	Friction factor.(defined in text.)	-
F	Function of.	-
g	Gravitational acceleration.	$ft./sec.^2$
G	Superficial mass velocity.	$lb./ft.^2 sec.$
G_o	Superficial mass velocity at the point of fluidization.	$lb./ft.^2 sec.$

h or L	Bed height.	ft.
h_o or L_o	Bed height at the point of fluidization.	ft.
k	Particle shape factor according to Heywood. ($k = \overline{V}_p / d_n^3$)	-
K	Volume shape factor. ($K = \overline{V}_p / d_M^3$)	-
K'	Volume shape factor. ($K' = (6K/\pi)^{1/3}$)	-
K_B	Dimensionless group = $C_D Re^2$ (Becker (30))	-
$K_{\Delta\rho}$	Dimensionless group (Wilhelm and Kwauk. (15))	-
l_e or R	Bed expansion ratio.	-
m	Slope of correlation proposed by Leva (2).	-
n	Slope V/ε .	-
$\bar{n}$	Number of particles/gm.	-
N	Number of particles per unit volume of bed measured at point of fluidization.	-
N_K	Drag number (Becker (30).)	-
P_A	Recorded air pressure.	mm.Hg.
P_2	Pressure downstream from orifice.	mm.Hg.
q	State of flow factor (Leva (2).)	-
Q_S	Volumetric flow rate (60°F. 760 mm.Hg.)	ft^3./min.
R.H.	Relative humidity of air supply.	%
Re	Modified particle Reynolds number.	-
Re_o	Modified particle Reynolds number at the point of fluidization.	-
Re_t	Terminal point of fluidization.	-
S_v	Surface area/unit volume of particles.	ft^{-1}
T_A or T_1	Temperature of air.	°R.
V	Superficial velocity.	ft./min.

V_o	Superficial velocity at the point of fluidization.	ft./min.
V_t	Terminal velocity.	ft./min.
$\overline{V}_p$	Particle volume.	$ft.^3$
W	Bed weight.	lb.
Z_s	Apparent weight of the particle (allowing for bouyancy.)	lb.
Δh	Manometer differential pressure.	cm. water
Δp	Pressure drop.	$lb./ft.^2$
ε	Average bed porosity.	-
ε_o	Average bed porosity at the point of fluidization.	-
$\varepsilon_{v\to o}$	Average bed porosity when the velocity is reduced to zero.	-
ε_c	Average bed porosity at the channelling point.	-
λ	Particle shape factor. (Leva (2).)	-
ϕ	Sphericity $= A_s/A_p = 1/\lambda$	-
ψ	'Form' sphericity. $= \pi d_s^2 / A_n$.	-
μ	Fluid viscosity.	lb./ft.hr.
ν	Fluid kinematic viscosity.	$ft.^2/hr.$
ρ_f	Fluid density.	$lb./ft.^3$
ρ_A	Air density.	$lb./ft.^3$
ρ_s	Particle density.	$lb./ft.^3$
ρ_{bo}	Bed density at the point of fluidization.	$lb./ft.^3$
Ar	Archimedes' criterion. $Z_s / \rho_s \nu^2$.	-
Ω	Criterion of similarity $V_t^3 \rho_f / \varepsilon \nu (\rho_s - \rho_f)$	

BIBLIOGRAPHY

1. D'Arcy, H.P.G., Les Fontaines Publique de la Ville de Dijon. Paris, (1856).

2. Leva, M., Weintraub, M., Grummer, M., Pollchik, M., Storch, H.H., Fluid Flow through packed&fluidized systems, U.S.B.M., Bull. 504, (1951).

3. Blake, F.C., Trans. A.I.Ch.E., 14, 415, (1922).

4. Chilton and Colburn. Trans. A.I.Ch.E., 26, 178-196, (1931).

5. Carman, P.C., Trans. Inst. Ch.E., (Lond.), 15, 150, (1937).

6. Ibid, Nature, 160, 301, (1947).

7. Kozeny, J., Sitzber. Akad. Wiss. Wien, 136, 11a, 217, (1927).

8. Ergun, S., Chem. Eng. Prog., 48, 89-94, (1952).

9. Brownell, L.E., Katz, D.L., Flow of fluids through porous media, Part 11., Chem. Eng. Prog., 43, 601, (1947).

10. Furnas, C.C., U.S.B.M., Bull. 307, (1929).

11. Rose, H.E., Proc. Inst. Mech. Engrs., 153, War Emergency issue No 5., 141-161, (1945).

12. Barclay, K.M., Wright, C.C., Walker, P.L., Bull. of the Mineral Industries Exp. Station Proceedings of the Anthracite Conference,(Oct. 1956), 29.

13. Parent, J.D., Yagol, N., Steiner, C.S., Chem. Eng. Prog., 43, 429, (1947).

14. Williamson, R.H., Garside, J.E., Inst. Gas Eng. Comm. 345.

15. Wilhelm, R.A., Kwauk, M., Chem. Eng. Prog. 44 201, (1948).

16. Lewis, W.K., Gilliland, E.R., Bauer, W.C., Ind. Eng. Chem., 41, 1104, (1949).

17. Toomey, R.D., Johnstone. H.F., Chem. Eng. Prog., 48, 220, (1952).

18. Ergun, S., Orning, A.A., Ind. Eng. Chem., 41, 1191, (1949).

19. Sinclair, C.G., Robinson, D.B., Can. J. of Ch.E., 36, 53, (1958).

20. Baerg, A., Klassen, J., Gishler, P.E., Can. J. Res., 28F, 287, (1950).

21. Agarwal, O.P., Storrow, J.A., Chem. and Ind., 278, (1951).

22. Jolley, L.J., Stanton, J.E., J. App. Chem., 2, 562, (1952).

23. Van Heerden, C., Nobel, A.P.P., Van Krevelen, D.W., Chem. Eng. Sci., 1, 37, (1951).

24. Miller, C.O., Logwinuk, A.K., Ind. Eng. Chem., 43, 1221, (1951).

25. Sinclair, C.G., M.Sc. thesis, Chem. Eng. Dept., U.of A. (1956).

26. Leva, M., Can. J. Chem. Eng., 35, 71, (1957).

27. Zenz, F.A., Petroleum Refiner, 36,147-155, (1957).

28. Richardson, J.F., Zaki, W.N., Trans. Inst. Chem. Eng., 32, 35-53, (1954).

29. Pinchbeck, P.H., Popper, F., Chem. Eng. Sci., 6, 57- 64, (1956).

30. Becker, H.A., M.Sc. thesis, Dept. of Chem. and Chem. Eng., U.of Sask., (1955).

31. Johnson, E., Inst. Gas Eng. Res. Fellowship Report Pub., 378/179, (1950).

32. Matteson, G.L., Herbst, W.A., Holt, P.H., Ind. Eng. Chem., 1099, (1949).

33. Leva, M., Shirai, T., Wen, C.Y., Genie Chem. 75, 33, (1956).

34. Hancock, R.T., Mining Mag., 55, 90, (1936).

35. Hancock, R.T., Ibid, 67, 179, (1942).

36. Hirst, A.A., Trans. Inst. Min. Engrs., 85, 236, (1932-33).

37. Hancock, R.T., Coke and Gas, 11, 386, (1949).

38. Steinour, H.H., Ind. Eng. Chem., 36, 618, (1944).

39. Morse, R.D., Ind. Eng. Chem., 41, 1117, (1949).

40. Jottrand, R., J. App. Chem., 2, 517, (1952).

41. Young, R.J., Ibid, 2, 855, (1952).

42. Lapple, C.E., Shepherd, C.B., Ind. Eng. Chem., 32, 605-17, (1940).

43. Beranek, I.J., Brit. Chem. Eng., 3, 358, (1958).

44. Wilhelm, R.H., Rice, W.J., A.I.Ch.E., 4, 423, (1958).

45. Yasui, G., Johanson, L.N., A.I.Ch.E., 4, 445, (1958).

46. Furukawa, J., Ohmae, T., Ind.Eng. Chem., 50, 821, (1958).

47. Leva, M., Chem. Eng. Prog., 47, 39, (1951).

48. Osberg and Charlesworth, Chem. Eng. Prog., 47, 566, (1951).

49. Hyman, D., Sc. D. Thesis, M.I.T., Dept. of Chem. Eng., (1952).

50. Richards, Ibid, (1954).

51. Lang, P.M., Ibid, (1955).

52. Gregory, S.A., J. App. Chem., 2, S1. (1952).

53. Zenz, F.A., Weil, N.A., A.I.Ch.E. Journal, 4, 472, (1958).

54. Wadell, H., J. Franklin Inst., 217, 459, (1934).

55. Heywood, H., Proc. Inst. Mech. Engrs., (Lond.) 140, 257, (1938).

56. Pettyjohn, E.S., Christiansen, E.B., Chem. Eng. Prog., 44, 157, (1948).

57. Herss, J.F., Coull, J., Chem. Eng. Prog., 48, 133, (1952).

58. Needham, L.W., Hill, N.W., Fuel, 26, 101, (1947).

59. Becker, H.A., Can. J. Chem. Eng., 37, 85, (1959).

60. Jacobs, J.K., Minet, R.G., United Engrs. and Constructors Inc., Philadelphia, Pa., (1956).

61. Lewis, E.W., Bowerman, E.W., Chem. Eng. Prog., 48, 603, (1952).

62. Zenz, F.A., Petr. Refiner, 36, 261, (1957).

63. Trawinski, H., Chem. Ing. Tech., 25, 201-3, 229-38, (1953).

64. Bakker, P.J., Heertjes, P.M., Brit. Chem. Eng., 3, 240, (1958).

65. Ergun, S., Anal. Chem., 23, 151, (1951).

66. Brown, Unit Operations, 13, 158, Equ. 103.

67. Sherlock, E., R.C.A. report, M.Sc. Thesis, Studies on some properties of Alberta coals, (1949).

68. Leva, M., Fluidization, Chem. Eng. Series, McGraw Hill, (1959).

69. Presler, A.F., Ph.D. Thesis, Iowa State College, (1956).

APPENDIX A.

Flow Equations for the Orifice Meter.

01. $D_o = 0.037$ in.

$$Q_s = 0.010 \sqrt{\Delta h \, P_2 / T_1}$$

02. $D_o = 0.0781$ in.

$$Q_s = 0.0421 \sqrt{\Delta h \, P_2 / T_1}$$

03. $D_o = 0.1875$ in.

$$Q_s = 0.242 \sqrt{\Delta h \, P_2 / T_1}$$

04. $D_o = 0.300$ in.

$$Q_s = 0.625 \sqrt{\Delta h \, P_2 / T_1}$$

05. $D_o = 0.500$ in.

$$Q_s = 1.66 \sqrt{\Delta h \, P_2 / T_1}$$

where:

Q_s = cu.ft./min. at 60°F. 76 cm.Hg.

Δh = inches of water.

P_2 = p.s.f.a.

T_1 = °R.

APPENDIX B.

FIXED-BED EXPERIMENTS.

1. APPARATUS.

The column used for these experiments was made from a 2 inch I.D. lucite tube, 30 inches long. The tube was split at its mid-point, and a screen and supporting disc were held between the two ends by a screwed sleeve which formed a union with the two halves of the column. This column replaced the fluidizing column, and arrangements were made so that air could be passed upwards or downwards through the bed. All other details of the apparatus are as described for the fluidization apparatus.

2. PROCEDURE.

A known weight of material was charged to the column and packed to the desired height. The flow of air through the bed was then increased (step-wise.), and readings were taken until the maximum pressure drop was reached in the apparatus. (Limited by the size of the mercury manometer used.) The readings taken are the same as those listed for the fluidization experiments (p. 64), pressure drop readings being taken on water or mercury manometers depending on the flow rate used.

3. RESULTS AND CALCULATIONS.

The results of the tests are shown in figures 41 and 42 as graphs of the friction factor f versus the modified Reynolds number $d_p \rho_s V/\mu$. Figure 41 shows graphs for glass beads, char and coal particles, and the results are calculated on the basis of the average particle diameter d_M. This graph also shows the correlations of Leva et.al. (2) and Lewis et.al. (16) for spherical particles. Figure 42 shows the results of the tests on glass beads based on the average microscopic diameter d_A. For these results, the porosity ε is calculated from the expression:

$$\varepsilon = 1 - \frac{\frac{W}{454} \times 12}{62.4 \times \rho_s \times L \times .0221}$$

or

$$\varepsilon = 1 - 0.192 \frac{W}{\rho_s L}$$

where W = weight of the bed (gm).

ρ_s = density of the particles (gm/cc).

L = height of the bed (inches).

The friction factor is then calculated directly from the

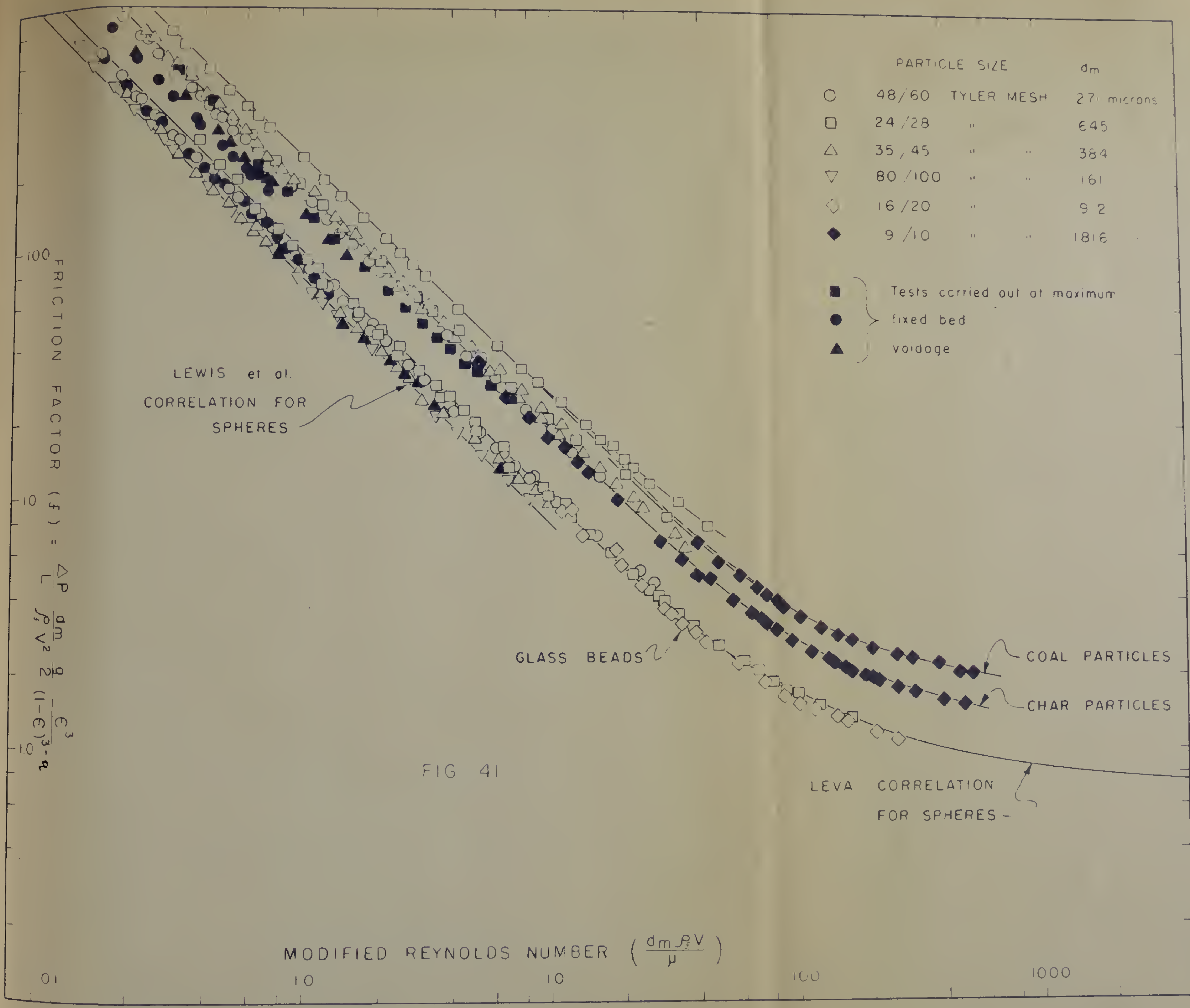
PARTICLE SIZE dm
48/60 TYLER MESH 271 microns
24/28 " 645
35/45 " " 384
80/100 " " 161
16/20 " 912
9/10 " " 1816
Tests carried out at maximum fixed bed voidage
LEWIS et al. CORRELATION FOR SPHERES
GLASS BEADS
COAL PARTICLES
CHAR PARTICLES
LEVA CORRELATION FOR SPHERES
FRICTION FACTOR (f) = $\frac{\Delta P}{L} \frac{dm}{\rho_f V^2} \frac{g}{2} \frac{\epsilon^3}{(1-\epsilon)^{3-a}}$
MODIFIED REYNOLDS NUMBER $\left(\frac{dm \rho_f V}{\mu}\right)$
100
10
1.0
01
10
10
100
1000

FIG 41

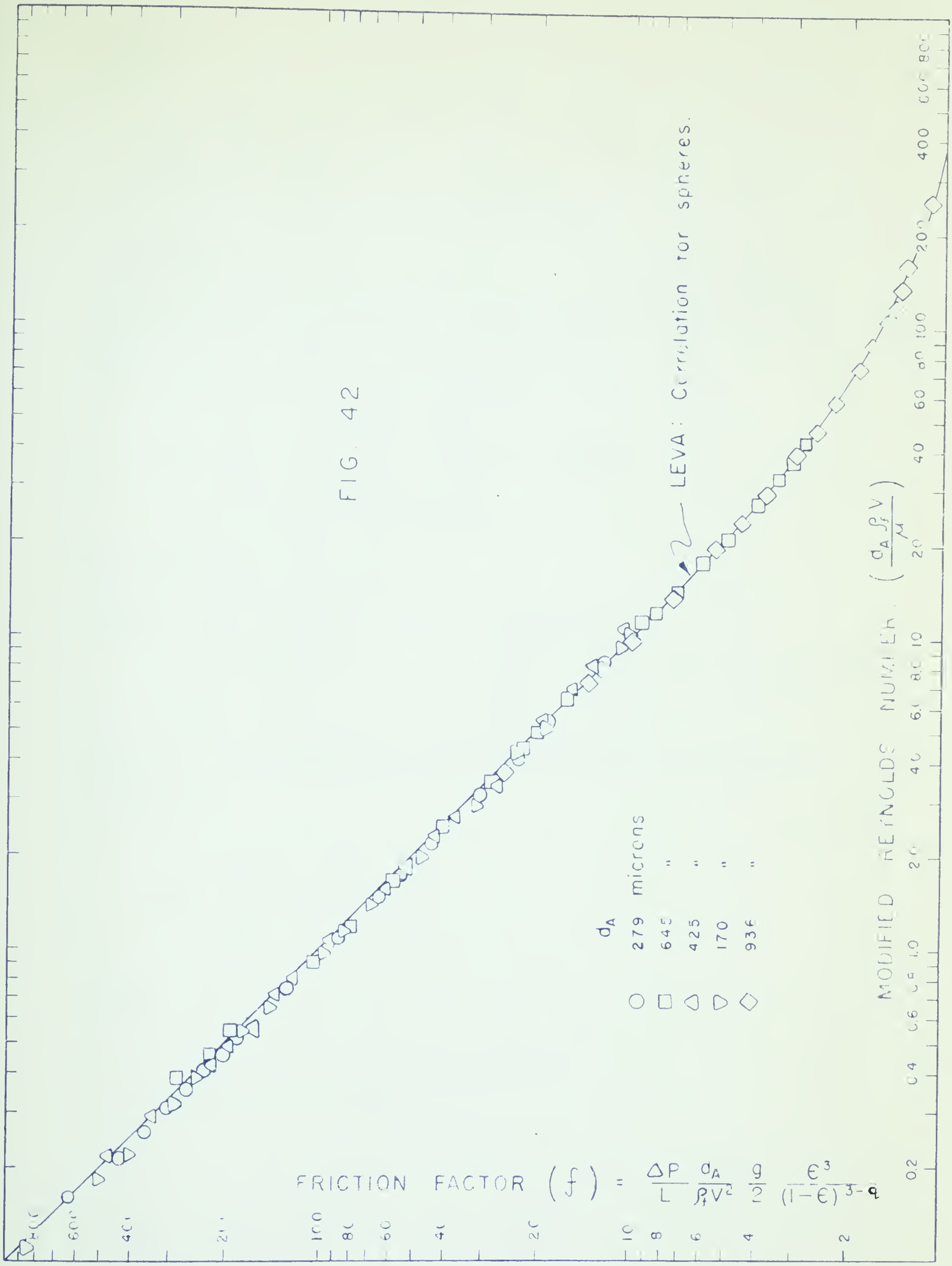
FIG. 42
LEVA: Correlation for spheres.
d_A
○ 279 microns
□ 645 "
△ 425 "
▷ 170 "
◇ 936 "
FRICTION FACTOR $(f) = \frac{\Delta P}{L} \frac{d_A}{\rho_f V^2} \frac{g}{2} \frac{\epsilon^3}{(1-\epsilon)^{3-q}}$
MODIFIED REYNOLDS NUMBER $\left(\frac{d_A \rho_f V}{\mu}\right)$

equation:

$$f = \frac{\Delta P}{L} \quad \frac{d_M}{\rho_f V^2} \quad \frac{g}{2} \quad \frac{\varepsilon^3}{(1-\varepsilon)^{3-q}}$$

where the index q is obtained from a plot of Re vs. q given by Leva et.al (2). In the case of laminar flow (when q = 1), this equation reduces to:

$$f = \frac{d_m}{L} \quad \frac{\varepsilon^3}{(1-\varepsilon)^2} \quad \frac{\Delta P}{Q_S^2} \quad \frac{P_A}{T_A} \quad x \quad (.0278)$$

for the tests described,

where: d_M = microns. ΔP = cm.Hg.

L = inches. Q_S = cu.ft./min. at S.T.P.

T_A = $^\circ$R. P_A = mm.Hg.

Similarly, the Reynolds number is calculated from the equation:

$$Re = \frac{6.81}{10^4} \quad x \quad \frac{d_m Q_S}{\mu}$$

where: d_M = microns.

Q_S = cu.ft./min. at S.T.P.

μ = lb./ft.hr.

From the graphs, we have, at Re = 1.0 for beads f = 95, for char f = 180 and for coal f = 245.

therefore for char $\lambda^2 = \dfrac{180}{95} = 1.90$

therefore $\underline{\lambda_{(char)} = 1.38}$

for coal $\lambda^2 = \dfrac{245}{95} = 2.58$

therefore $\underline{\lambda_{(coal)} = 1.61}$

This assumes that the beads have a shape factor $\lambda = 1$. It should be noted that $\lambda \equiv 1/\phi$, therefore ϕ(char) = 0.725 and ϕ(coal) = 0.622. The experimental results obtained from these experiments are tabulated in appendix C in a copy of this thesis at the Research Council of Alberta, Edmonton.

APPENDIX C.

CALCULATIONS.

A brief summary of the methods of calculation of the experimental results is reported here. The readings taken during a run are listed on p.64.

(a) FLOW RATE.

The group $\dfrac{\Delta h\ P_2}{T_1} = \dfrac{2116}{2.54} \times \dfrac{P_A}{760} \times \dfrac{\Delta h}{T_A}$ is calculated

where: P_A = mm.Hg. (taken as atmospheric pressure plus
T_A = °R the static pressure at the base of
Δh = cm.H_2O the column.)

from figure 3 (p.55.), the flow rate Q_s is obtained directly in cu.ft./min. at standard conditions.

The superficial velocity based on the whole cross-section of the column is then calculated by:

$$V = Q_s \times \frac{T_A}{P_A'} \times \left(\frac{0.0808}{A} \times \frac{760}{520} \right)$$

where: V = ft./min.
T_A = °R
A = ft.^{2} = cross sectional area of the column.

and $P_A' =$ mm.Hg. (taken as atmospheric pressure plus half the static pressure at the base of the column.

(b) BED POROSITY.

This is calculated directly from the properties of the particles, by the equation:

$$\varepsilon = 1 - \frac{W}{454} \Big/ \frac{62.4}{12} \rho_s \, h \, A.$$

where: W = weight of the bed (gm).

h = height of the bed (inches).

A = cross-sectional area of the bed (ft.^{2}).

ρ_s = apparent density of particles (gm/cc.).

(c) EQUIVALENT PARTICLE DIAMETER. (d_e)

As defined by Van Heerden et.al.(23), we have

$$\frac{N \pi d_e^3}{6} = 1 - 0.406$$

or $d_e = 1.043 / N^{1/3}$

where: N = number of particles/per unit volume of bed at maximum porosity and 0.406 is taken as the maximum porosity of a bed of spheres.

From this, if $\bar{n}$ = number of particles/gm. and ρ_{bo} = the density of the bed at maximum porosity (equivalent to ε_o) then $N = \bar{n}\rho_{bo}$

therefore $d_e = 1.043\ (\bar{n}\ \rho_{bo})^{1/3}$

ρ_{bo} could be calculated from the relationship

$$\varepsilon_o = 1 - \left(\frac{\rho_{bo}}{\rho_s}\right)$$

where ρ_{bo} and ρ_s are measured in the same units (gm./cc.).

TABULATIONS.

The results of the fluidization runs are listed* in the following tables, and have been calculated as described in this appendix.

The units are as follows:

ρ_s . . .	gm./cc.	T_A . . .	°F
ρ_f . . .	lb./ft.^{3}	R.H. . . .	%
μ . . .	lb./ft.hr.	h . . .	inches.
P_A . . .	mm.Hg.	ΔP . . .	cm.H_2O.
V . . .	ft./min.	E.V. . . .	ft./min.

All symbols and abbreviations are defined on page 154.

* The runs are tabulated in numerical order, this being the order in which the tests were made.

Co-ordinates for particulate type correlation (Zenz.)

for fluidization tests.

Run	$(C_D Re^2)^{1/3}$	$(Re/C_D)^{1/3} x10^3$	Run	$(C_D Re^2)^{1/3}$	$(Re/C_D)^{1/3} x10^3$
1a	13.2	6.48V	8a′	15.5	6.50V
1b	13.4	6.60V	8a″	17.7	6.45V
1c	13.2	6.50v	8b′	15.5	6.48V
1d	13.2	6.50V	8b″	19.7	6.53V
1e	13.2	6.50V	9a	13.3	6.55V
2a	10.0	8.62V	9b	13.3	6.59V
2b	10.0	8.62V	9a,	-	-
3a	10.0	8.62V	9a′	15.1	6.52V
3b	10.0	8.62V	9a″	18.0	6.54V
3c	10.[illegible]	[illegible].75V	9a‴	21.8	6.50V
3b′	11.1	8.57V	9b′	21.8	6.50V
3c′	13.25	8.57V	9b″	-	-
4a	13.3	6.55V	10a	10.0	8.70V
4b	13.3	6.55V	11a	10.0	8.75V
4c	13.25	6.51V	11a′	11.2	8.67V
4c′	14.4	6.52V	12a,	9.95	8.75V
4c″	15.4	6.49V	12a′	13.0	8.65V
5	14.1	8.59V	13	7.07	8.61V
6	18.8	6.66V	14	3.0	8.58V
7a	13.3	6.59V	15	5.04	8.68V
7b	13.3	6.59V	16	23.7	8.65V
7c	13.5	6.67V	17	33.9	8.75V
7a′	14.6	6.63V	18	3.97	6.65V
7b″	15.1	6.53V	19	6.7	6.71V
7b′	17.6	6.53V	20	9.45	6.61V
7c′	18.6	6.59V	21	31.8	6.60V
8a	13.2	6.52V	22	45.0	6.58V
8b	13.3	6.58V	23	56.5	8.70V

Run N° 1a. G.B. 48/60-1 (271 μ.) W = 300 g.

$\rho_s = 2.55$. $P_A = 709$. $\rho_f = .0695$

R.H. = 55 - 65 $T_A = 74$ $\mu = .0433$

h (limits)	h	ΔP	V	ε
6.45 - 8.55	7.5	10.6	120.5	.756
6.05 - 7.85	6.95	10.6	111.0	.737
5.65 - 7.55	6.6	10.7	102.0	.723
5.25 - 7.25	6.25	10.8	93.8	.707
5.05 - 6.85	5.95	10.7	85.0	.692
4.65 - 6.45	5.55	10.8	74.0	.670
4.45 - 5.85	5.15	11.0	62.2	.644
3.95 - 5.15	4.55	11.0	51.7	.598
3.75 - 4.45	4.1	11.1	37.6	.554
3.3 - 3.65	3.47	11.1	25.0	.472
	3.3	10.85	20.7	.445
	3.25	10.8	19.4	.436
	3.21	10.75	18.2	.430
	3.19	10.75	17.0	.426
	3.15	10.7	15.8	.419
	3.12	10.55	14.5	.414
	3.09	10.45	13.2	.409
	3.09	9.2	11.5	.409
	3.08	7.75	9.64	.407
	3.08	66.25	7.7	.407
	3.08	4.45	5.36	.407
	3.08	0	0	.407

Run N° 1b. G.B. 48/60-1 (271 μ.) W = 500 g.

$\rho_s = 2.55$ $P_A = 709.5$ $\rho_f = .0710$

R.H. = 60 - 75 $T_A = 62$ $\mu = .0428$

8.35 - 12.35	10.35	19.05	121.0	.706
7.45 - 11.85	9.65	19.05	108.5	.682
7.05 - 11.05	9.05	19.05	97.0	.663

Run N° 1b. continued:

h (limits)	h	ΔP	V	ε
6.85 - 10.45	8.65	19.05	89.0	.648
6.05 - 9.85	7.95	19.05	75.8	.616
5.95 - 9.05	7.5	18.95	63.5	.594
5.85 - 7.65	6.75	18.95	46.5	.548
5.55 - 6.55	6.05	18.9	34.3	.496
5.4 - 5.8	5.6	18.6	22.4	.455
5.4 - 5.7	5.55	18.55	21.0	.449
5.35 - 5.55	5.45	18.5	19.6	.441
5.31 - 5.45	5.38	18.4	18.2	.434
	5.29	18.25	16.7	.424
	5.23	18.1	14.9	.416
	5.18	17.0	13.3	.411
	5.18	13.86	10.9	.411
	5.17	11.65	8.73	.410
	5.17	7.65	5.64	.410
	5.16	0	0	.410
9.05 - 13.25	11.15	19.15	121.0	.727
8.25 - 12.45	10.35	19.2	108.5	.706
8.05 - 11.65	9.85	19.0	98.4	.690
7.05 - 11.25	9.15	18.95	85.3	.667
6.85 - 10.65	8.75	19.1	75.0	.652
6.55 - 9.75	8.15	19.2	64.2	.626
6.05 - 8.45	7.25	19.05	53.0	.580
7.55 - 5.55	6.55	19.0	41.6	.535
5.45 - 6.15	5.8	19.0	27.4	.475
	5.19	0	0	.413

Run N° 1c. G.B. 48/60-1 (271 μ.) W = 700 g.

$\rho_s = 2.55$ $P_A = 708.5$ $\rho_f = .0696$

R.H. = 73 - 84 $T_A = 74.$ $\mu = .0431$

11.28	27.5	70.5	.621
10.38	27.5	59.5	.588
9.98	27.5	50.4	.572

Run 1c. continued:

h (limits)	h	ΔP	V	ε
	9.13	27.4	40.8	.532
	8.4	27.3	32.4	.481
	7.7	27.0	21.9	.445
	7.68	26.8	19.6	.444
	7.58	26.75	18.4	.437
	7.5	26.6	17.4	.430
	7.4	26.3	16.0	.422
	7.36	25.00	14.1	.420
	7.31	23.55	13.0	.416
	7.31	21.3	11.8	.416
	7.31	18.85	10.4	.416
	7.31	16.85	9.26	.416
	7.31	14.55	8.0	.416
	7.31	12.0	6.55	.416

Run N^0 1d. G.B. 48/60-1 (271 μ.) W = 1000 g.

ρ_s = 2.55 P_A = 705.5 ρ_f = .0695

R.H. = 61 - 82 T_A = 69 μ = .043

12.4 - 22.4	17.4	41.5	80.4	.650
11.6 - 19.0	15.3	41.2	65.9	.601
12.4 - 17.4	14.9	40.5	53.8	.591
12.1 - 15.7	13.9	40.0	46.6	.561
11.4 - 14.4	12.9	39.5	35.7	.527
10.95 - 12.65	11.8	38.85	26.4	.484
11.03 - 11.73	11.38	39.0	22.1	.464
10.65 - 11.05	10.83	38.2	21.9	.437
10.78 - 11.38	11.08	38.9	20.5	.449
10.78 - 11.18	10.98	38.85	19.5	.444
10.68 - 11.03	10.85	38.8	18.4	.439
10.58 - 10.83	10.7	38.6	17.1	.430
	10.6	38.3	16.0	.425
	10.46	37.7	14.5	.416
	10.43	36.0	13.5	.415

Run N° 1d. continued:

h (limits)	h	ΔP	V	ε
	10.39	33.1	12.2	.413
	10.39	29.0	10.65	.413
	10.38	24.85	9.0	.412
	10.38	21.85	7.9	.412
	10.38	17.9	6.45	.412
	10.38	12.45	4.42	.412
	10.38	0	0	.412

Run N° 1e. G.B. 48/60-1 (271 μ.) W = 1000 g.

ρ_s = 2.55 P_A = 705 ρ_f = .0695

R.H. = 77 - 90 T_A = 70 μ = .043

10.83 - 11.43	11.13	38.95	20.5	.453
10.88 - 11.23	11.1	38.7	19.7	.450
10.73 - 11.08	10.9	38.75	18.7	.440
10.68 - 10.88	10.78	38.5	17.6	.434
10.53 - 10.68	10.6	38.3	16.1	.425
	10.43	38.5	14.8	.416
	10.21	39.2	13.2	.403
	10.11	36.1	11.2	.397
	10.0	31.95	9.4	.390
	9.96	28.6	8.0	.388
	9.96	23.7	6.6	.388
	9.96	16.85	4.66	.388
	9.95	0	0	.388

Run N° 2a. Char 48/60-1. (271 μ.) W = 500 g.

$\rho_s = 1.085$ $P_A = 704$ $\rho_f = .0694$

R.H. = 50 $T_A = 69$ $\mu = .043$

h (limits)	h	ΔP	V	ε
28.38 - 40.38	34.4	23.5	86.5	.792
24.38 - 37.38	30.9	23.8	73.6	.768
23.38 - 33.38	28.4	23.1	61.5	.748
20.88 - 30.38	25.63	22.8	56.7	.721
18.88 - 24.38	21.63	22.5	34.4	.669
17.18 - 19.18	18.18	20.5	23.0	.605
16.88 - 18.18	17.53	20.25	20.5	.591
16.78 - 17.98	17.38	20.2	19.4	.587
16.63 - 17.48	17.06	20.1	18.3	.580
16.33 - 17.03	16.68	19.9	17.1	.570
16.13 - 16.63	16.38	19.8	15.7	.562
15.83 - 16.23	16.03	19.6	14.3	.553
15.58 - 15.78	15.68	19.6	12.8	.542
15.13 - 15.38	15.25	19.35	11.3	.530
	15.03	19.0	10.3	.524
	14.87	18.15	9.15	.517
	14.80	17.15	8.36	.515
	14.77	17.4	8.2	.514
	14.75	16.1	7.8	.514
	14.70	15.5	7.31	.512
	14.70	14.7	6.95	.512
	14.68	13.25	6.25	.511
	14.65	12.8	5.9	.510
	14.65	11.15	5.6	.510
	14.60	10.1	5.25	.509
	14.53	0	0	.506

Run N° 2b. Char 48/60-1. (271 μ.) W = 300 g.

ρ_s = 1.085 P_A = 705 ρ_f = .0693

R.H. = 46 - 69 T_A = 71 μ = .043

h (limits)	h	ΔP	V	ε
15.9 - 24.4	20.15	12.8	94.2	.787
14.9 - 22.4	18.7	12.8	85.6	.770
15.0 - 21.0	18.0	12.6	75.0	.761
13.9 - 19.2	16.55	12.7	66.1	.740
13.4 - 17.9	15.65	12.6	58.5	.725
12.9 - 15.7	14.3	12.4	50.3	.700
12.1 - 13.9	13.0	12.4	42.2	.669
11.2 - 12.4	11.8	12.0	33.8	.636
10.38 - 11.4	11.2	12.0	27.2	.616
10.38 - 10.78	10.58	11.8	22.6	.593
10.13 - 10.68	10.42	11.6	20.6	.588
10.03 - 10.43	10.23	11.6	19.5	.580
9.98 - 10.28	10.13	11.6	18.62	.576
	9.9	11.55	17.1	.566
	9.73	11.55	16.1	.558
	9.60	11.45	14.5	.552
	9.40	11.40	13.0	.542
	9.20	11.3	11.3	.532
	9.05	11.2	10.3	.525
	8.93	11.0	9.42	.518
	8.87	10.2	8.36	.516
	8.84	9.05	7.26	.513
	8.81	7.5	5.7	.512
	8.80	5.5	4.3	.511
	8.77	0	0	.510

Run No 3a. Char 48/60-5; W = 400 g.

$\rho_s = 1.085$ $P_A = 705$ $\rho_f = .0692$

R.H. = 40 - 62 $T_A = 73$ $\mu = .043$

h (limits)	h	ΔP	V	ε
19.8 - 30.4	25.1	17.8	81.0	.772
18.9 - 28.9	23.9	17.8	71.9	.760
18.4 - 27.4	22.9	17.8	67.2	.750
17.4 - 26.6	22.0	17.8	61.1	.740
17.1 - 23.5	20.3	17.8	52.6	.718
15.9 - 21.1	18.5	17.2	47.6	.690
14.9 - 17.5	16.2	16.7	32.5	.646
13.6 - 14.9	14.25	16.2	22.4	.598
13.48 - 14.58	14.03	16.0	20.6	.591
13.38 - 14.08	13.68	15.95	19.5	.580
13.28 - 13.88	13.58	15.95	18.3	.577
13.08 - 13.78	13.43	15.75	17.5	.573
12.88 - 13.58	13.23	15.90	17.0	.565
12.88 - 13.58	13.23	15.7	16.0	.566
12.78 - 13.38	13.08	15.7	15.7	.560
12.68 - 13.08	12.88	15.6	14.6	.554
12.53 - 13.08	12.8	15.6	14.2	.551
12.38 - 12.78	12.58	15.5	13.0	.543
12.28 - 12.68	12.48	15.55	12.75	.540
12.13 - 12.38	12.25	15.55	11.3	.531
11.93 - 12.13	12.03	15.45	10.2	.523
11.83 - 11.93	11.88	15.35	9.42	.516
	11.69	15.15	8.5	.508
	11.58	14.10	7.3	.504
	11.51	12.5	6.34	.502
	11.49	10.5	5.24	.500
	11.45	8.55	4.14	.499
	11.39	0	0	.499

Run No 3b. Char 48/60-5. W = 200 g.

$\rho_s = 1.085$ $P_A = 703$ $\rho_f = .0692$

R.H. = 48 - 72 $T_A = 71.5$ $\mu = .043$

h (limits)	h	ΔP	V	ε
	6.88	7.40	20.5	.583
	6.76	7.40	19.05	.576
	6.70	7.35	18.25	.571
	6.60	7.35	17.4	.565
	6.40	7.25	16.1	.551
	6.42	7.30	15.3	.553
	6.25	7.20	13.8	.541
	6.20	7.25	12.2	.537
	6.06	6.95	11.4	.526
	6.07	7.20	10.95	.527
	5.98	7.10	9.9	.520
	5.93	7.0	9.0	.516
	5.84	6.85	8.02	.508
	5.80	6.20	6.9	.505
	5.77	5.05	5.47	.503
	5.76	4.10	4.38	.502
12.0 - 18.0	15.0	7.55	109.5	.821
11.0 - 16.4	13.7	7.75	101.0	.798
10.9 - 14.7	12.8	7.75	93.2	.783
10.4 - 13.9	12.15	7.75	83.1	.764
9.6 - 12.2	10.9	7.85	72.1	.727
9.0 - 11.2	10.1	7.75	62.9	.716
8.8 - 10.4	9.6	7.75	55.8	.701
	8.9	7.75	47.8	.678
	8.5	7.7	41.2	.662
	7.78	7.6	31.2	.631
	7.07	7.5	23.9	.594

Run No 3b'. Char 48/60-5. W = 142.1 g. E.V. = 150.

ρ_s = 1.085 P_A = 701 ρ_f = .0692

T_A = 73 μ = .043

h	ΔP	V	ε
4.45	5.1	20.5	.541
4.40	5.1	19.3	.535
4.33	5.05	18.1	.528
4.27	5.05	16.8	.521
4.20	5.05	15.5	.513
4.13	4.9	13.9	.505
4.08	4.87	12.3	.499
4.01	4.87	10.9	.490
4.00	4.55	9.63	.489
3.99	4.0	8.24	.488
3.98	3.5	7.18	.487
3.98	3.0	6.03	.487
3.96	2.35	4.51	.484
3.96	0	0	.484

Run N° 3b'. Char 48/60-5. W = 200 g. E.V. = 150.

	Unelutriated		Elutriated		Total	
Size	Weight	%	Weight	%	Weight	%
24/28	0.53	0.4			0.53	0.3
28/32	2.12	1.5			2.12	1.0
32/35	6.82	4.8			6.82	3.4
35/42	21.2	15.0			21.2	10.6
42/48	43.2	30.4	0.32	0.5	43.52	21.8
48/60	48.22	34.0	4.18	7.2	52.40	26.2
60/65	14.71	10.4	19.29	33.2	34.0	17.0
65/80	4.06	2.8	23.20	39.9	27.26	13.6
80/100	0.95	0.7	9.50	16.3	10.45	5.2
100/115	0.05	-	1.19	2.0	1.24	0.6
115/150	0.04	-	0.48	0.8	0.52	0.3
	141.9	100.0	58.16	100.0	200.06	100.0

Run N° 3c. Char 48/60-5. W = 250 g.

ρ_s = 1.085 P_A = 698 ρ_f = .0702

R.H. = 44 - 70 T_A = 61 μ = .0424

h (limits)	h	ΔP	V	ε
12.4 - 19.0	15.7	10.35	81.0	.771
11.8 - 17.0	14.4	10.33	70.0	.751
11.2 - 14.6	12.9	10.25	60.2	.722
10.6 - 13.4	12.0	10.25	53.0	.701
10.2 - 12.2	11.2	10.15	50.2	.680
9.6 - 11.0	10.3	10.15	35.8	.652
8.9 - 9.9	9.4	9.9	26.1	.618
8.65 - 9.0	8.83	9.85	20.5	.594
8.4 - 8.9	8.65	9.75	19.5	.585
8.25 - 8.75	8.50	9.75	18.4	.578
8.1 - 8.45	8.28	9.75	16.9	.566
	8.08	9.70	15.8	.556
	8.0	9.64	14.2	.551
	7.85	9.62	12.8	.543
	7.70	9.47	11.2	.534
	7.45	9.45	9.22	.518
	7.37	9.30	8.15	.513
	7.31	8.80	7.3	.509
	7.28	7.85	6.34	.507
	7.25	6.50	5.2	.505
	7.23	5.30	4.2	.503
	7.18	0	0	.500

Run No 3c′. Char 48/60-5. W = 61.0 g. E.V. = 222.

ρ_s = 1.085 P_A = 697.5 ρ_f = .0092

T_A = 72 μ = .043

h	ΔP	V	ε
3.1	2.25	84.1	.717
2.85	2.25	73.9	.693
2.60	2.22	63.1	.663
2.35	2.20	50.9	.628
2.08	2.15	37.7	.579
1.83	1.95	27.1	.521
1.72	2.0	20.8	.490
1.69	1.95	19.7	.482
1.66	1.90	18.8	.473
1.65	1.95	17.3	.469
1.65	1.95	16.2	.469
1.63	1.93	14.7	.463
1.63	1.80	13.1	.463
1.62	1.58	11.2	.460
1.62	1.30	9.0	.460
1.62	0.97	6.3	.460
1.62	0	0	.460

Run No 3c. Char 48/60-5. W = 250 g. E.V. = 222.

	Unelutriated		Elutriated		Total	
Size	Weight	%	Weight	%	Weight	%
20/28	0.55	0.9			0.55	0.2
28/32	2.96	4.8			2.96	1.2
32/35	9.29	15.2	0.13	0.1	9.42	3.8
35/42	23.60	38.5	3.74	2.0	27.34	10.9
42/48	18.30	29.9	24.28	12.7	42.48	17.0
48/60	5.67	9.3	67.88	35.6	73.55	29.4
60/65	0.83	1.4	51.04	26.8	51.87	20.4
65/80			25.95	13.6	25.95	10.4
80/100			14.33	7.6	14.33	5.7
100/115			1.72	0.9	1.72	0.7
115/150			0.78	0.4	0.78	0.3
-150			0.73	0.3		
	61.2	100.0	190.58	100.0	250.22	100.0

Run No 4a. G.B. 48/60-5 W = 788.5 g.

ρ_s = 2.54 P_A = 715.6 ρ_f = .0702

R.H. = 73 - 78 T_A = 74 μ = .043

h (limits)	h	ΔP	V	ε
12.4 - 20.9	16.05	31.6	110.3	.710
12.4 - 19.4	15.9	31.6	102.3	.696
11.9 - 18.9	15.4	31.6	92.4	.686
11.9 - 17.9	14.9	31.1	83.5	.675
11.8 - 16.4	13.6	30.9	75.5	.644
10.5 - 14.9	12.7	30.9	65.5	.619
10.2 - 13.8	12.0	30.6	55.4	.597
9.9 - 12.9	11.4	31.1	49.8	.575
9.4 - 12.0	10.7	31.0	43.0	.548
9.2 - 10.9	10.05	30.9	34.9	.519
8.88 - 9.78	9.33	30.4	24.5	.481
	9.05	30.4	20.6	.465
	8.9	30.3	19.5	.456
	8.68	30.3	18.5	.442
	8.5	30.3	17.3	.430
	8.4	30.2	15.9	.424
	8.3	30.1	14.4	.417
	8.13	29.8	12.8	.405
	8.07	28.9	11.6	.400
	8.03	27.3	10.7	.397
	8.03	25.1	9.8	.397
	8.02	23.3	8.75	.396
	8.01	19.9	7.7	.396
	8.01	16.85	6.41	.396
	7.98	13.05	4.94	.393

Run N° 4b. G.B. 48/60-5 W = 800 g.

ρ_s = 2.54 P_A = 724 ρ_f = .0704

R.H. = 65 - 70 T_A = 72 μ = .0431

14.9 - 27.9	21.4	33.0	173	0.770
12.4 - 23.4	17.9	34.0	142	.726
11.9 - 23.9	17.9	34.0	121	.726

Run No 4b. continued:

h(limits)	h	ΔP	V	ε
12.4 - 21.9	17.15	32.3	111.6	.714
11.8 - 20.8	16.3	32.3	103.6	.699
11.4 - 19.9	15.65	32.3	98.8	.686
11.4 - 18.9	15.15	32.3	88.5	.676
11.4 - 18.0	14.7	31.8	77.7	.666
11.4 - 16.6	14.0	31.8	71.7	.650
10.9 - 14.9	12.9	31.8	63.0	.620
10.3 - 13.9	12.1	31.8	55.0	.594
9.7 - 12.9	11.3	32.0	46.6	.565
9.4 - 12.0	10.7	32.0	39.0	.541
9.0 - 10.7	9.85	31.8	27.9	.500
8.63 - 9.33	8.98	31.2	20.5	.453
	8.88	31.1	19.4	.447
	8.73	30.9	18.2	.438
	8.63	31.1	16.95	.431
	8.58	30.8	16.05	.428
	8.48	31.0	15.65	.421
	8.40	30.3	14.65	.415
	8.23	30.3	14.25	.414
	8.30	29.5	13.45	.409
	8.23	30.4	12.90	.404
	8.15	30.0	11.45	.398
	8.13	28.0	10.5	.396
	8.11	26.2	9.85	.395
	8.11	23.4	8.70	.395
	8.11	20.8	7.70	.395
	8.07	17.7	6.4	.392
	8.06	19.9	5.06	.391
	8.06	0	0	.391

Run No 4c. G.B. 48/60-5 W = 400 g.

$\rho_s = 2.54$ $P_A = 715$ $\rho_f = .0698$

R.H. = 55 - 60 $T_A = 72$ $\mu = .0431$

11.0 - 15.0	13.0	14.3	202	.811
10.6 - 13.2	11.9	14.3	174	.794
9.0 - 11.6	10.3	14.4	143	.762

Run No 4c. continued:

h (limits)	h	ΔP	V	ε
7.7 - 10.5	9.1	14.2	108.5	.730
8.2 - 10.8	9.5	14.3	119.5	.742
7.7 - 10.2	8.95	14.3	110	.726
7.3 - 9.8	8.55	14.3	100.5	.713
7.0 - 9.4	8.20	14.3	91.0	.700
6.5 - 8.6	7.55	14.3	81.8	.676
6.2 - 8.0	7.10	14.3	70.5	.654
5.8 - 7.0	6.40	14.5	58.0	.616
5.35 - 6.25	5.80	14.7	46.7	.577
4.9 - 5.65	5.23	14.8	35.8	.531
	4.80	14.9	28.6	.489
	4.60	14.9	23.6	.467
	4.45	14.9	20.4	.449
	4.38	14.9	19.0	.440
	4.30	14.85	17.4	.430
	4.25	14.6	16.1	.423
	4.17	14.5	14.5	.412
	4.10	14.4	13.1	.402
	4.07	14.3	11.7	.398
	4.05	12.7	10.1	.395
	4.05	11.0	8.7	.395
	4.05	9.05	6.7	.395
	4.05	6.5	5.04	.395
	4.04	-	0	.393

Run No 4b. G.B. 48/60-5: E.V. = 173.

Size	Unelutriated.	
	wt.	%
24/28	1.37	0.2
28/32	7.47	1.0
32/35	38.95	5.0
35/42	85.94	11.0
42/48	133.97	17.2
48/60	271.0	34.8
60/65	130.20	16.7
65/80	40.81	5.1
80/100	69.91	9.0
100/115	0.29	-
Total	779.91	100.0

Run N° 4c'. G.B. 48/60-5: E.V. = 287. W = 306.5 g.

$\rho_S = 2.53$ $P_A = 711$ $\rho_f = .0699$

R.H. = 58 - 60 $T_A = 70$ $\mu = .0430$

h (limits)	h	ΔP	V	ε
5.6 - 7.6	6.6	11.2	91.0	.714
5.1 - 7.1	6.1	11.2	80.5	.691
4.7 - 6.6	5.65	11.2	71.3	.666
4.5 - 5.7	5.1	11.3	58.8	.630
3.85 - 4.75	4.3	11.3	46.3	.552
3.6 - 4.2	3.9	11.3	36.0	.517
3.3 - 3.6	3.45	11.3	25.8	.454
	3.25	11.1	21.3	.420
	3.20	10.93	19.8	.411
	3.18	10.9	18.4	.408
	3.17	10.95	17.1	.405
	3.17	10.2	15.7	.405
	3.16	9.6	14.4	.404
	3.16	8.5	12.7	.404
	3.16	7.0	10.5	.404
	3.12	5.85	8.3	.396
	3.12	4.05	5.65	.396
	3.12	-	0	.396

Run No 4c - 4c'. G.B. 48/60-5: E.V. = 287.

Size	Unelutriated wt.	Unelutriated %	Elut. wt.	Total wt.	Total %
24/28	0.66	0.2		0.66	0.2
28/32	3.71	1.2		3.71	0.9
32/35	16.50	5.4		16.60	4.1
35/42	43.88	14.4		43.88	11.0
42/48	80.38	26.4		80.38	20.2
48/60	123.68	40.5	0.80	124.48	31.4
60/65	34.83	11.6	47.47	82.30	20.6
65/80	0.66	0.2	30.43	31.09	7.8
80/100	0.27	0.1	11.30	11.57	2.9
100/115	0.04	-	2.72	2.76	0.7
115/150	-	-	0.81	0.81	0.2
Total	304.61	100.0	93.53	398.14	100.0

Run N° 4c". G.B. 48/60-5: E.V. = 360. W = 271.5 g.

$\rho_s = 2.53$ $P_A = 709$ $\rho_f = .0696$

R.H. = 68 - 70 $T_A = 70$ $\mu = .0430$

h (limits)	h	ΔP	V	ε
5.55 - 7.15	6.35	9.8	121	.738
5.25 - 6.55	5.90	9.6	111	.717
4.85 - 6.15	5.50	9.6	103	.697
4.35 - 6.05	5.20	9.6	102	.679
4.25 - 5.75	5.00	9.7	94.1	.666
4.75 - 5.85	5.30	9.8	88.0	.685
4.05 - 5.45	4.75	9.8	83.6	.649
4.05 - 5.35	4.70	9.9	74.3	.645
3.65 - 5.05	4.35	9.95	73.1	.616
3.65 - 4.55	4.10	10.0	63.5	.593
3.40 - 4.55	3.97	9.9	60.5	.580
3.35 - 4.05	3.70	9.95	53.4	.550
3.15 - 3.95	3.55	9.8	48.0	.530
3.15 - 3.8	3.47	10.0	46.8	.519
3.0 - 3.5	3.25	10.0	38.0	.487
	2.90	9.8	25.0	.425
	2.91	9.75	23.4	.427
	2.86	9.6	21.8	.417
	2.82	9.4	19.75	.409
	2.81	9.15	18.0	.406
	2.81	8.35	16.25	.406
	2.80	7.3	14.4	.405
	2.79	6.1	11.85	.402
	2.79	4.8	8.95	.402
	2.78	3.4	6.25	.400
	2.78	-	0	.400

Run N° 4c - 4c'' G.B. 48/60-5: E.V. = 360

Size	Unelutriated	
	wt.	%
24/28	0.88	0.3
28/32	6.01	2.2
32/35	21.92	8.0
35/42	54.13	19.8
42/48	96.90	35.4
48/60	90.56	33.2
60/65	2.97	1.1
65/80	0.05	-
80/100	0.02	-
100/115	0.04	-
Total	273.48	100.0

Run N° 5. Char 35/42-1. (384 μ.) W = 250 g.

ρ_S = 1.085 P_A = 700 ρ_f = .069

R.H. = 26 - 64 T_A = 72 μ = .043

h (limits)	h	ΔP	V	ε
14.9 - 24.9	19.9	10.3	130.7	.820
14.2 - 22.4	18.3	10.1	120.0	.804
13.1 - 20.5	16.8	10.1	110.0	.787
12.5 - 19.5	16.0	10.1	100.0	.776
12.1 - 18.9	15.5	10.1	92.5	.769
11.4 - 16.8	14.1	10.1	84.6	.746
11.2 - 15.8	13.5	10.1	75.3	.734
10.4 - 14.4	12.4	10.0	66.5	.711
10.0 - 12.4	11.2	9.75	55.7	.680
9.7 - 10.7	10.2	9.75	47.4	.648
8.9 - 9.6	9.25	9.55	38.2	.612
	7.94	9.20	24.8	.548
	7.76	9.20	22.0	.538
	7.54	9.15	20.2	.524
	7.47	9.05	18.9	.520
	7.38	9.0	17.8	.514
	7.30	9.0	16.4	.508
	7.26	8.85	15.6	.506
	7.24	8.45	14.7	.504
	7.21	7.80	13.0	.503
	7.18	6.85	11.2	.500
	7.18	5.60	9.08	.500
	7.17	4.8	7.74	.500
	7.17	3.9	6.22	.500
	7.16	3.0	4.64	.500
	7.15	0	0	.499

Run N° 6a, G.B. 35/42-1. (384 μ.) W = 500 g.

$\rho_s = 2.47$ $P_A = 719$ $\rho_f = .0709$

R.H. = 58 - 70 $T_A = 68$ $\mu = .0428$

h (limits)	h	ΔP	V	ε
8.2 - 11.4	9.8		123.0	.678
7.8 - 10.8	9.3		108.0	.660
7.4 - 10.2	8.8		103.0	.641
7.4 - 10.4	8.9		100.0	.645
7.2 - 9.6	8.4		92.0	.624
6.9 - 8.5	7.7		83.6	.590
6.8 - 8.9	7.85		79.0	.597
6.7 - 8.1	7.4		75.0	.573
6.4 - 8.0	7.2		70.6	.561
6.2 - 7.4	6.8	LEAK	65.0	.535
5.98 - 6.68	6.33		56.5	.500
5.68 - 6.18	5.93		48.1	.467
	5.88		47.0	.462
	5.63		40.9	.439
	5.48		37.2	.424
	5.38		34.4	.412
	5.25		30.0	.398
	5.23		26.0	.395
	5.22		20.5	.395
	5.22		17.0	.395
	5.21		0	.394

Run N° 6b. G.B. 35/42-1. (384 μ.) W = 450 g.

$\rho_s = 2.47$ $P_A = 697$ $\rho_f = .0709$

R.H. = 60 - 70 $T_A = 66$ $\mu = .0428$

7.7 - 10.0	8.85	119.0	.679
7.4 - 9.4	8.4	113.0	.662
7.5 - 9.5	8.5	106.2	.666

Run N° 6b. continued:

h(limits)	h	ΔP	V	ε
7.3 - 8.8	8.05		104.0	.647
7.3 - 8.05	8.05		101.0	.647
7.0 - 8.3	7.65		96.5	.629
6.4 - 7.9	7.15		94.6	.603
6.7 - 8.4	7.55		93.4	.624
6.3 - 7.4	6.85		77.5	.586
6.0 - 7.0	6.5	LEAK	69.8	.563
5.8 - 6.6	6.2		65.7	.542
5.8 - 6.5	6.15		62.5	.538
5.4 - 6.0	5.7		55.1	.502
5.28 - 5.68	5.48		51.1	.481
5.13 - 5.53	5.34		46.0	.468
	4.92		37.4	.423
	4.70		30.0	.396
	4.69		25.1	.395
	4.68		20.1	.393
	4.66		0	.391

Run N° 66. G.B. 35/42-1. (384 μ.) W = 450

$\rho_S = 2.47$ $P_A = 707$ $\rho_f = .0709$

R.H. = 60 - 74 $T_A = 67$ $\mu = .0428$

12.3 - 17.7	15.0		275.0	.810
11.3 - 16.0	13.65		247.0	.792
10.7 - 15.5	13.1		226.0	.783
9.9 - 13.6	11.75		203.0	.758
9.4 - 12.6	11.0		178.0	.742
8.4 - 11.8	10.1		152.0	.719
7.9 - 10.3	9.1		130.3	.688
7.5 - 9.8	8.65	LEAK	112.5	.672
7.6 - 10.6	9.1		110.7	.688
6.9 - 10.3	8.2		100.7	.654
6.9 - 9.8	8.35		96.3	.660
6.4 - 8.6	7.5		89.9	.621

Run N° 6b. continued:

h (limits)	h	ΔP	V	ε
6.3 - 8.1	7.2		77.6	.606
5.9 - 7.5	6.7		75.3	.576
5.6 - 6.7	6.15		63.2	.538
5.5 - 6.2	5.85	LEAK	53.4	.514
5.1 - 5.5	5.3		45.1	.465

Run No 6c. G.B. 35/42-1. (384 μ.) W = 600 g.

ρ_s = 2.47 P_A = 714 ρ_f = .0709

R.H. = 60 - 75 T_A = 68 μ = .0428

9.05 - 18.55	13.8	25.0	159.0	.726
8.05 - 16.05	12.05	24.2	138.5	.686
7.85 - 14.25	11.05	24.1	121.0	.657
8.95 - 14.35	11.65	24.0	113.2	.675
7.55 - 15.05	11.3	24.0	111.2	.665
8.05 - 13.05	10.55	23.6	101.0	.641
7.55 - 13.05	10.3	23.5	96.2	.632
7.55 - 12.15	9.85	23.4	91.0	.615
7.05 - 10.85	8.95	23.4	80.7	.576
6.85 - 10.05	8.45	23.2	72.7	.551
6.65 - 8.85	7.75	23.0	61.2	.511
6.65 - 8.05	7.35	23.0	53.3	.485
6.55 - 7.55	7.05	22.8	46.5	.463
6.55 - 7.25	6.9	22.75	44.1	.450
	6.46	22.5	35.2	.414
	6.39	22.25	33.8	.406
	6.24	19.1	24.2	.392
	6.24	15.6	19.9	.392
	6.23	0	0	.391

Run N° 7a. G.B. 48/60-10. W = 400 g.

$\rho_s = 2.52$ $P_A = 712$ $\rho_f = .0705$

R.H. = 55 - 60 $T_A = 66$ $\mu = .0429$

h (limits)	h	ΔP	V	ε
7.55 - 9.55	8.55	13.2	103	.710
7.05 - 9.05	8.05	13.3	93.6	.692
6.55 - 8.35	7.45	13.5	84	.668
6.05 - 7.75	6.90	13.5	72.6	.641
5.65 - 7.15	6.40	13.65	60.5	.613
5.15.- 6.25	5.70	13.7	47.4	.566
4.55 - 5.45	5.00	13.7	36.3	.505
4.00 - 4.30	4.20	13.7	20.0	.410
	4.08	13.7	18.5	.394
3.90 - 4.10	4.00	13.7	17.1	.381
3.85 - 4.05	3.95	13.7	15.7	.374
	3.89	13.5	14.0	.364
	3.88	13.5	12.4	.362
	3.75	11.5	8.6	.340
	3.73	9.9	7.13	.336
	3.72	8.3	5.84	.335
	3.70	6.2	4.43	.330
	3.69	-	0	.329
4.05 - 4.35	4.20	13.75	20.4	.410
	3.92	13.4	14.2	.368
	3.90	13.6	13.9	.365
	3.88	13.2	12.4	.362
4.00 - 4.35	4.17	13.7	20.2	.406
3.85 - 4.15	4.00	13.7	16.5	.381
	3.91	13.7	14.9	.367
	3,77	12.8	10.4	.344
	3.75	12.7	9.95	.340
	3.72	11.6	7.76	.335

Run N° 7b. G.B. 48/60-10 W - 500 g.

$\rho_s = 2.52$ $P_A = 713$ $\rho_f = .0704$

R.H. = 68 - 72 $T_A = 67$ $\mu = .0428$

n (limits)	h	ΔP	V	ε
10.05 - 14.05	12.05	18.0	133	.744
9.85 - 13.55	11.70	18.0	122	.736
9.35 - 13.15	11.25	18.0	114	.725
9.45 - 12.75	11.10	18.0	108	.722
9.25 - 12.05	10.65	18.0	102	.710
8.75 - 11.75	10.25	18.0	94	.698
8.05 - 11.05	9.55	18.0	84.5	.676
8.05 - 10.15	9.10	18.0	74.4	.660
7.55 - 9.25	8.40	18.0	65.5	.630
6.85 - 8.55	7.70	18.3	55.1	.599
6.45 - 7.85	7.15	18.3	46.8	.568
6.0 - 7.10	6.55	18.3	36.0	.528
5.75 - 6.35	6.05	18.9	22.4	.489
	5.80	18.9	21.6	.466
	5.70	18.9	20.0	.458
	5.55	18.9	18.4	.443
	5.45	18.85	16.8	.432
	5.35	18.85	15.4	.422
	5.31	18.8	14.5	.418
5.20 - 5.35	5.27	18.7	14.0	.414
	5.19	18.6	12.3	.404
	5.23	18.3	12.1	.409
	5.13	18.4	10.8	.397
	5.07	17.0	9.0	.390
	5.04	15.3	7.9	.386
	5.03		6.6	.385
	5.03	12.2	6.1	.385
	5.0	8.6	4.2	.381
	5.0	-	0	.381

Run N^{o} 7c. G.B. 48/60-10. W = 750 g.

$\rho_s = 2.52$ $\quad F_A = 716$ $\quad \rho_f = .0722$

R.H. = 45 - 67 $\quad T_A = 57$ $\quad \mu = .0422$

h (limits)	h	ΔP	V	ε
12.0 - 21.0	16.50	29.8	112	.720
11.2 - 19.1	15.5	29.8	99.5	.694
11.0 - 18.1	14.55	29.6	87.7	.681
9.5 - 15.9	12.70	29.6	77	.635
9.5 - 15.4	12.45	29.4	66.3	.627
9.0 - 13.1	11.05	29.4	52.2	.580
8.8 - 11.3	10.05	29.4	38.6	.538
8.25 - 9.35	8.80	29.2	24.6	.473
8.1 - 9.0	8.55	29.2	20.6	.459
8.05 - 8.8	8.43	29.2	19.0	.450
7.95 - 8.55	8.25	29.0	18.1	.437
7.85 - 8.35	8.10	29.0	16.6	.427
7.80 - 8.15	7.97	28.9	15.0	.418
7.75 - 8.05	7.90	28.7	13.5	.412
	7.85	28.3	12.7	.409
	7.79	28.4	11.8	.404
	7.75	26.8	11.2	.400
	7.73	26.5	10.6	.400
	7.67	25.8	9.9	.395
	7.63	22.6	8.35	.392
	7.62	20.9	7.75	.391
	7.59	19.4	6.95	.389
	7.55	13.9	4.92	.385
	7.52	-	0	.384
8.05 - 8.75	8.40	28.9	19.8	.448
7.95 - 8.45	8.20	28.8	17.8	.434
7.85 - 8.25	8.05	28.7	15.8	.424
7.80 - 8.05	7.92	28.2	14.3	.415
	7.85	27.0	12.7	.409
	7.77	24.1	10.7	.403
	7.69	20.2	8.6	.396
	7.65	17.2	7.2	.394
	7.63	12.8	5.2	.391
	7.59	-	0	.389

Run N° 7a'. G.B. 48/60-10: E.V. = 210. W = 315.5 g.

$\rho_s = 2.52$ $P_A = 715$ $\rho_f = .0710$

R.H. = 60 $T_A = 64$ $\mu = .0426$

h (limits)	h	ΔP	V	ε
6.85 - 8.05	7.75	11.1	119	.746
6.05 - 8.05	7.05	11.1	107	.720
5.95 - 7.65	6.80	11.1	97.4	.710
5.55 - 7.05	6.30	11.1	93.5	.687
5.25 - 6.85	6.05	11.1	79.5	.674
4.85 - 6.45	5.65	11.1	70.7	.651
4.35 - 5.55	4.95	11.1	57.6	.602
3.85 - 4.85	4.35	11.1	45.3	.540
3.55 - 4.45	4.00	11.2	35.8	.506
3.30 - 3.80	3.55	11.4	25.4	.445
	3.40	11.2	20.9	.429
3.3 - 3.50	3.40	11.2	19.5	.420
	3.30	11.2	18.0	.402
	3.30	11.2	17.6	.402
	3.27	11.1	17.0	.397
	3.27	11.1	16.6	.397
	3.24	11.2	15.7	.391
	3.21	10.8	14.1	.385
	3.19	10.7	13.5	.382
	3.23	9.5	12.4	.387
	3.23	9.1	11.9	.387
	3.21	8.2	10.4	.385
	3.19	6.7	8.1	.382
	3.19	5.3	6.2	.382
	3.19	-	0	.382

Run No 7a! 48/60-10: E.V. = 210. W = 315.5 g.

Analysis of unelutriable portion.

Mesh Size	wt. retained	%
24/28	9.36	3.0
28/32	16.18	5.2
32/35	27.75	8.8
35/42	45.76	14.5
42/48	53.00	16.8
48/60	87.32	27.7
60/65	28.02	8.9
65/80	25.26	8.1
80/100	22.07	7.0
100/115	0.08	7.0
	314.80	100.0

Run No 7b'. G.B. 48/60-10: E.V. = 370. W = 232 g.

$\rho_s = 2.51$ $P_A = 711$ $\rho_f = .0696$

R.H. = 68 - 80 $T_A = 69$ $\mu = .0429$

h (limits)	h	ΔP	V	ε
6.85 - 8.65	7.75	8.6	225	.814
5.80 - 7.90	6.85	8.6	200	.790
5.05 - 7.05	6.05	8.6	173	.762
4.65 - 5.85	5.25	8.6	143	.726
4.25 - 5.45	4.85	8.6	120.5	.703
4.05 - 5.35	4.70	8.55	112.5	.693
4.05 - 4.95	4.5	8.55	106.3	.680
3.95 - 4.75	4.35	8.6	98.5	.670
3.65 - 4.55	4.10	8.6	91.0	.649
3.40 - 4.05	3.73	8.6	80	.614
3.15 - 3.85	3.50	8.5	70	.588
2.95 - 3.45	3.20	8.5	58	.550
2.70 - 3.15	2.92	8.5	46.5	.507
	2.58	8.35	36.1	.452
	2.44	8.15	25.3	.410
	2.44	6.55	19.7	.410
	2.65	8.4	37.0	.405
	2.50	8.2	30.1	.426
	2.40	7.95	23.3	.400
	2.40	6.5	18.9	.400
	2.40	-	0	.400

Run Numbers 7b, 7b'', 7b'

		7b''			7b'		
Original Charge		E.V. = 288.			E.V. = 370.		
500 gm.		Unelutriated		Elut.	Unelutriated		Elut.
Size	wt.	wt.	%	wt.	wt.	%	wt.
16/20	0.5	0.5	0.2		0.6	0.3	
20/24	3.0	3.0	0.8		3.1	1.4	
24/28	8.25	8.25	2.3		8.05	3.5	
28/32	19.0	19.0	5.4		17.1	7.4	
32/35	36.5	36.5	10.3		44.1	19.0	
35/42	57.5	57.5	16.3		50.5	21.8	
42/48	75.0	75.0	21.2		69.1	29.8	0.18
48/60	97.5	93.5	26.4	4.0	38.3	16.6	80.0
60/65	74.0	41.3	11.7	32.7	0.73	0.3	74.0
65/80	60.0	16.8	4.8	43.2	0.04	-	46.1
80/100	37.5	1.04	0.3	36.5	0.02	-	37.2
100/115	19.0	1.04	0.3	18.0			16.3
115/150	8.5			8.5			7.3
150/170	3.0			3.0			4.1
170/200	0.75			0.75			1.04
-200	0.25			0.25			0.3
Total	500.0	353.43	100.0	146.9	232.65	100.0	266.52

Run N° 7c'. G.B. 48/60-10: E.V. = 410. W = 284.1 g.

ρ_s = 2.48 P_A = 710 ρ_f = .0699

R.H. = 60 - 70 T_A = 67 μ = .0428

h (limits)	h	ΔP	V	ε
5.45 - 9.05	7.25	10.5	197	.753
5.05 - 8.05	6.55	10.5	169	.727
4.35 - 7.15	5.75	10.5	139	.686
4.45 - 7.05	5.75	10.5	120	.689
4.15 - 6.55	5.35	10.5	112	.665
3.75 - 5.95	4.85	10.5	108.5	.631
3.95 - 5.95	4.95	10.6	101	.638
3.75 - 5.25	4.50	10.6	91.5	.602
3.25 - 5.05	4.15	10.5	82.3	.568
3.15 - 4.05	3.90	10.5	73.0	.541
3.15 - 4.55	3.85	10.65	67.0	.535
3.15 - 4.15	3.65	10.65	56.2	.510
3.05 - 3.80	3.43	10.5	47.8	.478
3.05 - 3.25	3.15	10.25	39.0	.422
	2.97	10.05	29.0	.397
3.1 - 3.55	3.32	10.4	45.7	.460
3.02 - 3.15	3.08	10.2	36.2	.419
	2.97	9.6	27.5	.397
	2.97	7.8	22.8	.397
	2.95	7.2	19.8	.394
	2.95	-	0	.394

Run No 7c'. G.B. 48/60-10: E.V. = 410.

Size	Unelutriated wt.	Unelutriated %	Elut. wt.	Total wt.	Total %
16/20	0.96	0.3		0.96	0.1
20/24	4.66	1.7		4.66	0.6
24/28	11.66	4.1		11.66	1.6
28/32	26.64	9.4		26.64	3.6
32/35	62.72	22.1		62.72	8.4
35/42	78.20	27.5	.05	78.25	10.4
42/48	85.64	30.1	8.54	94.18	12.6
48/60	13.74	4.8	175.4	189.17	25.2
60/65	0.04	-	95.62	95.63	12.8
65/80			51.62	51.62	6.9
80/100			89.44	89.44	11.9
100/115			23.34	23.34	3.1
115/150			11.55	11.55	1.6
150/170			7.53	7.53	1.0
170/200			1.68	1.68	0.2
200/250			0.71	0.71	-
Total	284.32	100.0	465.5	749.8	100.0

Run N° 8a. G.B. 48/60-25. W = 500 g.

$\rho_S = 2.52$ $P_A = 706$ $\rho_f = .0695$

R.H. = 60 - 70 $T_A = 70$ $\mu = .0430$

h (limits)	h	ΔP	V	ε
9.9 - 12.6	11.25	17.8	121	.725
9.0 - 11.8	10.40	17.8	108	.703
8.6 - 11.2	9.95	18.1	96.8	.690
8.0 - 10.8	9.40	18.0	86.4	.671
8.0 - 10.3	9.15	18.6	75.0	.662
7.35 - 9.15	8.25	18.8	62.8	.626
6.25 - 7.75	7.00	18.9	45.4	.558
6.05 - 7.25	6.65	18.7	36.5	.535
5.55 - 6.45	6.00	18.8	24.7	.485
5.45 - 6.15	5.80	18.5	20.7	.467
5.40 - 5.75	5.57	18.5	18.6	.445
5.35 - 5.65	5.50	18.4	18.4	.438
5.30 - 5.55	5.42	18.0	15.8	.430
	5.40	18.1	14.6	.428
	5.23	17.5	10.8	.410
	5.10	16.6	8.6	.394
	5.01	15.8	7.68	.384
	5.04	14.6	6.7	.386
	4.97	10.2	6.0	.379
	4.94	-	0	.374
	5.28	17.5	11.0	.414
	5.17	17.5	9.55	.403
	5.10	17.0	8.16	.394
	5.09	15.2	7.64	.392
	5.03	15.6	6.86	.385
	5.08	13.1	6.41	.390
	5.03	10.0	5.04	.385
	5.00	12.3	5.93	.381
	5.00	10.9	4.63	.381
	5.03	7.5	3.53	.385
	4.96	-	0	.377

Run No 8b. G.B. 48/60-25. W = 750 g.

$\rho_s = 2.52$ $P_A = 716$ $\rho_f = .0700$

R.H. = 60 - 66 $T_A = 68$ $\mu = .0429$

h (limits)	h	ΔP	V	ε
10.5 - 19.4	14.95	29.0	100.8	.690
10.5 - 17.6	14.05	28.8	90.1	.670
10.0 - 16.1	13.05	29.1	78.5	.644
9.5 - 15.1	12.30	28.8	68.0	.623
8.9 - 12.1	10.50	29.1	49.1	.558
9.0 - 13.1	11.05	29.1	56.4	.580
8.5 - 11.0	9.75	28.8	36.6	.524
8.05 - 9.45	8.75	28.7	24.6	.470
7.95 - 9.25	8.60	28.7	21.7	.460
7.85 - 8.90	8.37	28.6	19.7	.446
7.75 - 8.65	8.20	28.6	18.0	.435
7.75 - 8.45	8.10	28.5	16.4	.428
7.70 - 8.15	7.92	28.4	14.5	.415
7.65 - 7.95	7.80	28.0	12.3	.405
7.60 - 7.75	7.67	27.8	11.0	.395
	7.57	27.5	8.95	.388
	7.48	24.9	7.4	.380
	7.41	17.4	4.67	.375
	7.34	-	0	.369
7.95 - 8.75	8.35	28.5	19.75	.445
7.75 - 8.55	8.15	28.35	18.1	.430
7.65 - 8.25	7.95	28.15	16.0	.416
7.65 - 8.10	7.87	27.95	14.3	.410
7.65 - 7.85	7.75	27.30	12.1	.401
	7.70	23.9	10.2	.398
	7.65	20.8	8.3	.394
	7.57	17.3	6.15	.388
	7.53	13.1	4.35	.384
	7.45	-	0	.378

Run No 8a'. G.B. 48/60-25: E.V. = 254. W = 364 g.

$\rho_s = 2.53$ $P_A = 706$ $\rho_f = .0692$

R.H. = 65 - 70 $T_A = 70$ $\mu = .0430$

h (limits)	h	ΔP	V	ε
7.75 - 10.35	9.05	13.6	149	.751
6.95 - 9.25	8.10	13.5	125	.722
6.05 - 8.15	7.10	13.5	108	.683
5.95 - 7.55	6.75	13.6	97.7	.667
5.85 - 7.35	6.60	13.6	91.0	.659
5.55 - 7.05	6.30	13.6	81.0	.643
5.15 - 6.75	5.95	13.6	71.3	.622
4.55 - 5.95	5.25	13.6	61.0	.571
4.35 - 5.65	5.00	13.5	53.3	.550
4.05 - 4.95	4.50	13.8	44.4	.500
4.05 - 4.55	4.30	13.7	33.4	.477
3.85 - 4.20	4.02	13.7	27.7	.440
	3.81	13.4	21.8	.410
	3.75	13.2	20.0	.400
	3.73	12.9	18.7	.397
	3.69	12.3	17.2	.390
	3.67	11.6	15.5	.387
	3.66	10.7	14.6	.385
	3.65	9.85	12.8	.384
	3.65	8.3	10.8	.384
	3.64	6.7	8.71	.382
	3.64	4.6	5.86	.382
	3.64	-	0	.382

Run N° 8a" G.B. 48/60-25: E.V. = 352. W = 266 g.

$\rho_s = 2.52$ $P_A = 704$ $\rho_f = .0687$

R.H. = 70 - 75 $T_A = 73$ $\mu = .0432$

h (limits)	h	ΔP	V	ε
5.45 - 7.85	6.65	9.9	162	.753
4.75 - 6.75	5.75	9.75	130	.714
4.55 - 6.35	5.45	9.85	126	.698
4.15 - 5.95	5.05	9.85	116	.674
4.25 - 5.65	4.95	9.85	108	.668
3.95 - 5.05	4.50	9.85	98	.635
3.75 - 4.85	4.30	9.85	90	.618
3.45 - 4.75	4.10	9.85	81.8	.599
3.25 - 4.45	3.85	9.7	69.0	.573
3.05 - 4.05	3.55	9.8	58.5	.537
2.95 - 3.65	3.30	9.8	49.9	.502
2.9 - 3.25	3.07	9.8	39.8	.465
2.85 - 3.15	3.00	9.8	36.8	.451
	2.80	9.5	30.2	.415
	2.74	7.9	22.0	.400
	2.74	6.0	16.8	.400
	2.74	-	0	.400

Run No 8a'. G.B. 48/60-25. Run No 8a".

E.V. = 254. E.V. = 352.

Size	Unelutriated wt.	Unelutriated %	Elut. wt.	Unelutriated wt.	Unelutriated %	Elut. wt.	Total %
12/14	0.77	0.2		0.77	0.3		0.2
14/16	1.05	0.3		1.05	0.4		0.2
16/20	5.12	1.4		5.12	1.9		1.0
20/24	8.46	2.3		8.46	3.2		1.7
24/28	14.83	4.1		14.83	5.6		3.0
28/32	24.23	6.7		24.23	9.1		4.8
32/35	31.93	8.8		31.93	12.0		6.4
35/42	60.51	16.6		60.51	22.8		12.1
42/48	54.37	14.9		54.29	20.4	.08	10.9
48/60	92.52	25.4	.04	62.70	23.5	29.86	18.4
60/65	54.56	15.0	.41	2.09	0.8	52.88	11.0
65/80	9.11	2.5	23.81	0.02	-	32.90	6.6
80/100	6.50	1.8	50.55			57.05	11.4
100/115	0.07	-	25.30			25.37	5.1
115/150	0.04		15.86			15.90	3.2
150/170	0.02		11.54			11.56	2.3
170/200			4.70			4.70	0.9
200/250			2.46			2.46	0.5
250/270			0.73			0.73	0.2
-270			0.60			0.60	0.1
Total	363.9	100.0	136.0	265.9	100.0	234.1	100.0

Run No 8b'. G.B. 48/60-25: E.V. = 260. W = 532.6 g.

$\rho_s = 2.53$ $P_A = 713$ $\rho_f = .0692$

R.H. = 55 - 60 $T_A = 73$ $\mu = .0432$

h (limits)	h	ΔP	V	ε
8.03 - 13.1	10.55	20.7	122	.689
7.5 - 12.6	10.55	20.7	115.3	.674
7.1 - 12.6	9.85	20.7	108	.667
6.9 - 11.6	9.25	20.7	100	.645
6.0 - 11.1	8.55	20.7	91	.616
5.7 - 10.6	8.15	20.6	82.5	.597
5.75 - 9.55	7.65	20.6	75	.571
5.75 - 9.15	7.45	20.6	65	.560
5.55 - 8.35	6.95	20.6	55	.528
5.55 - 7.55	6.55	20.5	47	.499
5.55 - 6.75	6.15	20.5	38	.467
5.55 - 6.15	5.85	20.4	29.3	.439
5.45 - 5.75	5.60	20.1	22.9	.415
	5.55	19.9	19.9	.410
	5.45	19.5	19.3	.398
	5.43	18.7	17.5	.395
	5.40	16.8	16.2	.392
	5.38	15.3	14.3	.390
	5.38	13.4	12.7	.390
	5.36	10.7	10.5	.389
	5.36	7.6	7.12	.389
	5.36	-	0	0

Run N° 8b". G.B. 48/60-25: E.V. = 425. W = 295.6 g.

ρ_s = 2.50 P_A = 707 ρ_f = .0695

R.H. = 60 - 70 T_A = 70 μ = .0430

h (limits)	h	ΔP	V	ε
6.05 - 9.25	7.65	11.0	194	.759
5.05 - 8.15	6.60	10.9	170	.721
5.05 - 7.55	6.30	11.1	154	.708
4.65 - 7.05	5.85	11.0	137	.685
4.15 - 6.35	5.25	11.1	122	.641
3.95 - 6.15	5.05	11.1	115.3	.635
3.55 - 5.35	4.45	11.1	107.3	.586
3.35 - 5.35	4.35	11.05	98.7	.576
3.15 - 5.15	4.15	10.9	88.7	.556
3.15 - 4.75	3.95	11.0	79	.534
3.15 - 4.55	3.85	11.0	68.9	.522
3.05 - 4.05	3.55	11.0	56.3	.481
3.05 - 3.55	3.30	10.8	45.8	.441
3.05 - 3.25	3.15	10.6	38.0	.416
	2.99	9.9	28.0	.384
	2.99	7.8	21.8	.384
	2.99	-	0	.384

Run N° 8b'. G.B. 48/60-25. Run N° 8b".

E.V. = 260 E.V. = 425

Size	Unelutriated wt.	%	Elut. wt.	Unelutriated wt.	%	Elut. wt.	Total %
16/14	0.75	0.1		0.75	0.3		0.1
14/16	1.73	0.3		1.73	0.6		0.2
16/20	6.47	1.2		6.47	2.2		0.9
20/24	14.19	2.7		14.19	4.8		1.9
24/28	20.81	3.9		20.81	7.0		2.8
28/32	35.88	6.7		35.88	12.1		4.8
32/35	54.70	10.3		54.70	18.5	-	7.3
35/42	89.25	16.8		89.23	30.1	.02	11.9
42/48	77.25	14.5	-	64.53	21.8	12.72	10.3
448/60	151.88	28.5	0.12	7.59	2.6	144.41	20.2
60/65	73.02	13.7	4.15			77.17	10.3
65/80	0.83	0.2	54.87			55.70	7.4
80/100	5.66	1.1	74.64			80.30	10.7
100/115	0.03	-	35.08			35.11	4.7
115/150	0.11	-	19.89			20.00	2.7
150/170	-	-	16.60			16.60	2.2
170/200			7.70			7.70	1.0
200/250			2.60			2.60	0.3
250/270			1.09			1.09	0.2
-270			0.72			0.72	0.1
Total	532.6	100.	217.46	295.88	100.0	454.14	100.0

Run N° 9a. G.B. 48/60-100. W = 600 g.

$\rho_s = 2.50$ $P_A = 714$ $\rho_f = .0702$

R.H. = 50 - 60 $T_A = 72$ $\mu = .0431$

h (limits)	h	ΔP	V	ε
8.0 - 11.8	11.50	21.7	102.5	.687
9.7 - 13.3	9.90	21.7	90.6	.636
7.7 - 11.0	9.35	21.7	75.6	.615
8.0 - 10.8	9.40	22.3	64.0	.606
7.2 - 9.8	8.50	22.3	51.4	.560
6.8 - 9.1	7.95	22.4	42.8	.530
6.55 - 8.35	7.45	22.4	33.6	.499
6.15 - 7.75	6.95	22.4	26.3	.462
6.45 - 7.25	6.85	21.7	21.7	.455
6.25 - 7.05	6.65	21.5	19.8	.438
6.25 - 6.85	6.55	21.3	18.0	.429
6.15 - 6.75	6.45	21.1	16.4	.420
6.10 - 6.55	6.32	20.7	15.0	.409
6.05 - 6.35	6.20	20.3	12.4	.397
6.00 - 6.15	6.07	19.7	10.9	.385
	6.10	18.1	8.9	.387
	6.02	15.7	6.91	.379
	5.97	13.4	5.3	.375
	5.94	10.4	3.7	.370
	5.84	7.0	2.4	.359
	5.77	-	0	.351
6.25 - 6.85	6.55	21.5	18.1	.429
6.10 - 6.75	6.42	21.5	17.2	.418
6.05 - 6.65	6.35	21.3	16.1	.411
6.00 - 6.55	6.27	21.1	14.2	.405
6.05 - 6.35	6.20	20.5	13.0	.397
6.00 - 6.25	6.12	19.6	12.1	.390
5.95 - 6.15	6.05	19.5	9.2	.381
5.95 - 6.15	6.05	17.7	7.7	.381
	5.95	15.0	5.6	.372
	5.90	12.4	4.4	.366
	5.73	-	0	.346

Run N° 9b. G.B. 48/60-100. W = 750 g.

$\rho_s = 2.50$ $P_A = 712$ $\rho_f = .0690$

R.H. = 65 $T_A = 65$ $\mu = .0438$

h (limits)	h	ΔP	V	ε
8.4 - 12.1	10.25	28.5	52.0	.544
8.0 - 10.6	9.50	28.2	34.6	.507
7.8 - 9.3	8.55	27.6	22.2	.452
7.75 - 9.05	8.40	28.0	21.0	.443
7.75 - 7.85	8.35	27.0	20.3	.439
7.45 - 8.45	7.95	26.5	17.5	.411
7.45 - 8.25	7.85	26.0	15.6	.404
7.45 - 8.15	7.80	25.5	14.0	.400
7.55 - 7.95	7.75	24.9	12.4	.395
7.35 - 7.75	7.55	24.3	10.5	.380
7.45 - 7.65	7.55	22.0	8.7	.380
	7.51	19.7	7.1	.376
	7.44	16.4	5.1	.370
	7.37	13.2	3.8	.365
	7.27	-	0	.356
7.45 - 8.45	7.95	26.5	17.3	.411
7.55 - 8.15	7.85	25.7	14.4	.404
7.45 - 7.85	7.65	25.0	11.5	.388
7.35 - 7.60	7.47	22.2	8.25	.374

Run N° 9a′. G.B. 48/60-100: E.V. = 158. W = 504 g.

$\rho_s = 2.52$ $P_A = 715$ $\rho_f = .0699$

R.H. = 65 - 72 $T_A = 71$ $\mu = .0431$

h (limits)	h	ΔP	V	ε
9.05 - 11.65	10.35	19.1	116.5	.698
8.65 - 11.25	9.95	19.1	108.5	.686
8.55 - 10.85	9.70	19.2	100.5	.675
8.05 - 10.25	9.15	19.4	92.5	.659
7.35 - 10.05	8.70	19.2	82.5	.642
6.85 - 9.15	8.00	19.1	73.1	.610
6.05 - 8.85	7.45	19.1	63.5	.581
5.85 - 7.85	6.85	19.1	55.5	.545
5.65 - 7.55	6.60	19.1	47.8	.528
5.45 - 6.65	6.05	18.8	39.0	.484
5.25 - 6.05	5.65	18.7	29.7	.448
5.10 - 5.70	5.40	18.3	21.1	.422
5.10 - 5.55	5.32	18.1	19.5	.414
5.10 - 5.25	5.17	17.8	18.1	.397
	5.10	17.7	17.0	.388
	5.05	16.4	14.5	.382
	5.03	14.9	12.9	.380
	4.99	12.2	10.3	.375
	4.95	11.0	8.9	.370
	4.94	7.6	6.05	.369
	4.93	5.6	4.3	.368
	4.90	-	0	.363

Run N° 9a″. G.B. 48/60-100: E.V. = 262. W = 395 g.

$\rho_s = 2.52$ $P_A = 709$ $\rho_f = .0700$

R.H. = 70 - 75 $T_A = 70$ $\mu = .0430$

7.0 - 10.8	8.9	14.9	162	.725
7.05 - 9.85	8.45	14.9	141.5	.709
6.75 - 8.95	7.85	15.0	120.0	.690

Run N° 9a″ continued:

h(limits)	h	ΔP	V	ε
5.55 - 8.25	6.90	14.9	110.5	.646
5.55 - 7.95	6.75	14.9	102.8	.638
5.05 - 7.55	6.30	14.9	95.0	.612
5.05 - 7.25	6.15	14.9	87.3	.602
4.85 - 6.55	5.70	14.9	79.2	.571
4.65 - 6.15	5.40	14.9	68.0	.547
4.55 - 6.15	5.35	14.8	59.5	.543
4.45 - 5.65	5.05	14.8	55.8	.516
4.25 - 5.65	4.95	14.8	51.7	.506
4.25 - 4.85	4.55	14.7	44.9	.463
4.25 - 4.95	4.60	14.7	42.4	.469
4.15 - 4.55	4.35	14.5	35.2	.448
4.15 - 4.55	4.35	14.1	33.2	.448
4.05 - 4.35	4.20	14.0	29.3	.417
	4.01	11.9	23.4	.390
	4.00	12.3	21.7	.390
	3.95	9.2	17.0	.381
	3.94	-	0	.380

Run N° 9a‴ G.B. 48/60-100: E.V. = 382. W = 285.7 g.

$\rho_s = 2.53$ $P_A = 705$ $\rho_f = .0692$

R.H. = 60 - 65 $T_A = 69$ $\mu = .0430$

5.7 - 8.8	7.25	10.7	207	.757
5.4 - 8.2	6.80	10.5	182	.741
4.8 - 7.7	6.25	10.5	157	.719
4.35 - 6.75	5.55	10.5	140	.683
4.05 - 5.65	4.85	10.7	119.5	.638
3.85 - 5.55	4.70	10.65	110	.626
3.65 - 5.25	4.45	10.70	101.5	.605
3.45 - 5.05	4.25	10.6	93	.586
3.35 - 4.05	4.00	10.3	85.4	.560

Run No 9a" continued:

h (limits)	h	ΔP	V	ε
3.25 - 4.45	3.85	10.5	75.2	.543
3.05 - 3.80	3.43	10.5	62.1	.487
3.05 - 3.85	3.45	10.4	59.0	.490
2.95 - 3.45	3.20	10.4	54.5	.450
2.95 - 3.35	3.15	10.3	48.8	.441
2.95 - 3.09	3.02	10.2	44.7	.418
2.95 - 3.07	3.01	9.8	39.8	.415
	2.90	8.6	33.0	.394
	2.86	7.15	26.8	.385
	2.85	5.0	19.1	.383
	2.85	-	0	.383

Run No 9a, G.B. 48/60-100. Run No 9a'.

E.V. = 76. E.V. = 158.

Size	Unelutriated wt.	Unelutriated %	Elut. wt.	Unelutriated wt.	Unelutriated %	Elut. wt.
7/8	0.56	0.1		0.56	0.1	
8/10	5.70	1.0		5.70	1.1	
10/12	4.75	0.8		4.75	1.0	
12/14	0.19	-		0.19	0.1	
14/16	8.44	1.6		8.44	1.7	
16/20	17.75	3.1		17.75	3.5	
20/24	21.80	3.8		21.80	4.3	
24/28	28.45	5.0		28.45	5.7	
28/32	35.09	6.1		35.09	7.0	
32/35	37.18	6.5		37.18	7.4	
35/42	54.09	9.5		54.09	10.7	
42/48	47.69	8.3		47.69	9.5	
48/60	79.25	13.9		79.25	15.7	
60/65	46.63	8.2		46.63	9.3	
65/80	25.72	4.5		25.72	5.1	
80/100	60.63	10.6		60.44	12.0	0.19
100/115	34.72	6.1	0.02	26.19	5.2	8.58
115/150	28.48	5.0	0.04	2.78	0.6	25.75
150/170	23.96	4.2	0.10	0.06	-	24.00
170/200	9.00	1.6	3.81	0.01	-	12.80
200/250	0.75	0.1	11.34	-		12.09
250/270	-	-	4.05	-		4.05
-270	0.20	-	8.36	-		8.56
Total	571.03	100.0	27.72	503.77	100.0	96.01

Run No 9a''. G.B. 48/60-100. Run No 9a'''

E.V. = 262. E.V. = 381.

Size	Unelutriated wt.	Unelutriated %	Elut. wt.	Unelutriated wt.	Unelutriated %	Elut. wt.	Total %
7/8	0.56	0.1		0.56	0.2		0.1
8/10	5.70	1.5		5.70	2.0		1.0
10/12	4.75	1.2		4.75	1.6		0.8
12/14	0.19	0.1		0.19	0.1		-
14/16	8.44	2.1		8.44	3.0		1.4
16/20	17.75	4.5		17.75	6.2		3.0
20/24	21.80	5.5		21.80	7.6		3.6
24/28	28.45	7.2		28.45	10.0		4.8
28/32	35.09	8.9		35.09	12.2		5.9
32/35	37.18	9.4		37.18	13.0		6.2
35/42	54.09	13.7		54.05	19.0		9.0
42/48	47.69	12.1		47.54	16.6		8.0
48/60	79.25	20.1		24.00	8.4	55.25	13.2
60/65	46.24	11.7	0.39	0.21	0.1	46.42	7.8
65/80	1.96	0.5	23.76			25.72	4.3
80/100	5.41	1.4	55.22			60.63	10.1
100/115	0.13	-	34.71			34.74	5.8
115/150	0.10	-	28.42			28.52	4.8
150/170			24.06			24.06	4.0
170/200			12.81			12.81	2.1
200/250			12.09			12.09	2.0
250/270			4.05			4.05	0.7
-270			8.56			8.56	1.4
Total	394.7g.	100.0	204.7g.	285.7g.	100.0	313.4	100.0

Humidity tests.

Run N° 9b'. G.B. 48/60-100: E.V. = 395. W = 355.8 g.

ρ_s = 2.53 P_A = 706 ρ_f = .0693

T_A = 70 μ = .0430

h (limits)	h	ΔP	V	ε	R.H.
6.0 - 9.6	7.80	13.9	175	.717	70
5.5 - 8.4	6.95	13.8	141	.682	70
4.55 - 7.55	6.05	13.7	117	.635	70
4.85 - 7.05	5.95	13.85	112	.629	70
4.45 - 7.25	5.85	13.7	108	.622	60
4.35 - 6.25	5.30	13.9	99	.583	60
4.05 - 6.55	5.30	13.9	96.5	.583	60
4.05 - 5.85	4.95	13.6	89.1	.554	60
3.85 - 5.75	4.80	13.5	85.5	.540	65
4.35 - 5.55	4.95	13.6	74.9	.554	65
3.55 - 4.35	3.95	13.2	49.2	.441	65
3.65 - 3.85	3.75	13.1	45.2	.410	65
	3.57	12.0	34.2	.381	60
	3.49	8.5	23.2	.367	60
	3.49	-	0	.367	60
4.05 - 6.55	5.65	13.8	113.5	.583	60
4.65 - 6.65	5.30	13.8	113.5	.609	70
3.55 - 6.15	4.85	14.3	97.6	.545	60
4.55 - 6.55	5.55	13.7	97.6	.602	70
3.55 - 5.25	4.40	13.5	84.2	.498	60
4.25 - 5.75	5.00	13.5	84.2	.558	70
3.75 - 5.15	4.45	13.3	79	.506	60
4.05 - 5.85	4.95	13.3	79	.554	70
3.65 - 4.95	4.30	13.1	70.4	.486	60
4.05 - 5.55	4.80	13.1	70.4	.540	70
3.65 - 4.65	4.15	13.2	64.7	.468	60
4.05 - 4.95	4.50	13.2	64.7	.509	70
3.55 - 4.55	4.05	13.3	57	.455	60
3.75 - 4.65	4.20	13.3	57	.475	70
3.55 - 4.35	3.95	13.15	49.2	.441	60
	-	13.15	49.2	-	70

Run No 9b'. Run No 9b".

E.V. = 395. E.V. = 460.

Size	Unelutriated wt.	Unelutriated %	Elut. wt.	Unelutriated wt.	Unelutriated %	Elut. wt.	Total %
7/8	0.60	0.2		0.6	0.2		0.1
8/10	5.18	1.4		5.18	1.8		0.7
10/12	7.05	2.0		7.05	2.5		0.9
12/14	5.00	1.4		5.00	1.8		0.7
14/16	9.67	2.7		9.67	3.4		1.3
16/20	19.21	5.4		19.21	6.8		2.6
20/24	27.22	7.7		27.22	9.7		3.6
24/28	31.94	9.0		31.94	11.3		4.3
28/32	45.72	12.9		45.72	16.2		6.1
32/35	50.72	14.3		50.70	18.0		6.8
35/42	63.82	17.9		63.44	22.4	.38	8.5
42/48	64.00	18.0	0.35	16.18	5.7	48.17	8.6
48/60	24.95	7.0	59.92	0.45	0.2	84.42	11.3
60/65	0.50	0.1	68.00	-	-	68.50	9.2
65/80	0.13	-	30.07			30.20	4.0
80/100	0.08	-	76.57			76.65	10.2
100/115	0.02	-	43.28			43.30	5.8
115/150	0.01	-	33.99			34.00	4.6
150/170			31.35			31.35	4.2
170/200			18.44			18.44	2.5
200/250			15.08			15.08	2.1
250/270			4.74			4.74	0.7
270/325			5.67			5.67	0.7
-325			3.96			3.96	0.5
Total	355.8	100.0	392.2	282.4	100.0	465.5	100.0

Run N⁰ 10a. Char 48/60-10. W = 300 g.

ρ_s = 1.085 P_A = 711 ρ_f = 0.0701

R.H. = 30 - 50 T_A = 67 μ = 0.0428

h (limits)	h	ΔP	V	ε
14.4 - 12.9	19.05	12.3	94.2	.783
14.0 - 24.1	19.05	12.3	80.0	.775
13.2 - 19.7	16.45	12.3	67.0	.738
12.0 - 17.3	14.65	12.3	53.6	.706
11.4 - 15.7	13.55	12.1	44.0	.682
10.95 - 14.35	12.65	12.1	38.0	.659
10.55 - 12.55	11.55	11.9	30.0	.626
9.85 - 10.95	10.40	11.8	21.4	.585
9.65 - 10.75	10.20	11.6	19.2	.577
9.55 - 10.35	9.95	11.5	17.6	.566
9.35 - 10.35	9.75	11.5	16.1	.558
9.15 - 9.65	9.40	11.5	14.6	.542
9.05 - 9.35	9.20	11.3	12.9	.531
	9.07	11.3	10.8	.524
	8.90	11.2	9.7	.515
	8.89	11.1	9.2	.514
	8.75	8.9	6.6	.507
	8.55	-	0	.495
9.25 - 9.65	9.45	11.3	13.8	.543
9.05 - 9.45	9.25	11.3	12.05	.533
	8.97	11.2	10.4	.579
	8.87	10.7	8.8	.513
	8.81	9.4	7.3	.511
	8.72	7.3	5.72	.505
	8.65	5.90	4.12	.501
	8.57	-	0	.497
9.85 - 10.85	10.35	11.6	20.0	.583
9.40 - 10.00	9.70	11.5	16.6	.555
9.30 - 9.80	9.55	11.3	15.0	.549
9.05 - 9.55	9.30	11.3	12.8	.536
8.95 - 9.21	9.08	11.3	11.4	.525

Run N° 11a. Char 48/60-25. W = 300 g.

$\rho_s = 1.085$ $P_A = 711$ $\rho_f = 0.0701$

$T_A = 67$ $\mu = 0.0428$

h (limits)	h	ΔP	V	ε
15.0 - 27.1	21.05	11.7	100	.800
14.0 - 25.1	19.65	11.7	88.3	.780
12.9 - 22.6	17.75	11.8	77.0	.760
12.8 - 19.1	15.95	11.9	62.5	.731
12.0 - 17.7	14.85	11.9	53.7	.710
11.0 - 15.1	13.05	11.9	40.1	.670
10.6 - 13.1	11.85	11.8	30.7	.636
9.75 - 10.75	10.25	11.5	20.0	.580
9.65 - 10.55	10.10	11.3	18.0	.573
9.5 - 10.2	9.85	11.3	16.8	.562
9.5 - 9.9	9.70	11.2	15.6	.555
	9.20	10.8	12.8	.531
	8.98	9.5	8.24	.520
	8.57	-	0	.497
10.05 - 11.05	10.55	11.5	21.4	.591
9.75 - 10.75	10.25	11.4	19.2	.580
9.25 - 10.65	10.20	11.4	18.8	.577
9.55 - 10.45	10.00	11.4	17.6	.568
9.45 - 10.25	9.85	11.4	16.8	.562
9.40 - 10.05	9.72	11.2	15.8	.556
9.25 - 9.75	9.50	11.1	14.4	.546
9.05 - 9.55	9.30	10.8	10.8	.536
	9.15	10.6	11.7	.529
	9.05	10.3	10.4	.524
	8.96	9.8	9.23	.519
	8.90	9.2	7.9	.515
	8.81	7.9	6.1	.510
	8.73	6.3	4.4	.505
	8.57	-	0	.497

Run No 11a! Char 48/60-25: E.V. = 116. W = 238.3 g.

$\rho_s = 1.085$ $P_A = 703$ $\rho_f = 0.0695$

$T_A = 65$ $\mu = 0.0427$

h (limits)	h	ΔP	V	ε
11.0 - 17.1	14.05	9.4	89.0	.756
10.4 - 15.5	12.95	9.4	72.5	.735
9.5 - 13.6	11.55	9.4	58.6	.703
8.95 - 11.15	10.05	9.3	45.5	.659
8.45 - 9.95	9.20	9.1	34.6	.627
7.55 - 8.05	7.80	9.0	22.0	.560
7.55 - 8.05	7.80	9.0	21.5	.560
7.45 - 7.85	7.65	8.9	19.6	.551
7.35 - 7.65	7.50	8.9	18.2	.543
7.25 - 7.55	7.40	8.9	16.8	.536
7.15 - 7.35	7.25	8.7	15.5	.527
	7.05	8.6	13.6	.514
	6.92	8.5	11.8	.504
	6.83	8.3	10.8	.498
	6.77	7.4	9.3	.493
	6.75	6.4	7.7	.491
	6.73	5.0	6.0	.490
	6.70	3.5	3.9	.489
	6.66	-	0	.485
	6.82	7.3	8.54	.497
	6.75	6.1	6.8	.491
	6.71	5.0	5.3	.489
	6.67	3.4	3.6	.486
	6.63	-	0	.483

Run No 11a'. Char 48/60-25: E.V. = 116.

	Unelutriated.	
Size.	Weight.	%
12/14	0.51	0.2
14/16	1.19	0.5
16/20	3.02	1.3
20/24	4.73	2.00
24/28	8.99	3.7
28/32	15.16	6.4
32/35	19.55	8.2
35/42	34.47	14.4
42/48	35.12	14.7
48/60	41.67	17.4
60/65	32.60	13.6
65/80	24.12	10.10
80/100	16.60	6.9
100/115	1.29	0.5
115/150	0.22	0.10
through 150	0.10	0.04
	239.34	100.04

Sample weight 238.4 g.

Run N° 12a. Char 48/60-100. W = 400 g.

$\rho_s = 1.08$ $P_A = 708$ $\rho_f = 0.0703$

$T_A = 62$ $\mu = 0.0425$

h (limits)	h	ΔP	V	ε
16.0 - 24.1	20.05	16.5	56.0	.715
15.5 - 21.1	18.30	16.5	47.6	.686
15.0 - 20.1	17.55	16.5	41.2	.671
14.5 - 19.6	17.05	16.3	38.0	.661
14.0 - 17.4	15.70	16.1	32.0	.632
13.8 - 16.1	14.95	15.9	26.8	.614
13.55 - 14.55	14.05	15.6	21.3	.589
13.05 - 14.65	13.85	15.5	20.6	.582
13.05 - 14.25	13.65	15.4	19.4	.576
12.55 - 13.55	13.05	15.1	16.5	.557
12.35 - 13.05	12.70	14.8	15.25	.545
12.15 - 12.55	12.35	14.3	13.65	.532
11.95 - 12.20	12.07	13.8	12.0	.521
11.75 - 12.00	11.87	13.3	10.2	.513
	11.81	12.3	8.6	.511
	11.75	11.0	6.84	.508
	11.67	9.70	5.4	.505
	11.53	7.7	3.86	.500
	11.30	-	0	.489
12.85 - 14.15	13.90	15.4	18.8	.572
12.65 - 13.85	13.25	15.0	17.4	.564
12.35 - 13.25	12.80	14.7	15.9	.549
12.15 - 12.85	12.50	14.3	14.2	.538
11.95 - 12.35	12.15	13.8	12.4	.524
	11.90	13.3	10.3	.514
	11.85	12.0	8.34	.512
	11.75	10.4	6.4	.508
	11.66	8.8	4.7	.504
	11.31	-	0	.490

Run N° 12a'. Char 48/60-100: E.V. = 117. W = 289.7 g.

$\rho_s = 1.08$ $P_A = 706$ $\rho_f = 0.0698$

$T_A = 68$ $\mu = 0.0428$

h (limits)	h	ΔP	V	ε
13.5 - 24.6	19.05	11.6	99.0	.782
13.0 - 23.1	18.05	11.8	89.3	.768
12.0 - 21.1	16.55	11.8	78.7	.748
11.4 - 17.7	14.55	11.8	67.9	.714
11.05 - 16.35	13.70	11.7	58.1	.695
10.15 - 13.75	11.95	11.4	47.4	.650
10.35 - 13.05	11.70	11.4	44.4	.644
9.95 - 12.15	11.05	11.2	39.5	.622
9.85 - 11.65	10.75	11.3	36.7	.612
9.55 - 10.85	10.20	11.1	31.4	.592
9.05 - 9.85	9.45	10.8	25.8	.559
8.55 - 9.05	8.80	10.4	21.7	.526
8.65 - 8.95	8.80	10.3	20.8	.526
	8.62	10.0	19.3	.516
	8.53	9.7	17.6	.510
	8.42	9.2	15.9	.504
	8.34	8.5	13.9	.500
	8.25	7.8	11.7	.495
	8.16	6.8	9.9	.489
	8.14	6.0	8.4	.487
	8.12	5.0	6.9	.487
	8.10	3.9	5.13	.485
	8.07	-	0	.484

Run No 12a'. Char 48/60-100: E.V. = 117.

Unelutriated.

Size.	Weight.	%
8/9	1.0	0.4
9/10	1.8	0.6
10/12	2.9	1.0
12/14	4.1	1.4
14/16	6.1	2.1
16/20	11.2	3.9
20/24	14.3	5.0
24/28	17.5	6.0
28/32	24.1	8.3
32/35	25.3	8.7
35/42	36.9	12.7
42/48	44.3	15.3
48/60	40.4	14.0
60/65	32.9	11.3
65/80	17.7	6.1
80/100	8.8	3.0
100/115	0.8	0.3
through	0.3	
	290.4	100.0

Run No 13. Char 65/80-1. (192 μ.) W = 300 g.

ρ_s = 1.085 P_A = 699 ρ_f = .0695

T_A = 68 μ = .0429

h (limits)	h	ΔP	V	ε
10.85 - 12.05	11.45	11.6	21.5	.624
10.75 - 11.85	11.30	11.6	19.9	.618
10.65 - 11.55	11.10	11.6	18.6	.612
10.30 - 11.10	10.70	11.55	15.8	.601
10.15 - 10.65	10.40	11.50	13.8	.585
9.90 - 10.20	10.05	11.45	11.9	.571
	9.73	11.35	10.0	.557
	9.48	11.25	8.44	.544
	9.27	11.15	6.8	.535
	9.08	11.1	5.5	.525
	8.95	10.8	4.62	.518
	8.86	9.2	3.65	.514
	8.83	7.5	3.24	.512
	8.77	0	0	.509
14.35 - 21.95	18.15	12.1	75.0	.766
13.35 - 20.05	16.70	12.1	60.8	.742
12.85 - 17.85	15.35	12.05	48.7	.719
12.05 - 15.65	13.85	11.9	40.2	.689
11.55 - 14.55	13.05	11.85	32.9	.670
10.75 - 11.85	11.30	11.65	26.4	.644
10.55 - 11.35	10.95		17.9	.606
10.40 - 11.10	10.75		16.5	.599
10.15 - 10.75	10.45		15.0	.588
9.60 - 9.90	9.75		9.9	.558
	9.35		7.38	.538
	9.05	11.0	5.1	.524
	8.86	10.55	4.3	.514
	8.84	9.75	3.9	.512
	8.78	7.45	2.88	.509
	8.75	5.0	1.87	.508
	8.74	0	0	.508

Run No 14. Char 170/200-1. (81 μ.) W = 300 g.

$\rho_s = 1.10$ $\quad$ $P_A = 695.5$ $\quad$ $\rho_g = .0691$

$T_A = 66$ $\quad$ $\mu = .0427$

h (limits)	h	ΔP	V	ε
11.65 - 14.05	12.85	11.1	22.0	.668
11.85 - 14.05	12.95	11.1	20.5	.671
11.75 - 13.35	12.55	11.05	18.1	.660
11.55 - 12.85	12.2	11.12	16.7	.651
11.35 - 12.45	11.9	11.12	15.0	.642
11.15 - 12.05	11.6	11.1	13.4	.633
10.95 - 11.65	11.3	11.13	11.5	.623
10.75 - 11.35	11.05	11.15	9.5	.614
10.75 - 11.05	10.9	11.15	8.35	.609
10.45 - 10.85	10.65	11.1	6.5	.600
	10.4	11.05	5.0	.590
10.35 - 10.65	10.5	11.15	4.88	.594
10.35 - 10.55	10.45	11.15	4.48	.592
	10.45	11.05	4.28	.592
10.35 - 10.65	10.5	11.15	4.03	.594
	10.4	11.15	3.62	.590
	10.4	11.05	3.05	.590
	10.21	10.85	2.56	.583
	10.25	10.9	2.5	.584
	10.15	10.8	2.0	.580
	9.75	10.6	1.34	.563
	9.55	9.85	(0.8)	.554
	9.18	0	0	.536

Run N° 15. Char 100/115-1. (136 μ.) W = 300 g.

$\rho_s = 1.085$ $P_A = 703$ $\rho_f = .0698$

$T_A = 66$ $\mu = .0427$

h (limits)	h	ΔP	v	ε
11.55 - 12.75	12.05	11.65	21.4	.642
11.15 - 12.35	11.75	11.55	19.4	.633
10.95 - 12.05	11.5	11.55	17.7	.625
10.85 - 11.75	11.3	11.55	16.1	.618
10.65 - 11.35	11.0	11.5	14.2	.611
10.45 - 11.15	10.8	11.45	12.5	.601
10.25 - 10.75	10.5	11.4	10.2	.589
10.00 - 10.35	10.17	11.4	8.55	.575
9.75 - 10.05	9.9	11.3	6.6	.564
	9.6	11.2	4.84	.550
	9.45	11.1	3.8	.543
16.05 - 24.05	20.05	11.9	83.5	.791
14.55 - 20.55	17.55	11.9	62.0	.756
13.05 - 17.85	15.45	11.95	46.4	.721
12.95 - 16.15	14.55	11.9	37.5	.704
11.85 - 14.25	13.05	11.7	29.4	.670
11.25 - 12.65	11.95	11.7	21.4	.639
10.85 - 11.95	11.4	11.55	17.1	.622
10.65 - 11.35	11.0	11.45	13.8	.611
10.15 - 10.55	10.35	11.4	9.75	.584
	9.95	11.3	6.85	.566
	9.65	11.2	5.0	.553
	9.55	11.1	4.52	.548
	9.49	11.1	4.03	.546
	9.39	11.1	3.47	.540
	9.27	10.9	2.9	.535
	9.21	10.25	2.38	.532
	9.11	8.35	1.84	.527
	9.06	6.15	1.25	.524
	9.03	0	0	.522

Run No 16. Char 24/28-1. (645 μ.) W = 300 g.

ρ_s = 1.075 P_A = 700 ρ_f = .0095

R.H. = 40 - 50 T_A = 69 μ = .0429

h (limits)	h	ΔP	V	ε
12.55 - 25.05	18.8	12.8	116.5	.769
13.05 - 22.05	17.55	12.8	109.0	.752
11.55 - 21.55	16.55	12.8	107.5	.737
11.05 - 20.55	15.8	12.7	98.2	.725
10.75 - 18.55	14.65	12.6	91.7	.704
10.75 - 16.55	13.65	12.5	83.3	.682
11.05 - 16.25	13.65	12.4	81.1	.682
10.55 - 15.25	12.9	12.3	76.0	.663
10.05 - 13.15	11.6	12.15	66.5	.625
9.60 - 11.60	10.6	11.75	57.5	.590
9.50 - 10.45	9.98	11.5	52.7	.564
9.15 - 9.55	9.35	11.45	46.2	.535
	8.94	11.3	41.4	.513
	8.77	10.35	36.0	.504
	8.71	9.0	30.4	.502
	8.67	6.85	23.5	.499
	8.61	0	0	.495
9.45 - 10.15	9.8	11.4	50.5	.556
9.15 - 9.45	9.3	11.4	45.0	.532
	9.07	11.3	43.0	.520
	8.85	11.2	40.2	.509
	8.72	9.25	31.6	.502

Run No 17. Char 16/20-1. (912 μ.) W = 250 g.

ρ_s = 1.08 P_A = 700 ρ_f = .0701

T_A = 62 μ = .0425

h (limits)	h	ΔP	V	ε
9.45 - 15.65	12.55	10.15	117	.712
9.05 - 13.55	11.30	10.15	108	.680
8.75 - 12.55	10.65	10.19	102	.661
8.25 - 11.25	9.75	9.9	94	.630
8.15 - 10.25	9.2	9.65	87.6	.608
8.00 - 8.95	8.48	9.50	79.6	.574
7.75 - 8.35	8.05	9.50	73.5	.551
	7.65	9.4	68.5	.528
	7.52	9.1	64.0	.520
	7.46	8.7	60.0	.516
	7.42	7.95	54.5	.514
	7.37	7.0	47.8	.510
	7.34	5.65	39.3	.508
	7.33	4.55	32.0	.508
	7.30	3.20	23.2	.506
	7.29	0	0	.504
11.05 - 29.05	20.05	10.6	191	.820
10.75 - 22.75	16.75	10.5	156	.784
10.05 - 21.05	15.55	10.3	141	.768
9.75 - 18.15	13.95	10.3	132	.741
8.65 - 12.65	10.65	9.9	100	.661
8.95 - 12.35	10.15	9.85	99.2	.644
8.05 - 9.05	8.55	9.45	78.5	.578
7.75 - 8.35	8.05	9.45	73.2	.552
	7.70	9.4	70.0	.531
	7.35	8.25	54.0	.509
	7.27	0	0	.504

Run N° 19. G.B. 100/115-1. (136 μ.) W = 500 g.

$\rho_s = 2.47$ $P_A = 719$ $\rho_f = .0715$

R.H. = 40 - 55 $T_A = 66$ $\mu = .0427$

h (limits)	h	ΔP	V	ε
11.05 - 16.05	13.55	18.7	97.2	.707
10.05 - 14.05	12.05	18.8	84.6	.738
9.05 - 12.55	10.8	18.8	73.5	.708
7.95 - 10.75	9.35	18.75	60.6	.662
7.55 - 10.05	8.8	18.75	50.8	.642
7.05 - 9.05	8.05	18.75	40.6	.608
6.95 - 8.05	7.5	18.75	32.3	.579
6.55 - 7.2	6.87	18.8	23.6	.540
6.25 - 7.15	6.7	18.85	20.7	.529
6.15 - 7.05	6.6	18.9	19.2	.522
6.1 - 6.75	6.42	18.9	17.9	.509
	6.35	18.9	16.5	.503
	6.28	18.9	15.0	.498
	6.2	18.9	13.7	.490
	6.1	18.9	12.3	.483
	6.03	18.9	11.1	.476
	5.9	18.9	9.9	.465
	5.7	18.8	7.5	.446
	5.55	18.6	5.9	.431
	5.48	18.45	5.2	.425
	5.43	18.35	4.65	.419
	5.38	18.2	4.26	.414
	5.35	18.0	3.74	.410
	5.34	18.1	3.58	.409
	5.33	17.2	3.38	.408
	5.33	14.7	2.8	.408
	5.32	11.5	2.16	.407
	5.31	8.5	1.54	.406
	5.3	0	0	.405

Run N° 19a. G.B. 100/115-1. (136 μ.) W = 500 g.

$\rho_s = 2.47$ $P_A = 705.5$ $\rho_f = .0705$

R.H. = 40 - 60 $T_A = 67.5$ $\mu = .0427$

n (limits)	h	ΔP	V	ε
12.05 - 17.05	14.55	18.3	98.3	.783
10.05 - 14.25	12.15	18.3	86.3	.740
9.15 - 13.15	11.15	18.3	73.5	.717
8.35 - 11.35	9.85	18.4	67.5	.680
8.05 - 10.45	9.25	18.4	55.0	.659
7.65 - 9.05	8.05	18.4	46.1	.635
7.05 - 9.05	8.05	18.4	38.5	.608
7.05 - 8.25	7.65	18.6	32.1	.588
6.65 - 7.45	7.05	18.8	25.9	.552
6.35 - 7.05	6.7	18.8	20.5	.529
6.25 - 7.05	6.65	18.8	20.0	.525
6.15 - 6.95	6.55	18.8	18.2	.518
6.15 - 6.65	6.4	18.8	16.8	.507
6.05 - 6.55	6.25	18.8	14.8	.499
5.85 - 6.35	6.1	18.9	12.4	.483
	5.9	19.0	10.6	.465
	5.75	18.8	8.35	.451
	5.6	18.7	6.5	.436
	5.4	18.3	4.5	.415
	5.27	0	0	.402

Run N° 18a. G.B. 170/200-1. (81 μ.) W = 500 g.

$\rho_s = 2.38$ $P_A = 710$ $\rho_f = .0705$

R.H. = 50 - 61 $T_A = 66$ $\mu = .0427$

n (limits)	h	ΔP	V	ε
10.0 - 13.5	11.75		62.0	0.722
9.0 - 12.0	10.5		40.7	.690
8.0 - 11.0	9.5		39.3	.656
7.8 - 9.8	8.8	LEAK	30.9	.630
7.2 - 8.3	7.75		19.3	.580
7.0 - 8.0	7.50		17.7	.566

Run N° 18a. continued:

h (limits)	h	ΔP	V	ε
6.8 - 7.7	7.25		15.9	.551
6.6 - 7.2	6.90		13.9	.528
6.5 - 7.0	6.75		12.1	.518
6.5 - 7.0	6.75		11.5	.518
6.2 - 6.7	6.45		10.5	.495
	6.6		9.95	.507
	6.3	LEAK	8.38	.484
	6.23		7.0	.478
	6.15		5.8	.471
	6.03		4.8	.460
	5.97		4.5	.455
	5.95		4.3	.454
	5.93		4.2	.452
	5.89		3.77	.448
	5.86		3.28	.445
	5.86		3.00	.445
	5.82		2.72	.441
	5.80		2.60	.440
	5.77		2.28	.437
	5.74		1.96	.434
	5.72		1.72	.432
	5.72		1.36	.432
	5.64		0	.423

Run N° 18b. G.B. 170/200-1. (81 μ.) W = 478 g.

$\rho_s = 2.38$ $P_A = 725$ $\rho_f = .0700$

R.H. = 59 - 69 $T_A = 66$ $\mu = .0427$

6.5 - 8.0	7.25	17.3	19.7	.571
6.4 - 7.7	7.05	17.25	17.4	.558
6.3 - 7.4	6.85	17.3	15.7	.546
6.1 - 6.9	6.50	17.3	13.1	.522
6.1 - 6.6	6.35	17.45	11.5	.510
5.8 - 6.4	6.10	17.45	9.95	.490

Run No 18b. continued:

h (limits)	h	ΔP	V	ε
	6.0	17.45	8.78	.482
	5.97	17.45	8.35	.480
	5.90	17.5	7.5	.474
	5.82	17.5	6.5	.466
	5.70	17.5	5.6	.455
	5.63	17.5	4.84	.449
	5.5	17.35	4.0	.435
	5.25	-	0	.409

Run No 20. G.B. 65/80-1. (192 μ.) W = 500 g.

ρ_S = 2.52 P_A = 717 f_s = .0710

R.H. = 50 - 64. T_A = 69 μ = .0429

h (limits)	h	ΔP	V	ε
15.05 - 18.65	16.85	19.0	150	.816
	13.65	19.0	120	.774
9.95 - 15.55	12.75	19.0	109	.757
9.05 - 13.55	11.25	19.1	93.5	.725
8.55 - 13.05	10.75	19.0	82.3	.712
7.95 - 11.15	9.55	19.0	70.9	.676
7.45 - 10.25	8.85	19.0	59.8	.650
7.05 - 9.35	8.2	19.0	50.3	.622
6.65 - 8.45	7.55	19.0	40.0	.590
6.45 - 7.65	7.05	19.0	31.6	.560
6.15 - 6.95	6.55	19.1	24.6	.528
6.05 - 6.65	6.35	19.1	21.3	.512
5.95 - 6.45	6.2	19.1	19.5	.501
5.85 - 6.35	6.1	19.1	18.0	.493
5.85 - 6.15	6.0	19.0	17.0	.485
5.7 - 6.1	5.9	19.0	16.3	.475
5.65 - 6.0	5.82	19.0	15.0	.469
5.65 - 5.85	5.75	18.95	14.1	.461
5.55 - 5.85	5.7	18.9	13.3	.457
	5.57	18.8	11.7	.445
	5.47	18.65	10.8	.435
	5.42	18.7	10.0	.430
	5.29	18.4	8.6	.415
	5.26	18.2	8.05	.412
	5.24	18.2	7.5	.409
	5.22	18.1	6.78	.408
	5.20	15.05	5.5	.405
	5.19	11.1	4.1	.404
	5.18	0	0	.403

Run N° 21. G.B. 24/28-1. (645 μ.) W = 500 g.

ρ_s = 2.54 P_A = 715 ρ_f = .0708

R.H. = 45 - 68 T_A = 71.5 μ = .0430

h (limits)	h	ΔP	V	ε
8.75 - 19.35	14.05	19.5	248	.789
8.55 - 15.05	11.8	19.4	236	.740
9.05 - 17.05	13.05	19.5	225	.764
7.55 - 15.05	11.3	19.35	219	.728
7.55 - 13.55	10.05	19.7	207	.694
7.85 - 13.05	10.45	19.2	199	.706
7.05 - 14.05	10.55	19.8	192	.709
7.05 - 12.55	9.8	19.6	183	.686
6.05 - 12.55	9.3	19.5	167.5	.670
7.05 - 11.05	9.05	19.15	158.	.660
6.05 - 10.55	8.25	19.2	143	.628
6.05 - 9.05	7.55	19.0	132	.593
5.95 - 7.95	6.95	18.9	113	.558
5.8 - 7.3	6.55	18.8	107	.531
5.65 - 7.25	6.45	18.8	103	.524
5.7 - 7.05	6.37	18.8	99.5	.518
5.55 - 6.55	6.05	18.65	92.0	.492
5.55 - 6.15	5.85	18.65	87.5	.475
5.4 - 5.9	5.65	18.65	83.5	.456
	5.4	18.5	75.5	.431
	5.23	18.2	69.5	.412
	5.15	18.4	64.7	.405
	5.1	17.5	60.8	.398
	5.09	15.5	53.6	.396
	5.08	13.2	46.5	.395
	5.08	11.0	39.0	.395
	5.08	7.8	27.8	.395
	5.08	0	0	.395

Run N° 22. G.B. 16/20-1. (912 μ.) W = 500

ρ_s = 2.55 P_A = 714 ρ_f = 0.0708

R.H. = 40 - 70 T_A = 68 μ = 0.0429

h (limits)	h	ΔP	V	ε
6.95 - 15.35	11.15	20.5	271	.726
6.65 - 14.05	10.35	20.1	244	.705
6.25 - 12.05	9.15	19.3	218	.666
6.15 - 10.75	8.45	19.3	198	.638
6.35 - 10.05	8.2	19.1	198	.628
5.95 - 9.15	7.55	19.1	177	.596
	6.3	18.9	147	.515
5.7 - 7.1	6.4	18.9	147	.523
5.42 - 6.02	5.72	18.75	130	.466
	5.57	18.75	126	.451
	5.27	18.45	113	.420
	5.13	17.75	101	.405
	5.13	15.8	93.2	.405
	5.1	13.6	81.8	.401
	5.09	11.4	71.5	.401
	5.09	9.15	58.7	.401
	5.08	5.2	35.7	.399
	5.08	0	0	.399
8.05 - 18.05	13.05	20.1	308.0	.766
7.25 - 17.25	12.25	19.9	289.0	.750
6.75 - 14.55	10.65	20.6	257.0	.713
6.55 - 12.55	9.55	19.6	230.0	.680
6.05 - 11.05	8.55	19.4	209.0	.643
6.05 - 9.35	7.7	18.95	186.0	.604
5.75 - 7.95	6.85	18.85	163.0	.554
5.45 - 6.35	5.9	18.3	139.0	.483
5.45 - 6.05	5.75	18.3	132.0	.469
	5.29	17.9	116.0	.423
	5.15	17.75	105.5	.407
	5.1	13.4	86.1	.401
	5.08	0	0	.399

Run N° 23. Char 10/12-1. (1524 μ.) W = 300 g.

ρ_s = 1.075 P_A = 706 ρ_f = .0696

R.H. = 40 - 45 T_A = 67 μ = .0427

h (limits)	h	ΔP	V	$\mathcal{E}$
9.95 - 15.95	12.95	12.3	157	.664
9.35 - 12.15	10.75	11.85	138	.595
	9.25	11.45	123	.530
	8.85	10.6	112	.508
	8.75	9.3	98.8	.502
	8.65	7.8	84.3	.497
	8.57	5.9	67.9	.493
	8.53	0	0	.490
12.05 - 29.05	20.55	13.3	231	.788
11.55 - 25.05	18.30	13.0	204	.762
10.55 - 21.55	16.05	12.7	184	.729
10.55 - 21.55	16.05	12.7	181	.729
10.05 - 18.05	14.05	12.5	168	.690
9.95 - 17.15	13.55	12.5	162	.679
9.75 - 14.75	12.25	12.2	150	.645
9.45 - 13.45	11.45	12.0	141	.620
9.25 - 10.65	9.95	11.6	129	.562
9.25 - 10.25	9.75	11.4	125	.553
	8.65	10.2	104	.496
	8.53	8.1	85	.490
	8.45	5.4	61	.485
	8.43	0	0	.485

TERMINAL VELOCITY DATA:

BEADS;

Mesh Size	V_t	D_t (in)	V_t corrected	Sample wt.
14/16	1215	1	1380	37.5
16/20	1120	1	1200	37.0
24/28	886	1	906	39.5
35/42	544	2½	547	300
48/60	372	2½		300
65/80	239	2½		300
100/115	164	2½		300
170/200	91	2½		300
270/325	37	Roller		31.0

CHAR:

Mesh Size	V_t	D_t (in)	V_t corrected	Sample wt.
10/12	795	1	830	14.2
16/20	590	1	602	14.0
24/28	455	1	468	14.1
35/42	258	2½		200
48/60	190	2½		200
65/80	133	2½		200
100/115	100	2½		300
170/200	56	2½		200

MODIFIED DRAG COEFFICIENT PLOT.

$\varepsilon = 1.0$

$(Re/C_D)^{1/3}$		$(C_D Re^2)^{1/3}$
.00040		0.100
.00100		0.158
.00251		0.251
.00630		0.398
.0158(0)		0.630
.0398(0)	$(Re/C_D)^{1/3}$	1.000
0.100	from	1.580
0.251		2.510
0.530	fluid.	3.980
1.000	data	6.300
1.880		10.000
3.33	(3.00)	15.8
5.30	(4.65)	25.1
7.70	(6.95)	39.8
11.20	(9.75)	63.0
15.00	(12.9)	100.0
20.0	(16.3)	158.0
25.1	(20.7)	251.0
31.6	(25.5)	398.0
38.5	-	630.0
44.4	-	1000.0

$\varepsilon = 0.9$

$(Re/C_D)^{1/3}$	$(C_D Re^2)^{1/3}$
.000242	0.10
.00095	0.20
.0029	0.35
.0064	0.52
.0130	0.74
.0238	1.00
.0945	2.00
.278	3.50
.505	5.20
.845	7.40
1.22	10.00
2.70	20.0
4.50	35.0
6.30	52.0
8.00	74.0
9.70	100.0
14.0	200
18.75	350
-	520
-	740
-	1000

$\varepsilon = 0.8$

$(Re/C_D)^{1/3}$	$(C_D Re^2)^{1/3}$
.000140	0.1
.000555	0.2
.0017	0.35
.0037	0.52
.00745	0.74
.0139	1.00
.0550	2.0
.1650	3.5
.320	5.2
.540	7.4
.790	10.0
1.81	20.0
3.15	35
4.40	52
5.80	74
7.05	100
10.50	200
14.05	350

$\varepsilon = 0.7$

$(Re/C_D)^{1/3}$	$(C_D Re^2)^{1/3}$
.0000725	0.1
.000284	0.2
.000875	0.35
.00190	0.52
.00384	0.74
.00698	1.00
.0280	2.0
.0855	3.5
.180	5.2
.320	7.4
.500	10.0
1.210	20.0

$\varepsilon = 0.7$ continued:

$(Re/C_D)^{1/3}$	$(C_D Re^2)^{1/3}$
2.13	35
3.05	52
4.08	74
5.08	100.0
7.70	200
10.40	350

$\varepsilon = 0.8$

$(Re/C_D)^{1/3}$	$(C_D Re^2)^{1/3}$
.000035	0.10
.000134	.20
.00042	.35
.00091	.52
.0018	.74
.0033	1.00
0.0135	2.00
0.040	3.50
0.088	5.20
0.17	7.40
0.280	10.0
0.74	20.0
1.35	35
2.00	52
2.70	74
3.35	100
5.20	200
7.10	350
8.80	520

$\varepsilon = 0.5$

$(Re/C_D)^{1/3}$	$(C_D Re^2)^{1/3}$
.0000152	0.10
.0000600	.20
.000179	.35
.000390	.52
.000790	.74
.001420	1.00
.0056	2.00
.0180	3.5
.0375	5.2
.0840	7.4
.134	10.0
.415	20
.800	35
1.21	52
1.70	74
2.10	100
3.35	200
4.65	350
5.80	520

$\varepsilon = 0.4$

$(Re/C_D)^{1/3}$	$(C_D Re^2)^{1/3}$
.0000049	0.10
.000020	.20
.000062	.35
.00014	.52
.000284	.74
.00052	1.00
.0021	2.0
.0065	3.5
.0146	5.2

$\varepsilon = 0.4$ continued:

$(Re/C_D)^{1/3}$	$(C_D Re^2)^{1/3}$
.030	7.4
.054	10.0
.202	20.0
.44	35
.68	52
.94	74
1.38	10[illegible]
2.10	200
2.90	350
3.60	530